* DORIN LELEA *
DORIN.LELEA@UPT.RO
(L) LOCAL 08.07.2026 16:20
20.01.2026 20:28 - 20.01.2028 20:28
UNIVERSITATEA POLITEHNICA DIN TIMISOARA
Angajat UPT
20110420940401bd89332de2924a2697

Characterization of Sustainable Elastomeric Materials Used for Sealing Peripheral Components in Proton Exchange Membrane Fuel Cell Systems

A Thesis Submitted for obtaining
the Scientific Title of PhD in Engineering
from
Politehnica University Timișoara
in the Field of Materials Engineering
by

Eng. Daniel FOLTUȚ

PhD Supervisor: Prof. dr. ing. Viorel-Aurel Șerban †
Prof. dr. ing. Ion-Dragoș UȚU

Date of the PhD Thesis Defense: 28.05.2026

BUPT

The PhD thesis series of UPT are:

1.Automation
2.Chemistry
3.Energetics
4.Chemical Engineering
5.Civil Engineering
6.Electrical Engineering
7.Electronic Engineering and Telecommunications
8.Industrial Engineering
9.Mechanical Engineering
10.Computer Science and Information Technology
11.Science and Material Engineering
12.Systems Engineering
13.Energy Engineering
14.Computers and Information Technology
15.Materials Engineering
16.Engineering and Management
17.Architecture
18.Civil Engineering and Installations
19.Electronics, Telecommunications and Information Technologies

Politehnica University Timișoara, Romania, initiated the above series to disseminate the expertise, knowledge and results of the research carried out within the doctoral school of the university. According to the Decision of the Executive Office of the University Senate No. 14/14.07.2006, the series includes the doctoral theses defended in the university since October 1, 2006.

Copyright © Editura Politehnica – Timișoara, Romania, 2025

This publication is subject to copyright law. The multiplication of this publication, in whole or in part, the translation, printing, reuse of illustrations, exhibit, broadcasting, reproduction on microfilm or any other form is allowed only in compliance with the provisions of the Romanian Copyright Law in force and permission for use obtained in writing from the Politehnica University Timișoara, Romania. The violations of these rights are under the penalties of the Romanian Copyright Law.

Romania, 300223 Timișoara, Bd. Vasile Pârvan no. 2B
Tel./fax +40-(0)256 404677
e-mail: editura@upt.ro

BUPT

Foreword

The present doctoral thesis was developed on the basis of the scientific research carried out within the Department of Materials Science and Engineering, Faculty of Mechanics, Polytechnic University of Timișoara, Romania. The work was conducted in close collaboration with the Ostrava Laboratory of the Department of Common Engineering at Vitesco Engineering Romania SRL, Timișoara, Romania, providing both academic and industrial perspectives on the investigated topics.

The research activities underlying this thesis were motivated by the increasing demand for durable and reliable polymeric materials for proton exchange membrane fuel cell (PEMFC) applications, particularly in peripheral components where elastomeric sealing systems play a critical role in ensuring operational safety and long-term performance.

During these last four years, it would have been impossible for me to accomplish this work without the help, encouragement and support of my family, coordinating professor, colleagues and friends.

First and foremost, I would like to express my deepest gratitude to my wife, Naomi Foltut, whose constant encouragement, patience, and unwavering support made the completion of this doctoral work possible. From the moment I decided to embark on this journey until its completion, she stood by me and never allowed me to give up. Throughout these years, she carried an immense responsibility, taking care of our three wonderful children, Ioan, Ionatan, and Ana, all of whom were born during the course of my doctoral studies. The sustained pace and continuity of my research would not have been possible without her countless sacrifices, understanding, and strength. For all of this, I am profoundly grateful.

I would also like to express my sincere gratitude to Prof. Dr. Eng. Viorel Aurel Șerban from the Polytechnic University of Timișoara for offering me the opportunity to pursue this doctoral research under his academic guidance. His support, trust, and scientific insight were invaluable throughout my PhD studies. I am thankful for his continuous encouragement, constructive feedback, and for creating an academic environment that allowed this work to develop and mature.

Furthermore, I would like to thank Prof. Dr. Ing. Mircea Voda, Conf. Dr. Ing. Cosmin Codrean, Conf. Dr. Ing. Nicolae Crainic and Prof. Dr. Eng. Ion Dragoș Uțu from Polytechnic University of Timisoara for being part of my guidance committee and for their countless suggestions and advice regarding my scientific research.

Many thanks to my colleagues and friends from Vitesco Technologies, namely Dr. Eng. Monica Buzdugan, Dr. Eng. Dragoș Pascal, Eng. Jan Pospisil and Eng. Bjoern Pucher for the constructive discussions, their moral support, advices and friendship.

Last but not least, I am extremely grateful to my mother Foltuț Claudia and father Viorel Foltuț for their unconditional support, for trusting me and encouraging me to make important steps in my life.

Timişoara, December 2025 Daniel Foltuț

BUPT

To my wife, Naomi Foltuț, and our children Ioan, Ionatan and Ana.

FOLTUȚ, Daniel
Characterization of sustainable elastomeric materials used for sealing peripheral components in proton exchange membrane fuel cell systems
PhD theses of UPT, Series X, No. YY, Editura Politehnica, 200Z, 137 pages, 60 figures, 9 tables.
ISSN:
ISBN:

Keywords: elastomeric sealing materials, EPDM, TPV, sustainable elastomers, PEM fuel cells.

Abstract
This doctoral thesis addresses the characterization of sustainable elastomeric materials used for sealing peripheral components in proton exchange membrane fuel cell (PEMFC) systems. Although sealing elements are auxiliary components, their durability and reliability are critical for maintaining gas tightness, system efficiency, and operational safety under aggressive thermo-mechanical and chemical conditions.
The study focuses on ethylene–propylene–diene monomer (EPDM) rubbers, thermoplastic vulcanizates (TPV), and environmentally optimized EPDM materials incorporating circular and recycled carbon black fillers. The materials were subjected to accelerated thermal and chemical aging protocols representative of PEMFC cathodic air environments. Mechanical, thermal, chemical, and tribological properties were evaluated using standardized testing methods, including tensile testing, compression set, hardness measurements, thermal analysis, microscopy, leaching assessment, and pin-on-disk tribological experiments.
The results highlight distinct degradation mechanisms governed by polymer structure and filler type. EPDM exhibited superior chemical stability and elastic recovery, while TPV showed improved tribological behavior in dynamic sealing conditions but reduced resistance to acidic environments. Sustainable EPDM reinforced with circular carbon black demonstrated performance comparable to conventional formulations, whereas recycled carbon black variants showed increased degradation. The findings support the feasibility of sustainable elastomeric materials for PEMFC sealing applications when appropriate material design is employed.

BUPT

CONTENTS

ABSTRACT 1

1 Introduction 3

1.1 Motivation and importance of the work 7
1.1.1 Role of PEMFC systems in electric mobility 8
1.1.2 Market Status and Deployment Trends of PEMFC in Mobility 10
1.1.3 System Integration and Performance Considerations 11
1.1.4 Challenges and Limitations of using PEMFC in mobility 12

1.2 Importance of elastomeric gaskets in PEMFC operation 13

1.3 Need to investigate sustainable sealing materials 13

1.4 Structure of the thesis 14

2 State-of-the-art 16

2.1 Historical Background and Technological Development of Fuel Cells 16

2.2 PEMFC Architecture and Operating Environment 17

2.3 Operating Conditions and Environmental Stressors 20

2.4 Balance-of-Plant and Peripheral Components in PEMFC Systems 21
2.4.1 Air flux level control valve in PEMFC Systems 23

2.5 Sealing Concepts, Mechanisms, and Requirements in PEMFC Systems 25
2.5.1 Overview of Sealing Types in Engineering Systems 25
2.5.2 General Principles of Elastomeric Sealing 27
2.5.3 Mechanisms and Failure Modes of Elastomeric Sealing 29
2.5.4 Sealing Demands in PEMFC Balance-of-Plant Components and in the Cathodic Air Control Valve 31

2.6 Materials for sealing components in the cathodic side air-channel valve 32
2.6.1 Elastomeric Materials for Air-Valve Sealing 33

2.7 Sustainability Aspects of Synthetic Rubbers and Life-Cycle Considerations 37
2.7.1 Sustainable Feedstocks for Elastomer Synthesis 37
2.7.2 Sustainable Reinforcing Fillers: Recycled and Circular Carbon Black 38
2.7.3 Green Additives, Catalysts, and Compounding Strategies 40
2.7.4 Recycling and Circularity of Elastomers 40
2.7.5 Life-Cycle Assessment of Sustainable Elastomers 41
2.7.6 Relevance for PEMFC Cathodic-Side Sealing Components 41

2.8 Recent Developments in the Scientific Literature on Sealing Materials for PEMFC Applications and Identified Research Gaps 42

3 Scope and Objectives 46

3.1 Scope 46

BUPT

2
Scop și Obiective

3.2 Objectives 46

4 Methodology and equipment 48

4.1 Materials 50
4.1.1 Thermoplastic Styrenic Elastomer (TPS) – Heat Aging Study 50
4.1.2 EPDM-H, TPV and Eco TPV – Chemical and Thermal Aging 50
4.1.3 Low-Friction EPDM and Low-Frtiction TPV for Tribological Tests 51
4.1.4 EPDM-T – Temperature Dependent Mechanical Characterization 52
4.1.5 ECO EPDM with Circular and Recycled Carbon Black (CCB and RCB EPDM) – Chemical Stability & Leaching 52

4.2 Aging Protocols and Environmental Exposures 53
4.2.1 Thermal Aging of Thermoplastic Styrenic Elastomer 53
4.2.2 Chemical and Thermal Aging Protocols for EPDM-H, TPV, Eco TPV and ECO EPDM (CCB/RCB) 53

4.3 pH Tracking and Chemical Analysis of Leachates 54
4.3.1 pH Measurements 54
4.3.2 HPLC Analysis of Organic Leachates 54

4.4 Mass and Volume Change Measurements 56
4.4.1 General Mass and Volume Change under Acidic Immersion 56
4.4.2 Mass and Volume Change for ECO EPDM without Sinker 56

4.5 Hot Water Extraction and Ion Leaching Tests 57

4.6 Thermal Analysis 58
4.6.1 Thermogravimetric Analysis (TGA) and Differential Scanning Calorimetry (DSC) 58

4.7 Mechanical Testing 59
4.7.1 Tensile Testing Procedures 59
4.7.2 Compression Set Measurements 60
4.7.3 Hardness and Microhardness Testing 60

4.8 Dynamic Mechanical Analysis (DMA) 61

4.9 Tribological Testing 61

4.10 Microscopy and Surface/Elemental Analysis 62
4.10.1 SEM of TPS Before and After Thermal Aging 62
4.10.2 SEM of EPDM-H, TPV and Eco TPV after Acid and Heat Aging 62
4.10.3 SEM–EDS of ECO EPDM (CCB and RCB) 63

5 Results 64

5.1 Thermoplastic Styrenic Elastomer (TPS): Thermal Aging and Mechanical–Thermal Behavior [157] 64
5.1.1 Tensile Behavior Before and After Thermal Aging 64
5.1.2 Thermal Stability (TGA) 67
5.1.3 Thermal Transitions (DSC) 67
5.1.4 Surface Degradation After Aging (SEM) 68

BUPT

5.2 Chemical and Thermal Stability of Elastomeric Materials (EPDM-H, CCB EPDM, RCB EPDM, TPV and Eco TPV) 69
5.2.1 Swelling Behavior Under Acidic Environments 69
5.2.2 pH Evolution of Aging Media 72
5.2.3 Ionic Leaching Behavior (Hot Water Extraction Test) 75
5.2.4 Thermal Behavior After Aging (DSC) 77
5.2.5 Organic Leachate Profiles (HPLC-DAD) — ECO EPDM 80
5.2.6 Tensile Behavior After Chemical and Thermal Aging 84
5.2.7 Hardness and Microhardness Changes 90
5.2.8 Compression Set 91
5.2.9 Microstructural and Chemical Surface Evolution (SEM / SEM-EDS) 92
5.3 Temperature-Dependent Mechanical Behavior of EPDM-T [18] 97
5.3.1 Temperature-Dependent Tensile Behavior 97
5.3.2 Dynamic Mechanical Analysis 98
5.3.3 FEA Material Modelling 99
5.4 Tribological Behavior of LF-EPDM and LF-TPV Against PA66GF30 [21] 100
5.4.1 Coefficient of Friction (CoF) Evolution 100
5.4.2 Mass Loss 104
5.4.3 Wear Area and Wear Volume 105
5.4.4 FEA calibration and Simulation of Friction 110
5.4.5 Application-Level Push-In Simulation (Seal Actuation Case Study) 113
6 Conclusions 116
References 120

BUPT

ABSTRACT

The main goal of the present study was to comprehensively characterize and optimize sustainable elastomeric sealing materials—specifically EPDM, TPV, and Eco-friendly variants utilizing circular and recycled fillers—for the peripheral components of Proton Exchange Membrane Fuel Cell (PEMFC) systems.

The thesis has been structured into 6 chapters:

Chapter 1 presents the background and motivation of the chosen topic, emphasizing the role of PEMFC systems in electric mobility and the critical importance of sealing components.

Chapter 2 deals with the state of the art in the field of PEMFC sealing, presenting theoretical aspects regarding operating environments, current elastomeric materials, degradation mechanisms, and sustainability considerations in rubber manufacturing. Moreover, an introduction to the tribological and chemical challenges of peripheral components is made.

Chapter 3 outlines the scope and specific objectives of the doctoral research.

Chapter 4 describes the methodology and equipment used to achieve the experimental study. This chapter offers an outline concerning the applied investigation methods and presents different experimental techniques, such as accelerated aging protocols, chemical analysis (HPLC, HWET), and tribological testing, which can provide important information on the quality and performance of sustainable sealing materials.

Chapter 5 presents the experimental program concerning the mechanical, chemical, and tribological behavior of the materials, the results obtained during this study (including the specific effects of circular versus recycled carbon black), and highlights the most important aspects.

Chapter 6 points out the conclusions of this study and the personal contributions accomplished through this work.

In the current state of the art, sealing in PEMFC systems involves the use of specialized gaskets and O-rings made from synthetic rubbers, primarily EPDM, designed to withstand acidic environments, humid air, and temperature fluctuations. These seals are critical for preventing gas crossover and leakage, which are primary failure modes in fuel cell stacks. However, standard materials often rely on fossil-based feedstocks and virgin carbon black, contributing to a significant carbon footprint. The sealing process must ensure gas tightness under dynamic conditions, often involving compression against glass-fiber reinforced housings. During operation, the elastomers are exposed to temperatures between –40 °C to 60 °C and 90 °C, acidic condensates, and oxidative radicals, which can induce chain scission and crosslink degradation. No universal reference for the durability of sustainable elastomers containing recycled fillers in these specific conditions exists, because the degradation behavior depends strongly on the chemical composition of the base polymer (EPDM vs. TPV), the purity of the reinforcing filler (circular vs. recycled), and the specific interactions with the acidic environment. Considering that the majority of peripheral components are subjected to both static compression and dynamic sliding (as in air control valves), the material selection typically balances chemical resistance

BUPT

with tribological performance. The major limitation of current sustainable alternatives is the potential for leaching of ionic and organic species, which can poison the fuel cell membrane and catalyst. This process can have a negative effect on the system efficiency, leading to voltage loss or premature stack failure. Another current disadvantage of utilizing recycled materials is the variability in filler morphology, which can compromise the long-term mechanical stability and sealing force retention.

The present study assessed the possibility of overcoming the aforementioned limitations of standard and recycled sealing materials for PEMFC applications.

The personal contributions of this study refer to the possibility of utilizing accelerated aging protocols (acidic immersion and thermal exposure) in order to obtain sustainable elastomeric functional seals with superior chemical and mechanical resistance. In this regard, it was explored the possibility of combining circular carbon black (CCB) and recycled carbon black (RCB) as reinforcing phases with EPDM rubber, to develop eco-friendly sealing solutions. A careful selection of feedstock materials in order to favorably combine a manufacturing process as accessible, economic, and environmentally friendly as possible, with the production of seals with superior characteristics was also carried out. The successful employment of high-performance liquid chromatography (HPLC) and hot water extraction tests (HWET) to identify and quantify organic and ionic leachates, assessing the risk of membrane contamination was highlighted. The usage of the Arruda-Boyce hyperelastic model for Finite Element Analysis (FEA) allowed for the accurate prediction of sealing force retention and contact mechanics, thus reducing the need for extensive physical prototyping. Studies on the degradation mechanisms, as well as investigations on the influence of the acidic environment on the morphology of the coatings have been accomplished. Consequently, the optimization of material selection based on the trade-off between tribological performance (where TPV excelled) and chemical stability (where EPDM proved superior) was successfully performed. Experimental investigations revealed noteworthy characteristics and properties of the CCB-filled EPDM materials (including wear and corrosion resistance), which outperformed their recycled-black counterparts.

Accordingly, the method presented in this thesis leads to a rigorous and scientifically grounded way to develop sustainable functional seals with improved environmental footprints and verified durability, due to the comprehensive characterization of the polymer-filler network stability.

BUPT

1 INTRODUCTION

The transition toward a low-carbon economy has become a defining global objective of the 21st century. With increasing concerns about climate change, fossil-fuel depletion, and energy security, attention has shifted toward technologies that enable efficient, clean, and renewable energy conversion and storage. Among these, hydrogen technologies—and particularly proton exchange membrane fuel cells (PEMFCs)—have gained strategic significance due to their potential for decarbonizing transport, stationary power, and industrial processes.

Hydrogen offers the unique advantage of acting as both an energy carrier and a storage medium, complementing intermittent renewable energy sources such as wind and solar. When used in PEM fuel cells, hydrogen can be converted directly into electricity with only water and heat as by-products, making it one of the cleanest power-generation pathways currently available.

Global investments in the energy transition reflect this technological momentum. The global energy system is facing pressing challenges from multiple directions: rising greenhouse-gas emissions, increasing demand for mobility, and the need for sustainable, secure energy supply. In response, investment into the energy transition has surged. According to the International Energy Agency (IEA), it is estimated that clean-energy investment in 2024 exceeded US $2 trillion, and that total energy investment (including fossil fuels) may surpass US $3 trillion in the same year. Figure 1.1 showcases the yearly change of investments, starting with 2025. [1–3]

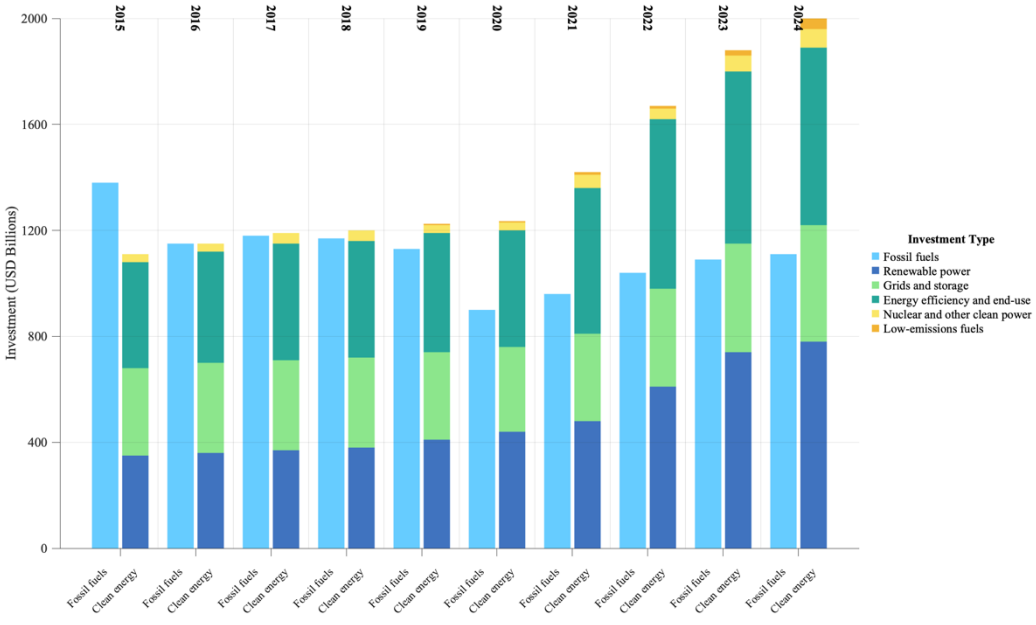


Figure 1.1. Comparison between fossil fuel and clean energy investments, 2015-2024 [1]

BUPT

These figures indicate a major shift in capital flows toward renewables, electric mobility, energy storage and hydrogen-based technologies.

Within this broader transformation, hydrogen and electrochemical energy systems play a pivotal role. The global demand for hydrogen surpassed 97 million tones in 2023 and is projected to approach 100 Mt in 2024, underscoring the scale of existing industrial hydrogen usage while signaling growth potential in low-emissions hydrogen production [4]. Meanwhile, the market for proton-exchange-membrane fuel cells (PEMFCs), pivotal for hydrogen conversion in transport and stationary applications, was valued at US $4.3 billion in 2024 and is forecast to grow to approximately US $10.3 billion by 2034 (CAGR ≈9 %) according to one estimate. [5,6]

Such growth trajectories reflect rising policy support, decarbonisation mandates, and increasing industrial deployment of hydrogen-based systems (including heavy-duty transport, backup power, and off-grid applications) where battery alone may face limitations.

Nevertheless, despite technological progress and stronger market signals, critical challenges remain for hydrogen and fuel-cell-based systems. These include:

- **The high capital cost and complexity of stack manufacture and hydrogen infrastructure.**

The capital cost of Proton Exchange Membrane (PEM) electrolyzer stacks can be a significant portion (e.g., 46%) of the total electrolyzer cost, and although cost reductions in stack manufacturing can reduce overall capital costs, the impact on hydrogen price can be limited due to other factors like electricity cost. This indicates the high capital cost and complexity associated with stack manufacture and infrastructure. [7]

Electrolyzer and hydrogen infrastructure capital costs constitute a large portion of the total installation cost due to multiple factors: the electrolyzer stack itself requires expensive materials like catalysts and membranes, and manufacturing these stacks involves complex processes with costs currently ranging roughly from $541 to over $700 per kW, with total installed system costs reaching $1,300 to $1,700 per kW; additionally, the balance of plant (BOP) systems, such as water purification, cooling, gas drying, power electronics, and control units, add significant cost and operational complexity, often contributing several hundred dollars more per kW; finally, infrastructure elements such as piping, compression, storage, safety systems, and installation activities including engineering and commissioning injections further drive up capital expenses, especially in early deployments where installation and indirect costs can approximately equal the uninstalled system costs; as a result, total installed capital costs typically range from $1,400 to $2,500 per kW, with the exact figure influenced by scale, technology maturity, and site-specific factors, making the capital investment for hydrogen production systems a complex interplay of materials, manufacturing, auxiliary systems, and infrastructure demands that challenges cost reduction but offers opportunities through economies of scale and process optimization. [8–10]

Hydrogen production via PEM electrolyzers currently incurs these high capital costs, yielding a levelized cost of hydrogen (LCOH) of about $5–$7 per kilogram when powered by renewable sources such as wind or solar [9]. By comparison, conventional electricity-generation technologies exhibit much lower capital expenditures and levelized costs of electricity (LCOE): natural-gas combined-cycle (NGCC) plants typically cost $700–$1,000 per kW with LCOE around $30–$50 per MWh; coal-fired

BUPT

plants average $1,000–$1,500 per kW with $40–$70 per MWh; and onshore wind and solar photovoltaic (PV) systems fall within $1,000–$1,500 per kW, yet achieve substantially lower LCOE values—$20–$40 per MWh—due to the absence of fuel costs[2, 4, 10]. The energy efficiency of PEM electrolysis (≈60–70%), coupled with the conversion losses incurred when hydrogen is reconverted to electricity through fuel cells or gas turbines, further widens the efficiency gap compared to direct electricity generation. [8,10,11]

Figure 1.2. compares the capital cost and levelized cost ranges of PEM electroliers with those of conventional and renewable power-generation technologies, highlighting the significantly higher investment intensity and energy cost associated with hydrogen production.

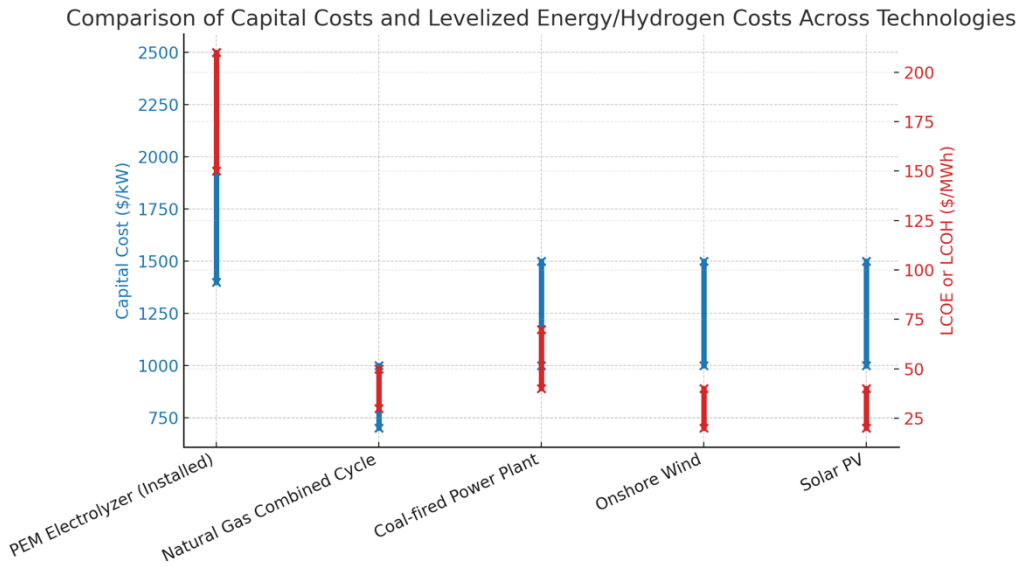


Figure 1.2 Comparison of capital costs and levelized energy or hydrogen production costs across representative technologies.

Despite these disadvantages, electrolyze-based hydrogen production enables carbon-free energy storage, grid balancing, and sector coupling between power and industrial systems—functions that traditional fossil or renewable plants cannot directly provide. Nevertheless, its economic and energy-efficiency challenges continue to constrain large-scale deployment. Bridging this gap will depend on reductions in capital cost, advances in electrolyze efficiency, scaling of renewable capacity factors, and policy mechanisms that internalize the environmental benefits of green hydrogen. These developments are essential for hydrogen to achieve parity with established electricity-generation pathways and to play a central role in future low-carbon energy systems.

- **The durability and reliability of peripheral components (seals, gaskets, polymers) which are often under-recognized but can determine lifetime and system-cost.**

The durability and reliability of peripheral components such as seals, gaskets, and polymers constitute critical challenges in fuel cell-based systems. These components, while sometimes overlooked compared to core elements like catalysts and membranes, are essential for maintaining gas tightness, structural integrity, and system efficiency. They operate in harsh environments characterized by large temperature ranges, high humidity, chemical exposure (such as acidic or oxidative conditions), and mechanical stresses including vibrations, compression, and cyclic loading. Over time, these stressors can induce physical and chemical degradation such as material embrittlement, cracking, swelling, and chemical breakdown, which compromise sealing capability and mechanical stability. For example, seal materials often face challenges in retaining elasticity and chemical resistance, leading to leaks and contamination issues that degrade fuel cell performance and safety. The failure of these "peripheral" components can cause significant operational interruptions and necessitate costly maintenance or replacement, directly impacting both system lifetime and total cost of ownership. [12–14]

Moreover, peripheral components are typically composed of polymeric materials that undergo complex degradation mechanisms, including oxidative damage from reactive oxygen species generated during fuel cell operation and physical fatigue from continuous mechanical cycling. Polymer membranes themselves, though central to the fuel cell function, suffer from chemical chain scission and mechanical wear, resulting in a loss of ionic conductivity and increased gas crossover, which lowers system efficiency and durability. Similarly, gaskets and seals often lose hydrophobic properties or suffer from chemical contamination, further undermining their sealing effectiveness. This degradation not only shortens the operational lifespan but can also propagate failures in the fuel cell stack, elevating replacement frequency and costs. Developing materials with enhanced resistance to chemical attack and mechanical degradation, alongside improved design strategies for durability testing and prediction, remains key research thrust within the fuel cell community and is the main subject if this thesis. [12–14]

The economic repercussions of peripheral component degradation can have a significant effect. Although these components may represent a smaller fraction of the initial capital cost compared to catalysts and membranes, their impact on operational expenditure and system availability is disproportionately large. Unscheduled maintenance driven by seal or gasket failures can result in significant downtime, loss of productivity, and increased labor and part replacement costs. Furthermore, premature degradation of these components typically limits the design operating conditions of fuel cells, constraining performance optimization and operational flexibility. Addressing these challenges necessitates multidisciplinary approaches including advanced polymer chemistry, improved manufacturing processes to ensure component uniformity and robustness, and comprehensive diagnostic tools to monitor component health in real time. In conclusion, enhancing the durability and reliability of peripheral components is essential to unlocking the full economic and performance potential of fuel cell systems, making them competitive for widespread commercial deployment. [12,15,16]

- **Material degradation and failure under harsh conditions (temperature, humidity, chemical attack, mechanical cycling) which can undermine system availability and economics.**

Material degradation and failure under harsh operating conditions—such as elevated temperature, high humidity, chemical exposure, and mechanical cycling—

BUPT

remain among the most critical challenges affecting the lifetime and economics of fuel-cell systems. Elastomeric sealing materials represent a relatively small subsystem, yet their performance has a disproportionately large influence on system reliability and maintenance cost. Even when the electrochemical components of a PEMFC achieve high efficiency, failure of seals or gaskets can cause gas leakage, cross-contamination, or electrical shorting, leading to rapid performance decay and safety risks. The environment in which these materials operate is extremely demanding, typically involving temperatures of 60–90 °C, high humidity, acidic condensates, and repeated mechanical compression cycles, all of which accelerate both chemical and physical degradation[13, 15].

At the same time, sustainability considerations are becoming increasingly important in the design of polymeric and elastomeric components for hydrogen technologies. Traditional sealing compounds often rely on petroleum-derived polymers and non-renewable fillers, contributing to a substantial environmental footprint throughout the system's life cycle. As hydrogen energy systems expand, there is growing emphasis on developing eco-efficient elastomeric materials that combine mechanical durability and chemical stability under aggressive PEMFC operating conditions with reduced life-cycle impact and enhanced recyclability [4,10].

1.1 Motivation and importance of the work

The long-term reliability of hydrogen energy systems depends not only on the electrochemical stability of membranes and catalysts but also on the durability of peripheral materials and interfaces that ensure structural integrity, sealing, and chemical stability. While PEMFC development has advanced significantly in catalyst and membrane technologies, the supporting elastomeric materials—such as seals and gaskets—remain a critical bottleneck in achieving reliable, cost-effective, and sustainable systems. [12,13,15]

The present research builds on a series of studies conducted throughout this doctoral work, which systematically examined the mechanical, chemical, and tribological degradation behavior of EPDM-based and thermoplastic vulcanizate (TPV) materials under conditions relevant to fuel-cell operation. Initial investigations addressed mechanical and physicochemical aging of EPDM, TPV, and ECO TPV under thermal and acidic environments, identifying significant differences in tensile retention and surface [17–20]. These findings established EPDM's superior resistance to acidic degradation and provided baseline mechanical data for further optimization.

Subsequent studies extended this work toward sustainable formulations through the use of circular and recycled carbon black (CCB and RCB) as eco-fillers, revealing that both filler morphology and carbon source significantly affect degradation kinetics, mechanical stability, and microstructural integrity after exposure to acidic and thermal stress [21–23]. Complementary analyses involving tribological testing against glass fiber-reinforced polyamide 66 (PA66GF30) demonstrated how contact-induced wear and friction correlate with mechanical softening and filler dispersion, providing insights into the surface degradation mechanisms of elastomers in dynamic sealing applications [21].

Together, these studies have defined the central hypothesis of the present thesis: that formulation design and filler circularity directly influence the durability and eco-efficiency of elastomeric sealing systems in hydrogen-based energy technologies. This thesis therefore integrates mechanical characterization, chemical aging, surface analysis, and numerical modeling to develop a comprehensive

BUPT

understanding of degradation mechanisms and to support material selection and design for next-generation PEM fuel-cell components.

While previous sections discussed the broader cost and performance challenges associated with hydrogen and fuel-cell systems, these issues gain practical significance in their most impactful application domain—electric mobility. Within this sector, proton exchange membrane fuel cells (PEMFCs) provide the technological foundation for fuel-cell electric vehicles (FCEVs), offering a pathway to deep decarbonization of transport while maintaining the convenience, performance, and range of conventional vehicles. Understanding their architecture and operational constraints is essential for contextualizing the material degradation phenomena addressed in subsequent chapters.

1.1.1 Role of PEMFC systems in electric mobility

PEMFCs convert hydrogen and oxygen electrochemically into electricity, producing only water vapor and heat as by-products. This direct conversion of chemical to electrical energy eliminates the combustion step, enabling higher efficiency and zero tailpipe emissions [2,4].

Globally, hydrogen and PEMFC technology are transitioning from demonstration to early commercialization.

By 2024, the worldwide fleet of fuel-cell electric vehicles (FCEVs) exceeded 85 000 units, with major deployments in Japan, South Korea, the United States, and several EU member states. The number of operational hydrogen refueling stations surpassed 1 100, marking a 30 % growth over 2022 [4].

These developments signal accelerating investment in hydrogen mobility infrastructure and reinforce the relevance of PEMFC systems as an enabling technology for transport decarbonization.

PEMFCs present several compelling advantages for mobility applications, driving significant interest in their use for vehicles such as cars, buses, trucks, and material handling equipment. One of the most significant advantages is their environmental friendliness: PEMFC vehicles emit only water vapor as a byproduct, producing zero tailpipe pollutants like CO2, NOx, or particulate matter, which makes them an important technology for reducing urban air pollution and greenhouse gas emissions in the transport sector [24–27]. This characteristic is particularly critical considering increasingly stringent emissions regulations worldwide. [28]

A PEMFC powertrain integrates the fuel-cell stack, hydrogen tanks (typically compressed to 700 bar for light-duty or 350 bar for heavy-duty vehicles), a DC/DC converter, traction inverter, electric motor and auxiliary battery. The hybridisation with a small lithium-ion battery smooths power transients and allows regenerative braking. Figure 1.3. shows the simplified configuration [29].

BUPT

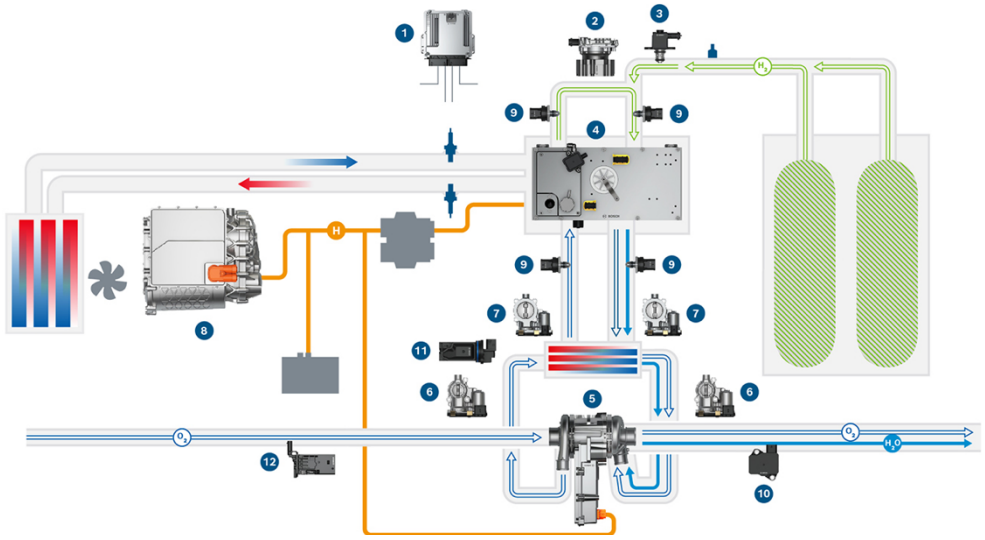


Figure 1.3. The PEMFC automotive system, from [29]

The operation of the system can be summarized as follows:

- Fuel-cell control unit (1) — Coordinates the operation of the stack, sensors, and balance-of-plant (BOP) subsystems, ensuring optimal efficiency and safety during dynamic load changes.
- Anode recirculation blower (2) — Recirculates unused hydrogen within the anode circuit, improving fuel utilization and maintaining a stable anode gas composition.
- Hydrogen gas injector (3) — Regulates the precise flow of hydrogen from the storage tanks into the anode inlet.
- Fuel-cell stack (4) — The electrochemical core where hydrogen and oxygen react across proton-exchange membranes to generate DC electricity and water.
- Electric air compressor (5) — Supplies compressed, filtered air to the cathode side, controlling stoichiometry and supporting membrane hydration.
- Humidifier and stack-bypass valve (6) — Maintains correct humidity and temperature; bypass control enables cold-start and transient-load management.
- Stack-isolation and control valves (7) — Manage hydrogen and air flow, isolating the stack for shutdown or safety events.
- Electric drive (e-Axle) (8) — Converts electrical power to mechanical torque for propulsion; regenerative braking energy is fed back into the DC bus.
- Sensor set (9–12) — Includes low-pressure, hydrogen-exhaust, and air-flow sensors that continuously monitor system parameters for diagnostic and control purposes.

BUPT

Blue, green, orange, and red flow lines in the schematic represent the air, water, hydrogen, and thermal/high-voltage circuits, respectively.

Hydrogen from on-board composite storage cylinders enters the fuel-cell stack, where the reaction of hydrogen and oxygen generates electric power ($2\ H_2 + O_2 \rightarrow 2\ H_2O$ + electric energy + heat). The generated electricity is conditioned by power electronics and distributed to the traction motor and auxiliary battery pack.

Hydrogen offers an exceptionally high gravimetric specific energy of around 120 MJ kg^{-1}—roughly three times that of gasoline (≈ 44 MJ kg^{-1}) on a mass basis—providing one reason why fuel-cell electric vehicles (FCEVs) can offer long driving ranges with lower battery mass penalty, when the hydrogen storage and fuel-cell stack are optimized. [30,31]

This architecture provides continuous high-power output combined with fast refuelling (≈ 3–5 minutes), long driving range (≈ 500–700 km), and zero tailpipe emissions. [28,29]

Recent reviews emphasize that a PEMFC stack is a multi-component system consisting of membrane–electrode assemblies, bipolar plates, gaskets and other peripheral components [22]. The overall efficiency and durability of FCEVs therefore depend not only on catalyst and membrane innovations but also on robust sealing solutions that maintain gas tightness and mechanical compression under demanding conditions.

1.1.2 Market Status and Deployment Trends of PEMFC in Mobility

Hydrogen mobility has shifted from prototype to early commercialization. According to the IEA Global Hydrogen Review 2024, global FCEV stock rose to about 85 000 vehicles by the end of 2024, while hydrogen-refueling stations exceeded 1 100 worldwide, with Japan, Korea, the EU and California leading deployment. [4]

Regional market analysis shows differing adoption models. In Asia, Japan's "Strategic Roadmap for Hydrogen and Fuel Cells" and Korea's "Hydrogen Economy Roadmap" target hundreds of thousands of FCEVs by 2030 [1].

Europe's regulatory and industry frameworks project substantial expansion of hydrogen fuel cell vehicle deployment through 2035. The EU's "Fit for 55" package establishes technology-neutral CO_2 emission reduction targets of 45% by 2030, 65% by 2035, and 90% by 2040 for heavy-duty vehicles. Within this regulatory context, industry projections from Hydrogen Europe anticipate that approximately 45,000 to 50,000 hydrogen-powered medium- and heavy-duty trucks and buses will be deployed across the European Union by 2030, with the fleet expanding to approximately 850,000 units by 2035. These projections reflect coordinated support from the Hydrogen Council and European hydrogen stakeholders, which envision hydrogen as a critical technology for achieving the decarbonization targets established under Fit for 55. The global hydrogen truck fleet is projected to reach 350,000 units by 2030 according to the Hydrogen Council roadmap, with Europe representing a significant portion of this deployment. [32–36]

The correlation between European decarbonization targets and projected deployment of hydrogen-powered vehicles is illustrated in Figure 1.4.

BUPT

The figure compares the expected growth of the hydrogen fuel-cell truck and bus fleet within the European Union to global hydrogen truck projections, overlaid with the official CO_2-emission reduction targets for heavy-duty vehicles defined under the Fit for 55 regulatory frameworks.

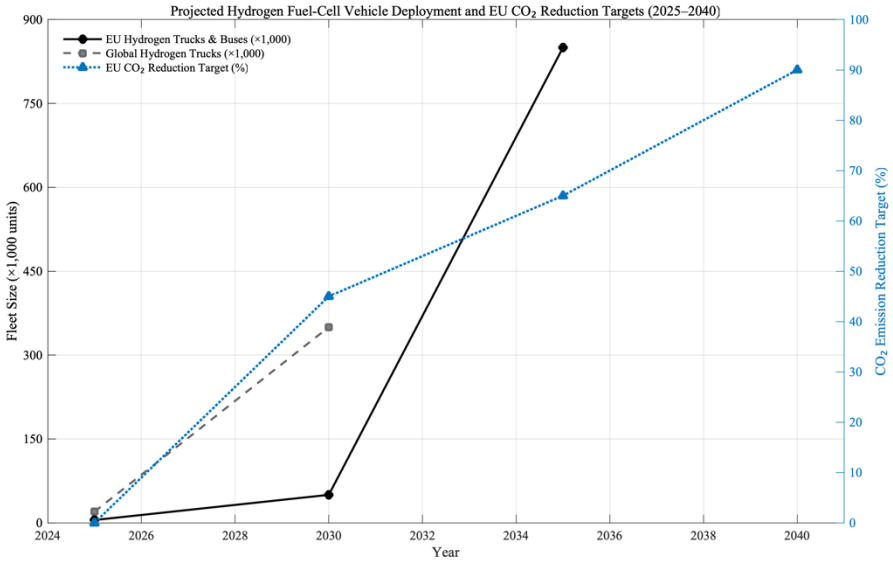


Figure 1.4. Projected hydrogen fuel-cell vehicle deployment and EU CO_2-reduction targets for heavy-duty transport (2025–2040)

The global Proton Exchange Membrane Fuel Cell (PEMFC) market is experiencing substantial expansion, with significant projections for the coming decade. The market was valued at approximately USD 3.5 billion in 2022 and is projected to reach USD 12.3 billion by 2030 [37]. Within the mobility sector specifically, the PEMFC vehicle market demonstrated even more aggressive growth trajectories, with market size estimates ranging from USD 1.24 billion in 2023 to USD 2.38 billion in 2024 [38]. Forecasts indicate the market will expand at a compound annual growth rate (CAGR) ranging from 25% to 36.60% through 2033, with some analyses projecting market valuations reaching USD 15.9 billion by 2032 and potentially USD 25 billion by 2035. Transportation applications have emerged as the dominant application segment, accounting for approximately 38.3% of the overall PEMFC market share in 2022, driven primarily by increased adoption of fuel cell electric vehicles (FCEVs). [39–41]

1.1.3 System Integration and Performance Considerations

Successful integration of PEMFCs in mobility applications requires optimized management of thermal, water, and hydrogen systems operating under dynamic load conditions. The fuel cell stack must maintain membrane hydration to sustain proton conductivity, yet excessive water accumulation causes flooding that blocks gas diffusion pathways and reduces performance. This fundamental control challenge—balancing opposing water management requirements—is intensified by dynamic

BUPT

vehicle operation, where rapidly fluctuating power demand creates temporal mismatches between water production and transport capacity. Advanced control strategies therefore employ variable-speed air compressors to modulate stoichiometric gas supply, membrane humidifier systems with feedback control to prevent both desiccation and flooding, and integrated coolant loops maintaining stack temperature within the narrow 55–80°C operating window. Load cycling studies demonstrate that automotive duty cycles, with current density variations from 0–1.0 A cm^{-2}, produce localized electrochemical stress, leading to platinum particle formation in membranes and preferential catalyst layer thinning. [42–47]

Contemporary automotive PEMFC stacks achieve volumetric power densities of 3–4 kW L^{-1} and specific power densities of approximately 2 kW kg^{-1}, with system-level electrical efficiency accounting for auxiliary loads typically ranging from 40–50%—substantially superior to internal combustion engines and with zero tailpipe CO_2 or NO_x emissions [48,49]. Passenger vehicle stacks are designed for operational lifetimes exceeding 5,000–8,000 hours, while heavy-duty bus and truck systems target 10,000–25,000 hours aligned with commercial duty cycles, with Class 8 tractor-trailer targets reaching 30,000 hours corresponding to 1,200,000-mile service life [50]. Recent materials research has established that bipolar plate coatings—particularly titanium nitride (TiN) and zirconium nitride (ZrN)—minimize interfacial contact resistance while maintaining corrosion resistance, and optimized gas diffusion layer architectures with strategically positioned grooves enhance oxygen transport while facilitating water removal. [51–54]

Polymer seals and elastomeric gaskets represent particularly vulnerable stack components under automotive cycling, with temperature fluctuations from −20°C to +90°C inducing de-crosslinking and chain scission in elastomer backbones. Cyclic pressure variations accompanying transient vehicle operation accelerate seal degradation through loss of elastic recovery and leakage of seal constituents [55–57]. Current analyses indicate that light-duty and bus platforms approach compliance with established U.S. Department of Energy and Clean Hydrogen Joint Undertaking durability targets (5,000–7,000 hours for passenger vehicles with <10% degradation; 10,000–16,000 hours for buses with >90% availability), while heavy-duty applications remain below targets due to integration challenges and limited transparency in commercial specifications. [58–60]

1.1.4 Challenges and Limitations of using PEMFC in mobility

Despite technological maturity, several obstacles still limit broad PEMFC adoption in mobility:

- High system and hydrogen cost. Stack manufacture involves precious-metal catalysts (Pt, Ir), fluorinated membranes, and graphite or titanium bipolar plates. Automotive cost targets call for reductions below USD 100 kW^{-1}, compared with current USD 700–1000 kW^{-1} [7–9]. Hydrogen fuel itself remains at USD 5–7 kg^{-1} from renewable sources [10].
- Durability under dynamic load. Start-stop cycling, humidity variations, and fuel starvation accelerate membrane thinning, catalyst corrosion, and carbon-support oxidation [15,61]. Automotive applications demand > 5 000 cycles with < 10 % performance loss—still a challenge even with advanced catalysts.
- Infrastructure limitations. Hydrogen distribution and refueling networks lag EV charging infrastructure. Station costs (≈ USD 1–2 million each) and safety regulations hinder rapid scaling [4].

BUPT

• Efficiency and energy-pathway considerations. Well-to-wheel efficiency depends on the hydrogen source. If produced from renewable electrolysis, overall efficiency is 25–30 %; fossil-based hydrogen without carbon capture offers minimal climate advantage [62].

1.2 Importance of elastomeric gaskets in PEMFC operation

Within a PEMFC stack, each membrane–electrode assembly is surrounded by gaskets that ensure a gas-tight seal between bipolar plates and prevent mixing of hydrogen, oxygen and coolant [63]. These gaskets, typically made of rubber-like polymers, play a decisive role in maintaining electrical insulation and the necessary compressive load on the stack [63]. The operating environment inside a PEMFC is harsh: temperatures of 60–90°C, high relative humidity and exposure to mildly acidic condensates formed by membrane degradation and catalyst reactions [22]. Under such conditions, elastomeric gaskets must retain their mechanical integrity, resist chemical attack and minimize leakage to ensure long-term fuel-cell performance and safety. Poor sealing can lead to fuel crossover, reduced power output, contamination of electrochemical components and accelerated degradation of the entire stack. Consequently, the selection and design of gasket materials are critical for the commercialization and reliability of PEMFC systems.

In addition to the internal sealing elements, a complete PEMFC stack is integrated with several peripheral components that manage reactant distribution, humidification, heat exchange, and pressure control. These include manifolds, flow-field plates, humidifiers, heat exchangers, valves, hoses, and sensor fittings, all of which rely on elastomeric interfaces to maintain gas and liquid tightness under cyclic loading. Among these, components located on the cathodic side—where air is supplied to the fuel-cell stack—are particularly demanding, as they operate under continuous exposure to oxidizing conditions, moisture, and fluctuating pressure.

One of the most critical of these subsystems is the air-management assembly, which regulates the flow and pressure of the oxidant stream through an air valve (or throttle valve). This valve ensures optimal stoichiometry and load response of the fuel-cell stack while maintaining controlled humidity and temperature. The sealing elements designed for this air valve must therefore endure repeated dynamic compression, contact with humid and acidic air streams, and extended service times at moderate temperatures. The present research focuses on the design and evaluation of sustainable elastomeric sealing materials specifically intended for such air-valve applications on the cathodic side of PEMFC systems, where chemical stability, wear resistance, and elasticity directly influence system efficiency and lifetime.

1.3 Need to investigate sustainable sealing materials

Ethylene–propylene–diene monomer (EPDM) rubber is the most widely adopted material for fuel-cell sealing applications due to its excellent thermal stability, elastic recovery, and resistance to ozone, oxidation, and polar media [64]. However, the demanding environment within a proton-exchange-membrane fuel cell—characterized by temperatures of 60–90 °C, high relative humidity, and acidic condensates—can lead to oxidative chain scission, surface cracking, and leaching of

BUPT

ionic species from the polymer matrix. These degradation phenomena progressively weaken the mechanical integrity of gaskets and shorten stack service life [17,22].

In parallel, the environmental impact of conventional elastomer compounding—especially the use of virgin carbon black derived from fossil sources—has become an increasing concern. To mitigate this, "ECO" EPDM systems have been developed that incorporate circular carbon black (CCB) or recycled carbon black (RCB) recovered from end-of-life tires. Comparative analyses have shown that CCB-filled EPDM retains superior mechanical strength, hardness stability, and dimensional integrity during acid and thermal aging, whereas RCB-filled EPDM tends to absorb more fluid, exhibits greater surface erosion, and suffers faster loss of tensile properties under identical exposure conditions [22,23].

Beyond EPDM, thermoplastic vulcanizates (TPVs) and ECO-TPVs—hybrid materials comprising dynamically cross-linked EPDM dispersed in a thermoplastic matrix—are emerging as promising alternatives due to their potential for recyclability and easier processing [19,21]. TPVs exhibit better dimensional stability and faster manufacturing cycles compared to conventional rubbers, yet their thermal and chemical resistance under fuel-cell conditions remains less well understood. Tribological studies further indicate that TPVs show higher friction coefficients and wear rates than EPDM when in contact with engineering thermoplastics such as PA66GF30, suggesting the need for filler and cross-link optimization to achieve equivalent sealing endurance [21].

These findings collectively underscore the need for systematic investigation of sustainable sealing materials for PEMFC applications. Future gasket compounds must simultaneously satisfy mechanical durability, chemical inertness, and tribological stability while aligning with circular-economy principles. Developing eco-efficient elastomeric formulations that maintain long-term sealing performance without releasing harmful leachates is therefore essential for the commercial viability and environmental compatibility of next-generation PEM fuel-cell systems.

1.4 Structure of the thesis

The thesis has been structured into 6 chapters:

Chapter 1 presents the background and motivation of the chosen topic, emphasizing the strategic role of PEMFC systems in electric mobility and the critical importance of sealing components for the reliability and efficiency of these systems.

Chapter 2 deals with the state of the art in the field of PEMFC sealing technology, presenting theoretical aspects regarding operating environments, degradation mechanisms of elastomeric materials, and the sustainability challenges associated with current manufacturing processes. Moreover, an analysis of the tribological and chemical requirements for peripheral components is made. Main limitations of current commercial solutions are also discussed.

Chapter 3 outlines the scope and specific objectives of the doctoral research, defining the main directions of investigation regarding sustainable elastomeric materials.

Chapter 4 describes the methodology and equipment used to achieve the experimental study. This chapter offers an outline concerning the applied

BUPT

investigation methods and presents the specific experimental techniques, such as accelerated aging protocols, chemical analysis (HPLC, HWET), and tribological testing, utilized to evaluate the quality and performance of the proposed sealing materials.

Chapter 5 presents the experimental program concerning the mechanical, chemical, and tribological behavior of the investigated elastomers, the results obtained during this study, and highlights the most important aspects regarding the influence of filler type (circular vs. recycled) and aging conditions.

Chapter 6 points out the conclusions of this study and the personal contributions accomplished through this work, along with directions for future research.

BUPT

2 STATE-OF-THE-ART

2.1 Historical Background and Technological Development of Fuel Cells

The concept of converting chemical energy directly into electrical energy predates many other modern electrochemical systems. The first successful demonstration of a rudimentary fuel cell was reported more than 160 years ago by the Welsh scientist Sir William Grove, who in 1839 built a device capable of generating electric current through the electrochemical reaction between hydrogen and oxygen gases [65]. Although Grove's "gas battery" was rudimentary, it established the fundamental principle of the fuel cell: the continuous generation of electricity through redox reactions rather than combustion. This discovery laid the groundwork for later developments in electrochemistry and catalysis, forming a bridge between the study of galvanic cells and emerging interest in alternative energy conversion technologies.

Throughout the late 19th and early 20th centuries, incremental progress was made in the understanding of electrode materials and electrolytes, yet practical implementation was limited by technological constraints. Fuel-cell efficiency, component degradation, and the lack of suitable membranes prevented early prototypes from achieving sustained operation. It was not until the mid-20th century that significant advancements took place. The pioneering work of Francis Thomas Bacon in the 1950s resulted in the first practical alkaline fuel cell (AFC), capable of delivering stable power output over extended durations [66]. The robust performance of these AFCs led to their adoption in NASA's Gemini and Apollo space missions, where they supplied both electrical energy and potable water. This period marked the transformation of fuel cells from laboratory curiosities to mission-critical power sources under extreme conditions.

The 1960s introduced a new class of fuel cells utilizing solid polymer electrolytes instead of alkaline or phosphoric acid systems. Researchers at General Electric, notably Willard Grubb and Leonard Niedrach, developed the first proton exchange membrane fuel cell (PEMFC) using a sulfonated polystyrene membrane, which later evolved into the perfluorosulfonic acid (PFSA) membranes commercialized as Nafion® [67,68]. These early PEMFCs were used in U.S. Navy programs and as auxiliary power sources for the Gemini spacecraft, demonstrating their high specific power and reliability in compact designs. Their success in spaceflight validated the concept of polymer electrolyte membranes and paved the way for terrestrial adaptation.

Despite these early breakthroughs, the subsequent two decades saw relatively slow progress in PEMFC development, primarily due to cost, durability, and material limitations. Precious-metal catalysts, notably platinum, dominated electrode design, leading to high manufacturing costs. Furthermore, membrane and sealing degradation under humid and acidic conditions limited system lifetime. Only in the 1990s did a major revival occur, driven by mounting environmental concerns and the quest for cleaner energy technologies. Rapid progress in polymer science, membrane chemistry, and catalyst engineering rejuvenated fuel-cell research. DuPont's introduction of chemically stable Nafion® membranes, with improved proton conductivity and oxidative resistance, revolutionized the performance of PEMFCs [68].

Parallel developments in electrode microstructure, bipolar-plate materials, and gas-diffusion layers improved water management and minimized mass-transport losses. Fuel-cell systems transitioned from laboratory test rigs to fully engineered

BUPT

power units, enabling applications beyond aerospace, particularly in automotive, stationary, and portable power sectors. During this period, automotive manufacturers such as Toyota, Honda, and Hyundai launched major R&D programs to develop fuel-cell electric vehicles (FCEVs), culminating in the introduction of commercial prototypes such as the Toyota Mirai and Honda Clarity Fuel Cell. These vehicles validated PEMFCs as a credible technology for zero-emission transportation, leveraging their high power density, fast start-up, and silent operation compared to internal combustion engines [69,70].

In parallel, PEMFC systems began to penetrate stationary energy applications, providing backup and distributed power generation for telecommunications, data centers, and hospitals. Industrial players such as Ballard Power Systems, Plug Power, and Siemens developed scalable PEMFC modules capable of delivering kilowatt- to megawatt-scale outputs. Combined heat and power (CHP) systems utilizing PEMFCs achieved overall efficiencies above 80 %, supporting both residential and industrial energy demands [4,71].

More recently, fuel-cell technology has advanced through improvements in stack architecture, system control, and material optimization. Current PEMFCs exhibit power densities exceeding 1 W cm^{-2}, start-up times below 60 seconds, and operational lifetimes surpassing 20,000 hours for automotive applications [32]. Ongoing research focuses on reducing platinum loading to below 0.1 mg cm^{-2}, enhancing membrane durability, and minimizing cost through manufacturing automation.

Despite these remarkable achievements, several technical and economic barriers persist. The cost of platinum-group catalysts, membrane degradation, peripheral component reliability, and the sustainability of polymeric materials remain major challenges for large-scale commercialization. This last issue is particularly critical for balance-of-plant components such as gaskets, valves, and seals—often made from elastomeric materials like EPDM, which are essential to maintaining gas-tight interfaces and mechanical stability within PEMFC stacks. As PEMFC technology moves toward wider industrial adoption, improving the chemical durability and sustainability of sealing materials has become a major research frontier.

In this context, the following sections of this chapter review the architectural features of PEMFC systems, the operational environment affecting polymeric components, and the state of knowledge regarding elastomeric materials—particularly EPDM and its sustainable variants—used in sealing and peripheral applications.

2.2 PEMFC Architecture and Operating Environment

A proton exchange membrane fuel cell (PEMFC) converts the chemical energy of hydrogen directly into electrical energy through electrochemical oxidation–reduction reactions, producing only water and heat as by-products. Its core unit—the membrane-electrode assembly (MEA)—is the locus of these reactions and defines the overall efficiency, durability, and power density of the system. A schematic representation of a single PEMFC cell is shown in Figure 2.1. illustrating the principal components and transport phenomena.

BUPT

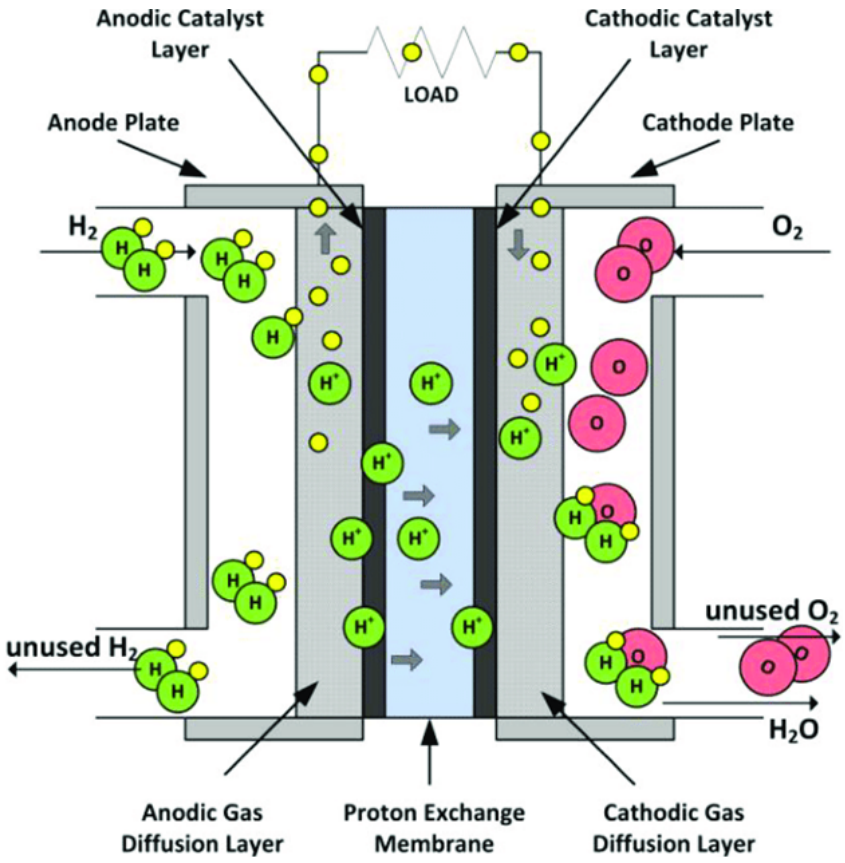


Figure 2.1. Schematic representation of a PEMFC [17]

The fundamental operation of a PEMFC entails a sequence of electrochemical operations that transform hydrogen fuel into electrical energy. The process commences with hydrogen gas being delivered to the anode (negative electrode). At the anode, hydrogen molecules (H_2) are catalytically dissociated into protons (H^+) and electrons (e^-) via a platinum-based catalyst, as in equation 1.

$$\boldsymbol{H_2 \rightarrow 2H^+ + 2e^-} \tag{1}$$

The proton exchange membrane, an essential component of fuel cells, permits only protons to traverse to the cathode (positive electrode). Simultaneously, the electrons traverse an external circuit, producing an electric current capable of powering electrical equipment.

At the cathode, oxygen is generally obtained from the environment, along with protons that have permeated the membrane and electrons that have traveled through the external circuit. This leads to the production of water (H_2O) and the

BUPT

emission of heat as byproducts of the electrochemical reaction. The comprehensive chemical equation for the reaction is:

$$H_2 + \frac{1}{2}O_2 \rightarrow H_2O + \text{heat} \quad (2)$$

This electrochemical mechanism enables PEMFCs to directly transform chemical energy into electrical energy without burning, yielding higher efficiencies, frequently above 60%, in contrast to the standard 20-30% efficiency of conventional internal combustion engines. The great efficiency and absence of hazardous pollutants, aside from water, render PEMFCs a compelling option for stationary and automotive energy applications. [72,73]

The theoretical open-circuit voltage (OCV) under standard conditions is 1.229 V, but practical cell voltages range between 0.6 and 0.8 V due to activation, ohmic, and mass-transport losses [74]. Figure 2.2 depicts the polarization curve showing the distinct loss regions.

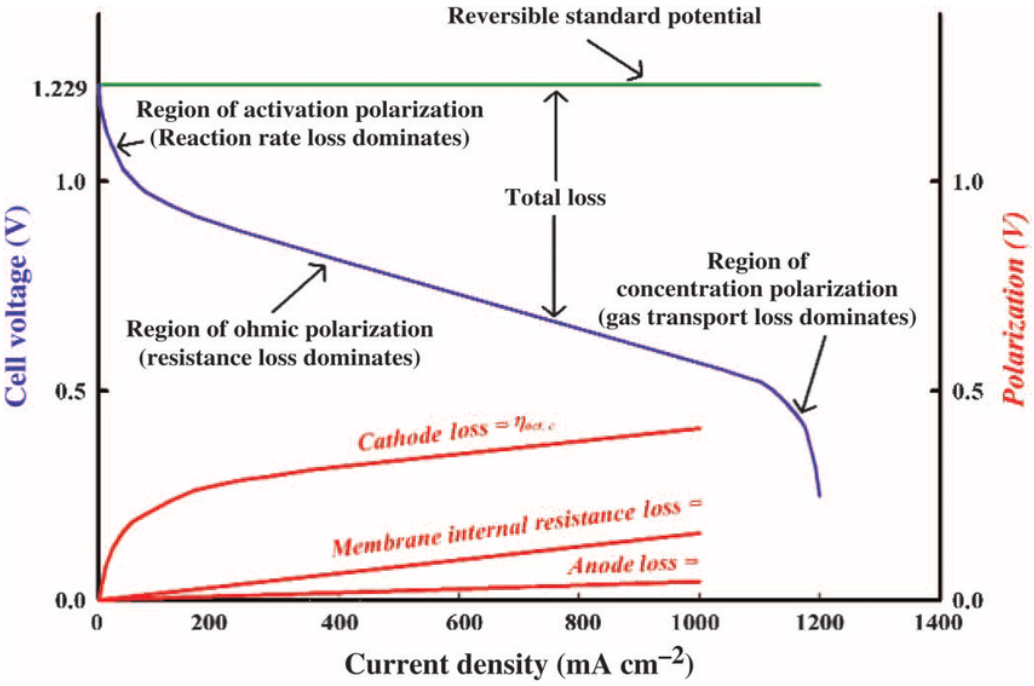


Figure 2.2. Polarization Curve of PEMFC, from [74]

Water and heat management are central to PEMFC operation. The membrane must remain hydrated to sustain proton conductivity (> 0.1 S cm^{-1}), yet excess water may flood the GDLs, hindering oxygen diffusion. Temperature control within 60–90 °C maintains optimum kinetics and mechanical stability; higher temperatures accelerate degradation of the membrane and peripheral seals, whereas lower temperatures promote condensation and liquid-water accumulation [75–77].

BUPT

2.3 Operating Conditions and Environmental Stressors

The internal operating environment of a PEMFC is defined by a combination of thermal, mechanical, and chemical stressors that arise intrinsically from the electrochemical reactions and the system-level requirements of high-efficiency operation.

Temperature within the stack typically ranges between 60–90 °C, a range selected to optimize proton conductivity, electrochemical kinetics, and water management. Several mechanisms contribute to heat generation. The cathodic oxygen reduction reaction (ORR) is strongly exothermic, releasing a considerable fraction of the reaction enthalpy as heat even under load. The fundamental electrochemical steps, expressed in Equations (1) and (2), illustrate the exothermic nature of water formation.

Because practical cell voltages (0.6–0.8 V) are significantly lower than the theoretical reversible voltage (1.229 V), 40–50% of the reaction enthalpy is released as thermal energy within the MEA [72]. Additional heating occurs through ohmic resistance in the membrane and electrodes, as well as from the compression of cathodic air. In automotive systems, air is commonly supplied at pressures of 2–3 bar using turbo-compressors, which raise the inlet temperature according to the isentropic relation

$$\boldsymbol{T_2 = T_1 * (P_2/P_1)^{(\gamma-1)/\gamma}} \quad (3)$$

, producing air streams that may temporarily exceed 100 °C before reaching thermal equilibrium [78]. These combined thermal loads accelerate polymer oxidation, chain scission, and cross-link rearrangements in elastomers such as EPDM, making the thermal environment one of the primary initiators of material degradation within PEMFCs [79].

Humidity plays an equally central role in defining the internal conditions of a PEMFC. Proton exchange membranes, typically composed of perfluorosulfonic acid (PFSA) polymers such as Nafion®, require a high degree of hydration to sustain proton conductivity. Conductivity decreases sharply when the membrane hydration level falls below approximately 10–12 water molecules per sulfonic acid group [80], making high relative humidity, often approaching 100% RH near the membrane, essential for proper operation. Water produced at the cathode during the ORR contributes to this saturation, creating a wet environment that varies spatially within the MEA. Water transport occurs through a combination of electro-osmotic drag (from anode to cathode), back-diffusion (from cathode to anode), and evaporation–condensation cycles. During dynamic load changes, characteristic of mobility applications, rapid shifts in gas flow and temperature induce hydration cycling, subjecting polymeric sealing materials to repeated swelling and deswelling. These fluctuations impose volumetric strain and can initiate microcracking, softening, and surface degradation in elastomers exposed to the cathodic air channels [64,81].

Pressure is another fundamental parameter governing PEMFC performance and internal stresses. Cathode pressures of 2–3 bar are commonly used to increase oxygen partial pressure, thereby enhancing oxygen reduction kinetics and delaying mass-transport limitations at high current densities [82]. Simultaneously, the PEMFC stack is assembled under substantial compressive loads—typically 1–2 MPa—to

BUPT

ensure uniform contact between MEA layers and the adjacent gaskets. The operational pressure environment, however, is highly dynamic. Start–stop cycles, rapid load changes, and fluctuations in compressor output result in continuous variations in gas pressure across the stack. Such cyclic pressures impose repeated compressive deformation on gaskets, O-rings, valve seals, and other elastomeric components, promoting compression set, stress relaxation, and fatigue microcracking. These degradation processes are well documented in EPDM-based sealing systems used in PEMFC technology [55,83].

In addition to thermal and mechanical effects, the **chemical environment** within PEMFCs is intrinsically acidic and oxidative. PFSA membranes release sulfonic acid groups ($-SO_3H$) into condensed water, producing localized pH levels as low as 2–4 during operation [15]. Furthermore, under certain conditions the ORR follows a two-electron pathway, generating hydrogen peroxide (H_2O_2):

$$\boldsymbol{O_2 + 2H^+ + 2e^- \rightarrow H_2O_2} \tag{4}$$

Hydrogen peroxide can diffuse within the MEA and participate in subsequent reactions. In the presence of trace metal ions, originating from stainless steel corrosion or contaminants introduced during system operation, H_2O_2 undergoes Fenton-type reactions that produce highly reactive hydroxyl radicals:

$$\boldsymbol{H_2O_2 + Fe^{2+} \rightarrow OH^- + OH\cdot + Fe^{3+}} \tag{5}$$

These radicals are known to cause membrane thinning, catalyst degradation, and severe chemical attack on elastomeric materials.

In real operation, PEMFC components are rarely exposed to these stressors in isolation. Instead, degradation is driven by their synergistic interaction. Elevated temperature accelerates chemical reaction rates; humidity enhances hydrolytic and ionic processes; acidic water promotes leaching and cross-link breakdown; and pressure fluctuations amplify mechanical fatigue.

This complex environment is particularly severe on the cathodic air side, where hot, humidified, oxygen-rich air interacts continuously with elastomeric sealing interfaces. For this reason, the performance and durability of EPDM and related elastomeric materials under coupled thermal-humid-acidic-mechanical stress conditions represent a critical research area for improving PEMFC reliability. These considerations strongly motivate the experimental work presented in later chapters of this thesis, which focus on the mechanical, chemical, and tribological behavior of sustainable EPDM formulations under PEMFC-relevant conditions.

2.4 Balance-of-Plant and Peripheral Components in PEMFC Systems

While the membrane–electrode assembly (MEA) defines the intrinsic electrochemical performance of a PEM fuel cell, a complete system incorporates a broad set of auxiliary subsystems, collectively referred to as the Balance-of-Plant (BoP). These subsystems manage reactant supply, thermal regulation, water distribution, electrical control, and safety. Their coordinated operation enables the fuel cell stack to function under the highly dynamic load profiles typical of automotive

BUPT

applications. As noted by Barbir [72] and Larminie & Dicks [84], BoP components are essential for transforming the MEA from a laboratory-scale electrochemical device into a robust powertrain capable of meeting automotive response rates, efficiency requirements, and lifetime expectations.

A modern PEMFC BoP typically includes the air-supply assembly (compressor, turbine or expander, air-flux control valve, humidifier, intercooler), the hydrogen subsystem (injection valve, recirculation blower or ejector, purge valves, pressure regulators), thermal management (coolant pumps, radiators, heat exchangers), water handling (humidifiers, separators, drains), and sensor–actuator networks governed by an electronic control unit (ECU). Several studies, including recent industrial assessments by Toyota and Hyundai, show that BoP hardware may represent 40–60% of total system mass and cost, and frequently dictates the overall reliability of the PEMFC system [85,86].

In automotive PEMFC powertrains, such as the Hyundai Nexo system illustrated in Figure 2.3, the Balance-of-Plant (BoP) plays a decisive role in enabling the stack to operate under real-world transient conditions. While the fuel cell stack provides the electrochemical core, the integrated power module is built around three major BoP subsystems: the fuel (H_2) processing system, the air processing system, and the thermal management system [87]. The hydrogen processing subsystem ensures controlled delivery, recirculation, and purging of hydrogen through injectors, recirculation blowers/ejectors, and pressure regulation devices, maintaining stable anode stoichiometry even under rapid load changes. The air processing subsystem, comprising the compressor, humidifier, air-flux control valve, and related ducting, conditions the incoming air to appropriate pressure, temperature, and humidity before feeding the cathode. This subsystem is particularly critical in FCEVs because air supply must track power demand instantaneously while preventing membrane dehydration, oxygen starvation, or excessive flooding.

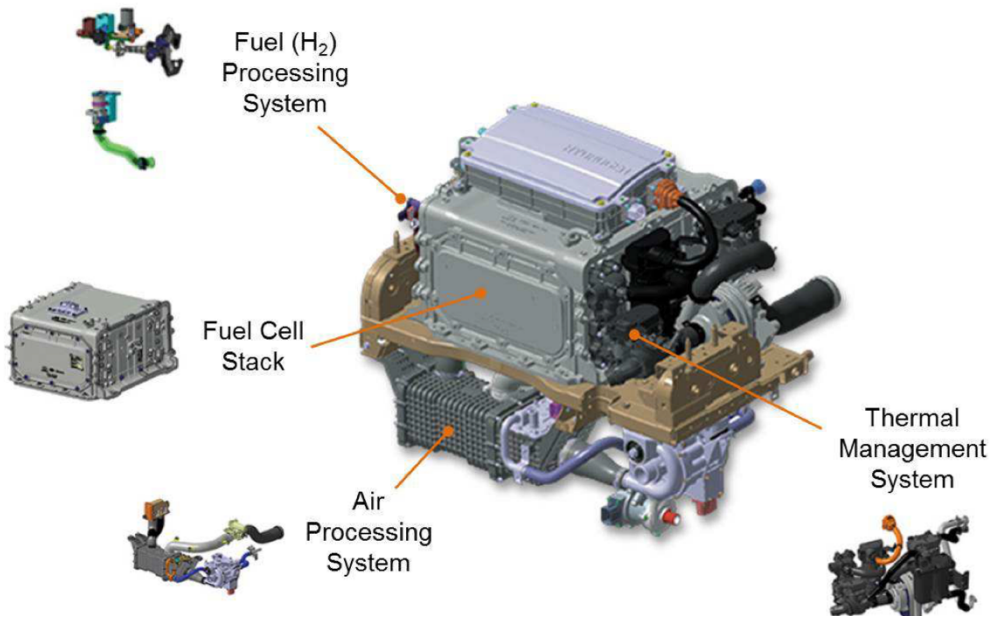


Figure 2.3. Typical PEMFC powertrain, taken from [87]

BUPT

The thermal management system provides precise heat removal from both the stack and the BoP components, maintaining membrane hydration and preventing thermal excursions that accelerate chemical degradation of catalysts, membranes, and elastomeric seals. Hyundai's Nexo platform integrates these BoP subsystems tightly with the stack to achieve substantial improvements over its previous ix35 generation, raising system efficiency from 55% to 60%, extending driving range from 415 km to 609 km, and nearly doubling durability from 80,000 km to 160,000 km, achievements explicitly attributed not only to improved stack design but also to advancements in BoP architecture, controls, and component materials [87]. As emphasized in the original study, the BoP is not a peripheral addition to the stack but a core performance-defining subsystem, responsible for reactant management, water balance, freeze-start capability, and robust operation under dynamic driving cycles. Its components, many of which rely on elastomeric interfaces, are therefore central to system reliability and constitute a major engineering focus for next-generation PEMFC vehicles.

2.4.1 Air flux level control valve in PEMFC Systems

Many BoP components incorporate polymeric housings, elastomeric gaskets, O-rings, and dynamic sealing elements, making them especially sensitive to the thermo-hygro-chemical environment of the cathode side. The air-management subsystem is particularly demanding. As highlighted by Zhao et al. [88], this subsystem operates with compressed air at temperatures often exceeding 80–120 °C after compression, near-saturated humidity, and high oxygen partial pressures, conditions known to accelerate oxidative and hydrolytic degradation of elastomeric materials used for sealing. The presence of trace acidic condensates, originating from membrane decomposition and water management processes, further increases chemical aggressiveness, as shown in material aging studies by Pehlivan-Davis [81] and Kimura et al. [89].

Peripheral components, although not directly part of the MEA, frequently experience stress conditions comparable to or more severe than those inside the membrane environment. Misoperation or degradation of BoP subsystems can propagate rapidly to the fuel cell stack, causing effects such as oxygen starvation, membrane dehydration or flooding, thermal imbalance, or loss of sealing integrity leading to gas crossover. For example, instabilities in the air-supply pathway may induce oscillations in cathode pressure, which deepen membrane hydration fluctuations and accelerate mechanical fatigue of seals and gaskets [80]. Consequently, the durability of elastomeric components within BoP actuators has become a recognized bottleneck for PEMFC system lifetime, as noted in recent assessments from the Hydrogen Council and the IEA [4,32].

BUPT

Within this context, the air flux level control valve represents a particularly critical peripheral component.



Figure 2.4. Air Valve for PEMFC systems, made by [90]

The cathodic air control valve, often referred to as the stack control valve, is a central actuator within the air-processing subsystem of PEMFC BoP architecture, responsible for precisely metering the compressed air delivered to the cathode and maintaining the required oxygen stoichiometry, cathode pressure, and dynamic load response. During operation, the valve must rapidly adjust its opening angle—often within <120 ms—to match airflow with the instantaneous current demand of the stack, while simultaneously stabilizing backpressure to support membrane hydration and effective water management. Many modern designs, including those used in automotive PEMFC systems, perform dual functions by acting as both a flow-control device during operation and an isolation valve during shutdown, preventing uncontrolled air ingress that could accelerate catalyst corrosion or membrane oxidative degradation. Internally, the valve operates in a highly aggressive environment characterized by temperatures ranging from −40 °C to 120 °C after compression, high oxygen concentration, near-saturated humidity, and exposure to acidic condensates formed within the cathode supply line. These conditions impose severe demands on the elastomeric sealing elements, which must maintain extremely low leakage rates—on the order of 0.5 mL min^{-1} at typical automotive pressure

BUPT

differentials—while enduring millions of sliding and compressive cycles against polymeric housings and glass-fiber reinforced components. As such, the cathodic air control valve constitutes one of the most demanding BoP components for sealing materials, directly linking elastomer durability to overall system efficiency, stability, and lifetime in PEMFC applications. [90]

Although the sealing elements inside this valve account for only a small fraction of system mass and cost, their degradation can lead to increased leakage, reduced metering accuracy, higher parasitic loads (through frictional resistance), and ultimately stack malfunction. Because the valve operates at the interface of hot compressed air, variable humidity, condensed acidic droplets, and sliding tribological contacts, the selection and formulation of sealing materials must satisfy exceptional durability requirements.

For these reasons, a detailed understanding of the operating environment and stressors described in the next sections of the thesis is essential for evaluating the performance of EPDM, TPV, and sustainable ECO-EPDM compounds in air-management components. This provides the foundation for subsequent chapters addressing the mechanical, chemical, and tribological behavior of these materials under PEMFC-relevant conditions.

2.5 Sealing Concepts, Mechanisms, and Requirements in PEMFC Systems

2.5.1 Overview of Sealing Types in Engineering Systems

Sealing technologies form a foundational part of fluid-handling systems, enabling the containment of gases or liquids and the maintenance of pressure differentials across interfaces. In engineering practice, seals are commonly classified according to their operating mode and loading direction. The primary distinction is between static seals, used between stationary components, and dynamic seals, which accommodate relative motion such as reciprocating, oscillating, or rotary movement.

Static seals, typically O-rings, flat gaskets, and compression sheets, derive their performance from enforced elastic deformation and surface conformity and are governed by established principles in polymer contact mechanics [91,92].

Dynamic seals, including rotary lip seals and reciprocating shaft seals, must withstand not only compressive loading but also frictional heating, abrasion, and shear forces, making material selection and lubrication critical [93]. Figure 2.5 illustrates both type of rubber seals in a piston application.

A second classification concerns the direction of applied preload: axial seals operate under compression normal to the sealing plane, while radial seals rely on interference or compression along a cylindrical direction, as in O-rings or gasketed housings [94]. In addition, sealing systems may be designed as either dry or lubricated interfaces; lubricated seals reduce wear in high-speed dynamic applications, whereas dry seals are preferred when contamination or volatilization is unacceptable, as is the case in PEMFC systems [72,95].

A fundamental criterion for sealing performance is the ability of the compressed elastomer to generate a contact stress that exceeds the internal fluid pressure. For a seal compressed with a force F_c over an effective contact area A, the average interfacial stress can be expressed as:

$$\sigma_c = F_c/A \tag{6}$$

BUPT

For the seal to remain leak-free, the classical inequality defined in sealing theory must be satisfied [91]:

$$\sigma_c \geq P_m \tag{7}$$

where
$\boldsymbol{\sigma_c}$ = contact stress (Pa),
$\boldsymbol{P_m}$ = internal medium pressure (Pa).

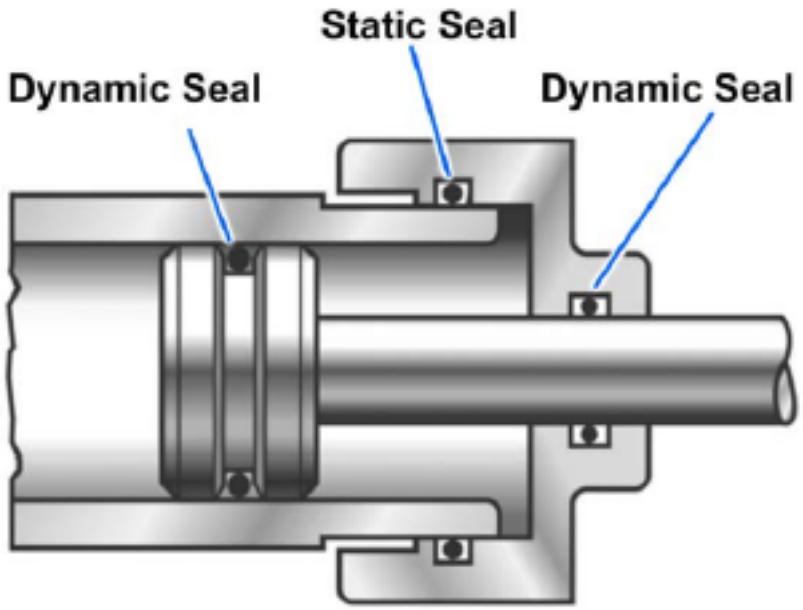


Figure 2.5. Exemplification of Dynamic and Static Sealing [93]

Because most sealing interfaces exhibit roughness at the micro- and nanoscales, the elastomer must deform sufficiently to penetrate surface asperities. Under an imposed displacement $\boldsymbol{\Delta h}$, the sealing force follows a simple stiffness relationship:

$$F_c = k_e * \Delta h \tag{8}$$

where
$\boldsymbol{k_e}$ = effective stiffness of the elastomer, dependent on its elastic modulus, crosslink density, and filler morphology.

For toroidal or O-ring seals, classical Hertzian contact theory approximates the peak contact pressure as [96]:

$$p_0 = (2 * F_c)/(\pi * b * L) \tag{9}$$

BUPT

where
b = contact half-width (m),
L = length of the sealing interface (m).

This localized high-pressure region acts to "close" leakage pathways. When the sealed medium exerts internal pressure, the seal may experience self-energization, meaning the effective sealing stress increases as the medium pressure acts on the elastomer profile:

$$\sigma_{\text{eff}} = \sigma_c + \alpha * P_m \tag{10}$$

where $0 < \boldsymbol{\alpha} < 1$ accounts for geometric pressure transmission [97].

These relationships illustrate that sealing performance depends on the interplay between externally applied compression, elastomeric stiffness, contact mechanics, and the pressure of the sealed fluid. They form the theoretical foundation for understanding static and dynamic sealing in more complex environments such as PEMFC systems.

2.5.2 General Principles of Elastomeric Sealing

The fundamental purpose of a seal is to prevent fluid leakage by creating a barrier that interrupts potential flow paths across an interface. Even highly machined surfaces exhibit microscopic asperities that form leakage channels; elastomeric materials, by virtue of their high compliance, deform under compression to fill these voids and establish a contiguous sealing contact. In classical sealing theory, the seal must generate a contact stress exceeding the internal medium pressure, ensuring that no interfacial gap opens under operating conditions [91,98]. This requirement is central in gas sealing, where low viscosity and high diffusivity make leakage more sensitive to surface topology.

Elastomers provide exceptional sealing performance due to their combination of elastic deformation and viscoelastic damping. Upon compression, elastomers flow laterally and penetrate surface valleys, increasing the real contact area well beyond what rigid materials can achieve [99]. Under fluid pressure, the elastomer may undergo additional deformation, sometimes described as *self-energizing*, which enhances sealing at higher pressures, especially for O-ring geometries [97]. However, elastomeric materials also exhibit time-dependent behaviors. Stress relaxation reduces contact stress under constant strain, while compression set represents the permanent deformation after long-term loading; both mechanisms degrade sealing effectiveness and are strongly accelerated at elevated temperatures and high humidity [100,101].

The mechanics of sealing are governed by the interaction between elastomer properties and surface roughness. According to Greenwood–Williamson and Persson contact models, sealing performance depends on achieving sufficient real contact area across a multiscale roughness profile [96,102]. In dynamic seals, frictional forces generate heat that contributes to viscoelastic softening, wear, and potential leakage. Tribological considerations—friction coefficient, abrasion resistance, and counterface roughness—are central to the performance of dynamic sealing elements such as those in PEMFC air valves [21,103].

BUPT

Sealing reliability is influenced not only by interfacial mechanics but also by bulk permeation through the elastomer. Gas transport follows solution–diffusion mechanisms described by Fick's law, and permeability increases with temperature and decreases with filler loading or crosslink density [104].

Gas permeation in elastomeric sealing materials does not occur solely through interfacial leakage but also through the bulk of the polymer, following the classical solution–diffusion mechanism characteristic of gases in rubbery materials. In this process, gas molecules first dissolve into the elastomer at the high-pressure surface, diffuse through the polymer network, and then desorb at the low-pressure surface. The driving force for this transport is the concentration gradient across the material thickness, and the resulting flux is governed by Fick's law of diffusion, first formulated for molecular transport in solids [104]. According to Fick's First Law, the steady-state diffusive flux J ($mol \cdot m^{-2} \cdot s^{-1}$) is proportional to the concentration gradient ($\boldsymbol{dC/dx}$) across the material thickness, such that:

$$J = -D * (dC/dx) \tag{11}$$

where D is the diffusion coefficient, a temperature-dependent parameter reflecting the mobility of gas molecules within the polymer matrix. For a uniform elastomeric seal of thickness L, this relationship simplifies to a linear dependence between flux and concentration difference. Because the concentration of a gas dissolved in an elastomer is itself proportional to the partial pressure of the gas—following Henry's law—gas transport can also be described in terms of a pressure gradient. Substituting the solubility relation $C = S * P$ into Fick's expression yields the classical permeation equation, where the effective permeability coefficient

$$P_{perm} = D * S \tag{12}$$

incorporates both diffusion and solubility effects:

$$J = P_{perm} * (P_1 - P_2)/L \tag{13}$$

This relationship demonstrates that permeation increases with the pressure differential across the seal and decreases with increasing seal thickness. More critically, both diffusion and solubility coefficients rise with temperature, often following an Arrhenius-type dependence, meaning permeation becomes increasingly significant under the elevated thermal conditions typical of PEMFC operation. Filler loading and crosslink density also strongly influence permeation: carbon black, silica, and other reinforcing fillers create more tortuous diffusion pathways and reduce molecular mobility, while higher crosslink density restricts chain segment motion, thereby lowering both D and S [97,104].

In PEMFC systems, where sealing materials operate at temperatures of 60–120 °C, under high humidity and continuous pressure cycling, permeation is non-negligible. Hydrogen, oxygen, and water vapor can diffuse through elastomeric components even when interfacial sealing is intact, contributing to gradual pressure equalization, changes in local humidity, and long-term degradation of the polymer network. These diffusion processes, combined with chemical and mechanical aging, form a crucial part of the sealing-performance landscape in fuel cell stacks and

BUPT

balance-of-plant actuators. Understanding and accurately modeling Fickian permeation is therefore essential for predicting lifetime, selecting appropriate elastomer formulations, and designing seals capable of meeting the severe operating requirements of modern PEMFC systems.

2.5.3 Mechanisms and Failure Modes of Elastomeric Sealing

Elastomeric seals function by generating and maintaining a compressive contact stress that exceeds the internal system pressure, ensuring that microscopic surface asperities are bridged and leakage paths eliminated. Over time, however, elastomers experience mechanical, viscoelastic, and chemical changes that progressively reduce their ability to sustain this contact stress. In PEMFC environments, where temperatures of 60–90 °C, near-saturated humidity, oxidative species, and pressure cycling are prevalent—multiple degradation mechanisms interact to undermine sealing reliability. These mechanisms can be categorized into viscoelastic relaxation, mechanical fatigue and wear, and chemical/environmental degradation, all of which are strongly temperature dependent and accelerated under fuel-cell operating conditions. [105–107]

A major source of sealing failure is **stress relaxation**, the time-dependent decay of internal stress under constant strain. For an elastomer compressed by an imposed deformation $\boldsymbol{\Delta h}$, the initial sealing stress $\boldsymbol{\sigma_0}$ decays exponentially according to viscoelastic constitutive behavior:

$$\sigma(t) = \sigma_0 * exp(-t/\tau) \tag{14}$$

where

t = relaxation time constant, dependent on temperature, crosslink density, and chemical environment.

At 80 °C, EPDM typically exhibits a 25–40% loss of sealing stress over 100–300 hours, whereas at 23 °C the same loss may require several months [97]. Such mechanical softening directly reduces the ability of the seal to maintain interfacial pressure.

Closely related is **compression set**, the irreversible deformation remaining after compressive load removal. It quantifies permanent molecular rearrangement and filler–matrix debonding, both of which diminish the seal's ability to recover and sustain contact:

$$CS(\%) = [(h_0 - h_r)/(h_0 - h_s)] * 100 \tag{15}$$

where

$\boldsymbol{h_0}$ = original thickness,

$\boldsymbol{h_s}$ = thickness under compression,

$\boldsymbol{h_r}$ = recovered thickness after decompression.

Recent studies report that EPDM and peroxide-cured elastomers can exhibit compression-set increases of 30–50% after only 500–1.000 h at 100–125 °C, driven by thermal rearrangement of the polymer network and relaxation of crosslinks under sustained load [108,109]. Similar research shows that the incorporation of recycled

BUPT

or low-structure carbon blacks tends to increase compression set by 20–35%, as weaker filler–matrix interactions promote permanent deformation and diminish elastic recovery under fuel-cell-relevant humidity and temperature conditions [110,111].

Dynamic sealing applications, such as the cathodic air valve in automotive PEMFC systems, also involve **tribological degradation**. Repeated sliding against polymeric or glass-fiber-reinforced counterfaces causes abrasion, micro-cutting, and surface fatigue. The wear volume V under sliding contact can be approximated using Archard's law:

$$V = (k * F_n * s) / H \tag{16}$$

where
$\boldsymbol{k}$ = dimensionless wear coefficient,
$\boldsymbol{F_n}$ = normal force,
$\boldsymbol{s}$ = sliding distance,
$\boldsymbol{H}$ = hardness of the elastomer.

Mechanical motion also contributes to frictional heating, which accelerates both oxidative and thermo-mechanical degradation. The local temperature rise can be estimated by:

$$\Delta T \approx (\mu * F_n * v)/(\rho * c_p * A_{contact}) \tag{17}$$

where
$\boldsymbol{\mu}$ = friction coefficient,
$\boldsymbol{v}$ = sliding velocity,
$\boldsymbol{\rho}$ and $\boldsymbol{c_p}$ = density and heat capacity, respectively.

Chemical and environmental degradation is another dominant failure pathway. In PEMFC systems, elastomers are exposed to reactive oxygen species (ROS) such as hydrogen peroxide (H_2O_2), superoxide ($\boldsymbol{O_2^{-\bullet}}$), and hydroxyl radicals ($\bullet OH$), all produced by incomplete oxygen reduction at the cathode. These species induce chain scission, crosslink modification, and surface oxidation:

$$-\boldsymbol{C}-\boldsymbol{C}- + \bullet \boldsymbol{OH} \rightarrow -\boldsymbol{C}\bullet + -\boldsymbol{C}-\boldsymbol{OH}(\boldsymbol{chainscission}) \tag{18}$$

Oxidative attack is strongly accelerated under high humidity and elevated temperature.

Finally, **permeation-induced damage** occurs when gases diffuse into the elastomeric network following Fickian transport (Equation 13). Under long-term pressure cycling, permeated gases expand and contract, producing internal mechanical stresses that contribute to micro-cracking and swelling.

Gas transport through EPDM, for example, follows the classical solution–diffusion mechanism, where permeability P increases exponentially with temperature according to Arrhenius behavior. Typical hydrogen permeabilities for EPDM lie in the range of 10^{-8} to 10^{-7} mol·m^{-1}·s^{-1}·Pa^{-1} between 25 and 80 °C, consistent with values reported for non-polar elastomers [104,112]. Carbon-black-filled EPDM formulations generally exhibit lower permeability (by 20–40%) due to the formation of tortuous diffusion paths that restrict molecular transport [113]. Although specific permeation

BUPT

data for PEMFC-grade EPDM are limited, these trends remain valid for the sealing materials used at the cathode side of PEMFC systems.

These degradation processes rarely occur in isolation. Mechanical wear exposes fresh surfaces to chemical attack; oxidative degradation reduces modulus and accelerates stress relaxation; swelling from permeation lowers hardness and increases friction. The synergistic coupling of mechanical, tribological, and chemical aging ultimately determines sealing lifetime, especially in PEMFC BoP components subjected to millions of actuation cycles.

Understanding these interacting mechanisms is therefore critical to the design of robust sealing materials and forms the scientific foundation of the experimental investigations presented in later chapters.

2.5.4 Sealing Demands in PEMFC Balance-of-Plant Components and in the Cathodic Air Control Valve

Sealing requirements extend beyond the fuel cell stack itself and into the BoP, where numerous components operate under conditions markedly different from the largely static compression of MEA perimeter gaskets. BoP devices, including air compressors, humidifiers, hydrogen recirculation valves, purge valves, and flow-control actuators, experience rapidly fluctuating pressures, humidity, and temperatures, often cycling between ambient conditions and 120–150 °C in the compressed air pathway [112,114]. These gradients generate swelling–deswelling stresses in elastomers and accelerate viscoelastic processes such as stress relaxation and creep. Acidic condensates formed from membrane degradation (pH 3–5) and oxygen-rich environments further promote oxidative aging in polymeric seals, emphasizing the need for materials with strong resistance to hydrolysis, radical-driven chain scission, and changes in mechanical stiffness under long-term exposure [64].

Among BoP components, the cathodic air control valve represents one of the most demanding sealing applications. Unlike static MEA gaskets, this actuator incorporates a dynamic sealing interface, typically involving the sliding rotation of a throttling plate against a polymeric housing made from materials such as PA66GF composites. Dynamic seals are exposed to abrasive and adhesive wear, micro-cutting by protruding glass fibers, and fretting damage caused by repeated small-amplitude oscillatory motion, phenomena well documented in polymer–polymer and polymer–composite contacts [115]. In such interfaces, local flash temperatures can rise 10–20 °C above the bulk temperature, promoting thermo-oxidative degradation and surface embrittlement of the elastomer. This tribo-thermal environment also elevates friction coefficients and accelerates surface fatigue, demanding sealing materials with low wear coefficients, stable modulus, and resistance to friction-induced aging.

In addition to wear and thermo-chemical stresses, the cathodic air valve must maintain very low leakage rates to ensure accurate oxygen stoichiometry and stable stack backpressure. Leakage tolerances in automotive PEMFC control valves often fall below 1 $mL \cdot min^{-1}$ at 50–100 kPa differential pressure, requiring seals that preserve intimate contact despite prolonged cyclic loading and changing thermal conditions [29,112]. Because oxygen-rich and humid conditions promote the formation of reactive oxygen species (ROS), elastomers in the valve are vulnerable to radical-mediated oxidation, chain scission, and filler–matrix debonding, all of which reduce

BUPT

elasticity and sealing stress over time [16]. Moreover, dynamic actuation results in fluctuating compression loads that amplify compression set and stress relaxation, compromising long-term sealing force. These combined tribological, chemical, and mechanical stressors make the cathodic air control valve one of the harshest environments for elastomeric sealing materials within PEMFC systems, demanding formulations specifically engineered for high humidity, elevated temperatures, oxidative atmospheres, and repeated dynamic motion.

2.6 Materials for sealing components in the cathodic side air-channel valve

Sealing components located in the cathodic-side air-channel valve of a PEM fuel-cell system operate under some of the most demanding conditions encountered by polymeric materials in electrochemical energy devices. Unlike the static gaskets compressed between bipolar plates, valve seals are exposed to dynamic mechanical loading, transient pressure variations, sliding or reciprocating contact, and continuous exposure to humidified oxidizing gases. The cathode stream typically contains O_2, N_2, and water vapor at temperatures between 60 °C and 80 °C, and may also contain acidic degradation species, including fluoride, sulfate ions, and hydrogen peroxide, originating from PFSA membrane decomposition. As highlighted by Zhao et al., the mechanical integrity and chemical stability of cathodic sealing components are essential for safe and efficient fuel-cell performance, because leakage or premature degradation can lead to reactant crossover, local starvation, and even catastrophic hydrogen–air mixing [116].

These conditions impose strict requirements on the materials used for valve sealing. Chemical resistance is essential because the cathode environment can become mildly to strongly acidic, especially under high-load operation or membrane degradation events, where condensates may reach pH values of 2–4. Over time, the presence of reactive oxygen species accelerates oxidative chain scission in elastomers lacking sufficient backbone saturation or stabilizing fillers. Furthermore, Xu et al. demonstrated that permeation through elastomeric gaskets is not negligible; in fact, gas permeation can exceed interfacial leak rates under normal stack pressures, especially when thin-section seals are used in compact architectures such as valves or manifolds [117]. Therefore, an ideal valve-seal material must feature inherently low gas diffusivity, strong chemical stability, and good retention of mechanical elasticity.

Mechanical durability is equally important. Elastomers undergo stress relaxation, a time-dependent reduction of internal stress under constant strain, due to molecular rearrangements in the polymer network. In dynamic sealing components, this loss of sealing force may be accelerated by temperature cycling. Cui et al. showed that liquid silicone rubber (LSR) subjected to thermal cycling between 23 °C and 80 °C experienced a sealing-force decrease of more than 40%, far exceeding predictions based solely on thermal contraction [118]. Their modified Maxwell model, incorporating stiffness evolution due to thermal aging, more accurately captured the stress-loss behavior and demonstrated that elastomers operating under variable temperatures are prone to accelerated relaxation. Such findings are directly relevant to cathodic valve seals, where rapid temperature changes occur frequently during start-up, shut-down, and load transitions.

BUPT

2.6 - Materials for sealing components in the cathodic side air-channel valve 33

2.6.1 Elastomeric Materials for Air-Valve Sealing

Elastomers dominate sealing applications in PEMFC components due to their elasticity, ability to conform to irregularities, and resilience to moderate temperature fluctuations. Among the elastomers evaluated for PEMFC sealing, EPDM and TPV are the most widely studied and the most relevant for the present work, while AEM, FKM, VMQ, and LSR serve as alternatives with distinct advantages and limitations.

EPDM exhibits superior resistance to humidity, steam, acidic environments, and oxidative conditions. These attributes arise from its saturated backbone, which suppresses uncontrolled radical-driven oxidative scission, and from its nonpolar character, which minimizes water uptake. Numerous uploaded studies confirm its dominant suitability for PEMFC environments.

Stress-relaxation studies on EPDM under PEMFC-relevant temperature cycling (60–120 °C, humidified air) show that a significant portion of sealing force is lost within the first 100 h, followed by a slower decay phase; nevertheless, peroxide-cured EPDM retains substantially higher residual force than sulfur-cured grades [118].

Typical EPDM formulations exhibit tensile strengths between 7–12 MPa, elongations at break of 300–600%, and densities near 0.85–0.90 g/cm³. EPDM also maintains good chemical resistance toward dilute acids and chlorides, making it suitable for humid and acidic environments. However, Qiu et al. demonstrated that EPDM exhibits pronounced stress-relaxation behavior under compression, losing approximately 0.45 MPa of contact stress across tested conditions—representing the widest stress-loss range among EPDM, NBR, fluororubber, and silicone rubber [119]. This vulnerability raises concerns for dynamically actuated seals that depend on sustained contact stress.

Thermoplastic Elastomers

Thermoplastic vulcanizates (TPVs)—composed of a crosslinked EPDM phase finely dispersed within a polypropylene matrix—offer an alternative with improved tribological performance. Their tensile strengths typically range from 10–14 MPa, elongation at break from 300–500%, and densities between 0.90–0.95 g/cm³. The presence of a semi-crystalline PP matrix imparts enhanced wear resistance and lower friction compared to conventional EPDM. While TPVs maintain good elasticity and recoverability, their chemical resistance depends strongly on the stability of the PP phase. Polypropylene is susceptible to oxidative degradation at temperatures above ~90 °C, especially in the presence of oxygen radicals or acidic condensation. This vulnerability limits the use of TPVs in cathodic regions unless the valve architecture minimizes exposure to acidic condensates or unless additional protective coatings or barriers are implemented. [120]

Styrenic Thermoplastic Elastomers (TPS), specifically hydrogenated grades like SEBS (Styrene-Ethylene-Butylene-Styrene), offer a distinct manufacturing advantage through their ability to chemically bond with rigid valve substrates (e.g., Polyamide or PBT) via multi-shot injection molding. This capability eliminates adhesive interlayers and assembly steps, reducing leak pathways. However, the thermal stability of TPS is physically limited by the glass transition temperature (*Tg*) of the polystyrene hard domains, which act as physical crosslinks. Drobny notes that while the saturated ethylene-butylene mid-block resists oxidation, the styrenic domains begin to soften near 95 °C, causing rapid stress relaxation and permanent

BUPT

deformation if the valve operates near the upper limit of PEMFC exhaust temperatures [121].

Of greater concern for PEMFC durability is the issue of leachate contamination. To achieve the low durometer required for valve sealing, TPS formulations rely on significant loadings of paraffinic plasticizer oils. Schulze et al. identified that these low-molecular-weight organic species can migrate from the seal into the gas stream, depositing onto the Membrane Electrode Assembly (MEA). This contamination results in catalyst poisoning and increased hydrophobicity loss in the Gas Diffusion Layer (GDL), directly increasing mass transport resistance [122]. Consequently, the utility of TPS is restricted to low-temperature air-intake locations where manufacturing cost reduction is prioritized over long-term electrochemical stability.

Silicone rubbers (VMQ) possess a unique combination of flexibility, thermal stability, and low glass-transition temperature, enabling operation even at sub-zero start-up conditions. However, extensive studies have shown that silicone rubbers degrade quickly in environments combining high temperature, humidity, and acidity. Chang et al. systematically investigated the aging behavior of silicone rubbers of various hardness grades and reported that exposure to humidified air above 100 °C leads to decomposition of crosslinker units and cleavage of methyl substituents on the siloxane backbone [123]. This degradation resulted in increased compression set, reduced tensile strength, and substantial surface cracking. Their data suggested that silicone rubbers may perform adequately below 80 °C, but suffer pronounced deterioration above 100 °C. Additionally, siloxane migration poses contamination risks. Yang et al. reported that volatile silicone species can interfere with gas diffusion layers and catalyst layers, reducing the electrochemical performance of operating fuel cells [124]. These issues render silicone rubbers unsuitable for cathodic valve seals, where humidity and transient temperatures frequently exceed their stability thresholds.

Fluoroelastomers (FKM, FSR) are among the most chemically resistant elastomeric materials available for PEMFC systems. They offer tensile strengths of 10–20 MPa, elongation at break between 150–300%, and densities of 1.7–1.9 g/cm³. Their resistance to acids, hydrocarbon species, and reactive oxygen intermediates is excellent. Furthermore, FKMs exhibit exceptionally low gas permeability, making them attractive for applications requiring minimal reactant crossover. Nevertheless, their mechanical behavior under temperature cycling can be problematic. Cui et al. reported (based on Derham's measurements) that FKM O-rings experienced sealing-force reductions exceeding 50% when cycled from 80 °C down to 23 °C, with the observed losses far exceeding those predicted by thermal contraction alone [118]. Their higher stiffness also reduces conformity in complex sealing geometries, potentially preventing the formation of effective dynamic sealing contacts. For these reasons, while FKMs excel in static seals exposed to aggressive chemistry, they are not ideal for dynamically actuated cathode valves requiring flexible sealing lips and rapid recovery.

Table 2-1 synthesizes the principal mechanical, thermal, chemical, and tribological properties of the most relevant elastomeric materials considered for cathodic-side valve sealing, providing a comparative basis for evaluating their suitability under PEMFC operating conditions.

BUPT

2.6 - Materials for sealing components in the cathodic side air-channel valve 35

Evaluating these materials collectively, EPDM remains chemically stable but mechanically challenged in dynamic conditions; TPV offers improved wear resistance but reduced chemical resilience; silicone provides temperature flexibility but fails under humid acidic loads; and FKM provides excellent chemical protection but poor dynamic compliance. Driven by the need for a sealing material capable of resisting acidic humidity, repeated deformation, and variable temperature, modern PEMFC valve-design literature increasingly favors elastomers with saturated backbones and optimized filler networks, such as EPDM-based compounds. Although advanced formulations and sustainable variants are being explored, the current state of the art indicates that EPDM remains the most balanced material for cathodic-side air-channel valve seals, provided that appropriate reinforcement strategies or surface treatments are implemented to mitigate wear and stress-relaxation effects.

BUPT

Table 2-1. Comparative Properties of Elastomers Used in PEMFC Cathodic-Side Valve Sealing

Property	**EPDM**	**TPV (EPDM/PP)**	**Silicone Rubber (VMQ / LSR)**	**Fluoroelastomer (FKM/FSR)**
Tensile strength (MPa)	7–12 (typical EPDM gasket grades)	10–14 (due to PP matrix reinforcement)	7–9 (VMQ), 6–8 (LSR)	10–20
Elongation at break (%)	300–600	300–500	400–700	150–300
Density ($g \cdot cm^{-3}$)	0.85–0.90	0.90–0.95	1.10–1.20	1.75–1.90
Thermal stability (°C)	−40 to 120	−40 to 110	−60 to 150 (but degraded >100 °C in humidity) [5,6]	−20 to 200
Resistance to humid heat	Very good	Moderate (PP phase vulnerable)	Poor at >100 °C (rapid modulus loss) [5]	Excellent
Acid resistance (H_2SO_4, condensates)	Good	Fair to moderate	Poor (acid-catalyzed degradation)	Excellent
Oxidation resistance	Good (saturated backbone)	Moderate	Fair–poor (methyl group oxidation) [5,6]	Excellent
Resistance to ROS ($\bullet OH$, H_2O_2)	Moderate	Low–moderate	Poor	Very high
Gas permeability (relative)	Medium	Medium–low	High	Very low
Compression set (100–120 °C)	Moderate–good (peroxide-cured best)	Moderate	Poor (25–35% strength loss) [5]	Moderate–poor under cycling [3]
Stress relaxation under thermal cycling	Significant at 80–120 °C [Qiu et al.]	Moderate	Very high (40%+ force loss) [3]	Very high (50%+ loss under 80→23 °C) [3]

BUPT

2.7 Sustainability Aspects of Synthetic Rubbers and Life-Cycle Considerations

The transition toward sustainable energy systems—among them PEMFC technologies—has intensified the demand for elastomeric materials that can deliver both high durability and reduced environmental impact. Conventional synthetic rubbers such as EPDM, FKM, AEM, NBR, HNBR, CR, and various polyurethanes remain predominantly petrochemical in origin. Their manufacturing relies on fossil-derived monomers, high-energy polymerization routes, and compounding packages containing activators, oils, antioxidants, and fillers whose production can exhibit significant environmental burdens. As a consequence, sustainability challenges arise across the entire life cycle, from monomer production to end-of-life disposal. Recent advances summarized in the literature indicate that sustainable elastomer science now moves beyond incremental improvements at the formulation level toward genuinely new feedstocks, low-energy catalytic routes, and recycling concepts. The following sections synthesize these developments using the provided references.

2.7.1 Sustainable Feedstocks for Elastomer Synthesis

A major pathway toward sustainability lies in replacing fossil monomers with renewable carbon sources. Several reviews highlight that plant-derived terpenes, vegetable oils, carbohydrate-derived diols, lactones, and even CO_2 can serve as primary synthons for next-generation elastomers.

Terpene-based elastomers represent one of the most promising families. Monomers such as β-myrcene, trans-β-farnesene, and alloocimene can be sourced from conifers, citrus waste, or biotechnologically fermented plant sugars [125]. Their polymerization yields elastomers with microstructures closely resembling classical diene rubbers. For example, emulsion-polymerized polymyrcene exhibits a glass transition near −73 °C, with 1,4-cis, 1,4-trans and vinyl linkages similar to polybutadiene and SBR, providing a direct route to sustainable analogues of common rubbers [125,126]. Likewise, poly(trans-β-farnesene) has been successfully introduced industrially for tire tread compounds due to its low-temperature elasticity and strong interfacial compatibility with silica-based reinforcing systems [125].

Another robust category is **vegetable-oil-derived polyols** and diols used in polyurethane (PU) elastomers. Soybean oil, palm oil, and other triglycerides can be epoxidized or transesterified to produce polyols for PU networks, replacing fossil-derived polypropylene oxide or polycaprolactone. Such routes significantly reduce hazardous isocyanate requirements and allow solvent-free polymerization, lowering toxicity and energy demand [127]. When combined with biobased diisocyanates, elongations at break exceeding 800 % and tensile strengths above 25 MPa have been reported, demonstrating that sustainable chemistry does not necessarily impose performance penalties [127].

Beyond biofeedstocks, emerging catalytic processes enable partial substitution of fossil monomers with **captured CO_2**. Polyether-carbonate polyols

BUPT

synthesized via copolymerization of CO_2 with propylene oxide and maleic anhydride can be chain-extended into cross-linkable CO_2-based rubbers. A full cradle-to-grave life cycle assessment (LCA) indicates that although these systems do not sequester carbon, replacing fossil epoxides reduces global warming potential by 18–34% (Figure 2.6) depending on the substituted rubber (HNBR, NBR, EPDM, or CR) [128].

This establishes CO_2-utilizing elastomers as a viable pathway to decarbonize sealing materials while maintaining conventional processing.

2.7.2 Sustainable Reinforcing Fillers: Recycled and Circular Carbon Black

A critical frontier in sustainable compounding is the decarbonization of reinforcing fillers, specifically carbon black (CB), which traditionally accounts for a substantial portion of a rubber compound's embodied carbon (approx. 2.5 kg CO2 per kg of CB) [129]. Recent literature distinguishes between two emerging pathways to mitigate this impact: Recycled Carbon Black (rCB) and Circular Carbon Black.

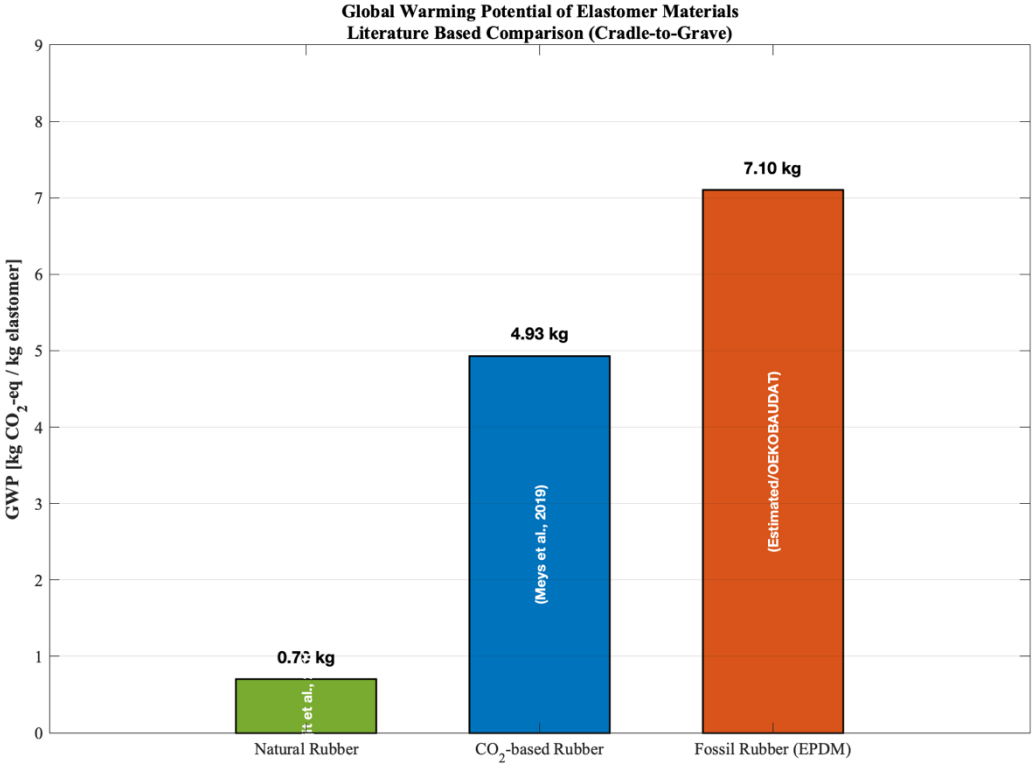


Figure 2.6. Global warming potential (GWP) reduction achieved when CO_2-based elastomers replace conventional rubbers, based on cradle-to-grave LCA data from Meys et al. (2019)

Recycled Carbon Black (rCB) is recovered directly from the solid char residue of end-of-life tire (ELT) pyrolysis. While rCB offers a greenhouse gas reduction of up to 80% compared to virgin variants, its application faces technical constraints due to surface heterogeneity and high residual ash content (typically 15–25 wt%, composed

BUPT

largely of zinc sulfides and silica) [130]. Investigations into Styrene-Butadiene Rubber (SBR), Natural Rubber (NR), and Nitrile Rubber (NBR) reveal that these impurities can disrupt the filler-polymer network, often manifesting as a pronounced Payne effect (strain-dependent modulus) and increased hysteresis [130,131]. Consequently, rCB is currently favored as a semi-reinforcing replacement (analogous to N500/N700 grades) for carcass compounds or static sealing applications—typically using Butyl Rubber (IIR) or NBR—where dynamic heat buildup is less critical [131].

Quantitative analysis of this substitution strategy highlights a distinct trade-off. While increasing rCB content drives a linear reduction in Global Warming Potential—potentially lowering the footprint from ~2.5 to 0.5 kg CO2/kg—mechanical reinforcement typically exhibits a non-linear decline. Data derived from Schuster et al. [131] suggests an optimal "sweet spot" near 20% substitution, where mechanical properties (such as tensile strength) remain comparable to virgin baselines. Beyond this threshold, performance degrades sharply as the negative effects of ash content and weak polymer-filler interaction outweigh the environmental benefits.

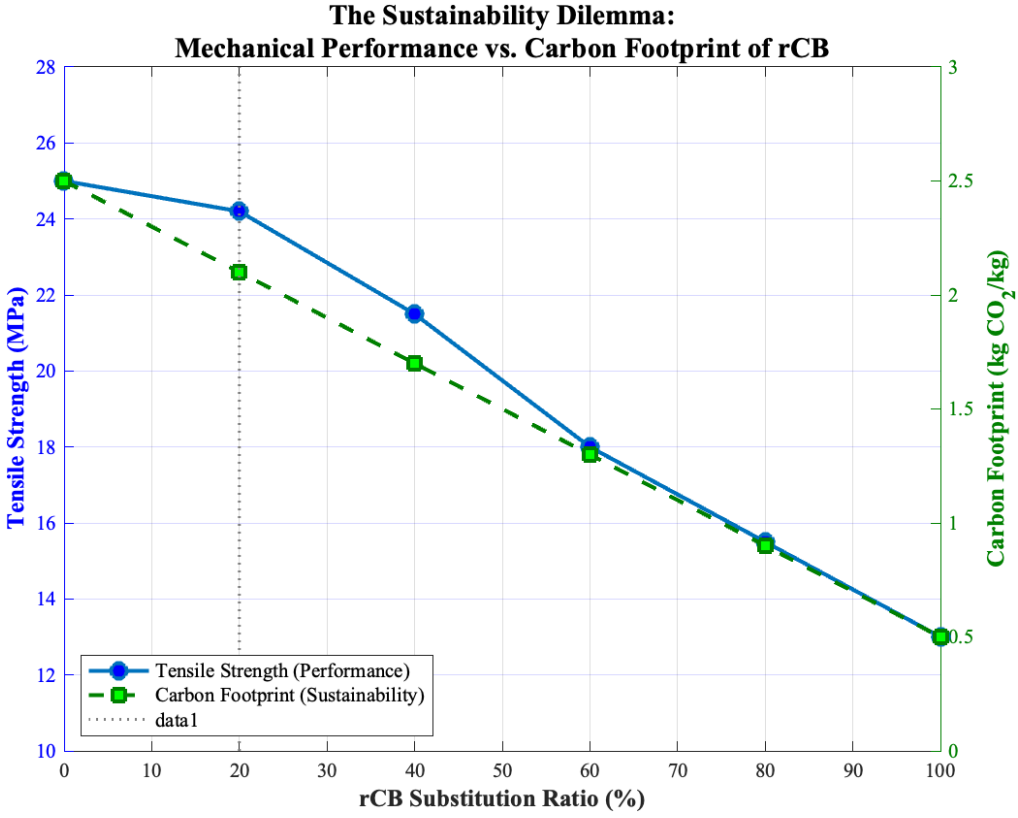


Figure 2.7. The trade-off between mechanical performance and sustainability in rCB substitution [131]

Conversely, Circular Carbon Black represents a "drop-in" solution, produced via the conventional furnace black process but substituting fossil feedstocks with tire

BUPT

pyrolysis oil (TPO) or renewable biomethane. Because this material is manufactured under controlled reactor conditions, it yields a filler chemically and morphologically identical to virgin grades (including high-structure N100/N200 series) [129]. This allows for its use in demanding applications—such as tire treads or PEMFC gaskets—without the performance penalties associated with char-based fillers. Current compounding strategies increasingly adopt hybrid approaches, blending rCB, circular black, and bio-based silica to optimize the trade-off between mechanical reinforcement, processing rheology, and life-cycle circularity.

2.7.3 Green Additives, Catalysts, and Compounding Strategies

Material sustainability also depends on the auxiliary chemicals incorporated into elastomer compounds. Conventional additives—aromatic process oils, ZnO activators, nitrosamine-forming accelerators—are associated with toxicity, poor biodegradability, or aquatic ecotoxicity. Consequently, a strong movement toward green compounding has been documented.

Biobased processing oils such as soybean, palm, tea, or coconut oils provide effective plasticization of natural rubber and synthetic elastomers while reducing polycyclic aromatic hydrocarbon (PAH) content. Their ester functionalities promote specific interactions (e.g., hydrogen bonding) with silica surfaces, improving filler dispersion and lowering compound viscosity without compromising mechanical strength[132].

Similarly, zinc oxide—an essential vulcanization activator—faces regulatory pressure due to environmental toxicity. Nano-ZnO, zinc-carboxylates, and ZnO supported on silica have been shown to reduce necessary Zn loadings by up to 75 % while maintaining cure kinetics and cross-link density [132]. These approaches mitigate leaching and reduce environmental footprint during tire wear or long-term weathering.

Catalytic innovations also contribute. Non-isocyanate PUs (NIPUs) formed via cyclic carbonate–amine reactions eliminate phosgene-derived isocyanates entirely, reducing toxicity and lowering energy consumption compared with classical PU synthesis. Their performance continues to improve, supported by new biobased diols and optimized polymer architectures [125,132,133].

2.7.4 Recycling and Circularity of Elastomers

Because rubbers are cross-linked, they are inherently difficult to recycle. Nevertheless, several recycling pathways are gaining momentum and represent an essential pillar of sustainability.

Mechanical recycling techniques—including fine grinding of vulcanized rubber to produce ground rubber powders—allow partial reintegration into new rubber compounds or polymer composites, such as recycled-rubber-reinforced concretes, improving crack resistance and damping characteristics [134]. Chemical devulcanization using controlled thermomechanical or catalytic processes can partially restore the polymer network, enabling re-processing while reducing waste accumulation. Such approaches also support the valorization of large waste streams such as end-of-life tires.

These recycling strategies fit into a broader vision of circular elastomer technology in which renewable feedstocks, low-toxicity additives, efficient energy use,

BUPT

and closed-loop material flows converge to reduce environmental burdens across the life cycle [125].

2.7.5 Life-Cycle Assessment of Sustainable Elastomers

Life-cycle assessment provides a quantitative framework to evaluate environmental improvements delivered by sustainable elastomer technologies. Across the reviewed studies, several consistent trends emerge:

1. Feedstock substitution dominates environmental impact.

Replacing fossil monomers with biobased or CO_2-derived feedstocks produces the most significant reductions in global warming potential (typically 20–40 %). This is because petrochemical monomer synthesis is highly energy-intensive and carbon-intensive. [14]

2. Additive and catalyst selection significantly affect toxicity-related impact categories.

PAH-rich aromatic oils, nitrosamine-forming accelerators, and ZnO disproportionately contribute to ecotoxicity and human toxicity; their replacement with bio-oils, non-nitrosamine accelerators, or nano-ZnO has measurable impact benefits. [125]

3. End-of-life remains a challenge.

Most rubbers end in incineration; for CO_2-based elastomers, incineration returns CO_2 to the atmosphere, meaning they are not carbon sinks. However, their overall global warming impact remains markedly lower than conventional rubbers thanks to reduced upstream burdens. [128]

4. Recycling pathways yield localized benefits.

Incorporating recycled elastomer waste reduces material demand and affects impact categories such as fossil depletion, waste generation, and particulate matter formation. While the mechanical properties of recycled compounds may drop, hybrid rubber-concrete and rubber-plastic composites mitigate this limitation [134].

Overall, LCA evidence strongly supports the potential of sustainable elastomer systems to reduce life-cycle environmental burdens while maintaining performance suitable for demanding applications such as PEMFC sealing.

2.7.6 Relevance for PEMFC Cathodic-Side Sealing Components

For PEMFC air-channel valves and sealing components, sustainability considerations must be balanced against strict operational requirements—chemical stability against O_2, radicals, and acidic humid condensates; low gas permeability; and longevity under compressive strain. The reviewed sustainable elastomers increasingly approach or match the mechanical and chemical performance of conventional EPDM and FKM systems, making them viable candidates for future fuel-cell component designs.

BUPT

CO_2-based rubbers are particularly attractive for PEMFC balance-of-plant applications. Their LCA shows reduced global warming potential and fossil resource use without major changes to processing routes or formulation practice compared to conventional EPDM or NBR systems [128]. Likewise, terpene-based diene rubbers offer a sustainable route to hydrocarbon elastomers with tunable cross-link density and glass transition behavior analogous to established PEMFC sealing materials.

2.8 Recent Developments in the Scientific Literature on Sealing Materials for PEMFC Applications and Identified Research Gaps

Recent advances in PEMFC technology have intensified interest in improving the performance and lifetime of elastomeric sealing materials, which remain critical determinants of stack reliability. As PEMFCs operate at elevated temperatures, under continuous humidification, and in chemically aggressive environments, the elastomeric gaskets are subjected to simultaneous thermal, chemical, and mechanical stressors that, over extended operation times, induce significant material degradation. Understanding these degradation pathways—and how they are influenced by formulation, curing chemistry, and environmental exposure—has become a central theme in contemporary sealing-materials research. The literature published over the past decade reveals a considerable expansion in analytical methods and mechanistic insights, yet persistent gaps remain in linking the various degradation phenomena to real-world PEMFC operating conditions.

One of the most substantial developments in recent research lies in elucidating the **chemical degradation** processes occurring within sealing elastomers, particularly EPDM, which remains a widely deployed material due to its intrinsic resistance to water, polar media, and ozone. EPDM's relatively saturated backbone provides good oxidative stability, yet studies have demonstrated that prolonged exposure to acidic condensates—typically involving H_2SO_4 and HF generated by membrane and catalyst degradation—can initiate chain scission, de-crosslinking, and oxidative surface modification.

Tan et al. demonstrated that immersion of EPDM in 1 M H_2SO_4 with 10 ppm HF at 60–80 °C leads to measurable weight change, carbonyl formation, and mechanical softening, with indentation modulus decreasing despite limited alterations in bulk Tg [135,136]. The same work demonstrated a clear contrast with fluoroelastomers, which exhibited more rapid chemical breakdown, emphasizing EPDM's superior resistance under PEMFC-relevant acidic conditions.

Complementary insights were provided by Lin et al. [137], who aged EPDM in humidified air at 120 °C and observed a roughly 30 % reduction in storage modulus accompanied by broadening of tan δ peaks and subtle modifications in viscoelastic relaxation behavior. These studies collectively highlight the role of hydrolysis- and oxidation-induced microstructural changes that remain difficult to detect through conventional thermal analysis alone, yet manifest clearly in surface chemistry and mechanical behavior.

Another important area of recent development concerns the **influence of curing systems and crosslink structure** on degradation resistance. Nah et al. [138] demonstrated that peroxide-cured EPDM retains structural integrity more effectively in simulated PEMFC environments than sulfur-cured EPDM, with reduced

BUPT

formation of oxidative byproducts and significantly lower swelling and de-crosslinking. The work of

Liu et al. [139] further clarified this point by showing that peroxide-cured EPDM undergoes chain scission and carbonyl formation under strong acid exposure, but the inclusion of a coagent such as triallyl isocyanurate (TAIC) mitigates degradation by forming more hydrolysis-resistant crosslinks. Without TAIC, peroxide-cured EPDM continues to react during aging, forming ether-linked structures that compromise elasticity. These findings underscore the necessity of carefully tailored crosslinking chemistry when developing EPDM formulations intended for long-life operation in PEMFC cathodic environments.

The role of fillers in enhancing chemical and mechanical durability has also been central to recent investigations. Carbon black—long recognized as the primary reinforcing filler for EPDM—has been shown to significantly improve resistance to hydrogen uptake, volume expansion, and oxidative degradation under high-pressure conditions.

In studies of hydrogen-induced damage, Ono et al. [83] observed dramatic differences between unfilled and carbon-black-filled EPDM when subjected to pressure cycling. While unfilled EPDM developed extensive microcracking, with crack densities increasing from approximately 20 to over 140 cracks/mm² after cycling, carbon-black-filled EPDM showed markedly reduced damage progression, demonstrating the stabilizing influence of fillers in suppressing cavitation and strain localization.

Shamsabadi et al. [140] confirmed that EPDM reinforced with smaller particle size carbon black exhibits superior resistance to chemical and mechanical deterioration under combined thermal and acidic stress, retaining mechanical integrity while showing minimal swelling and reduced peroxide-induced oxidative pathways. These results point to the central role of filler morphology and dispersion quality in stabilizing EPDM networks within aggressive PEMFC environments.

Parallel advances have been made in understanding **the thermomechanical aging behavior of EPDM**. Long-term exposure to elevated temperatures provokes oxidation, increased hardness, and reductions in elongation at break due to crosslink reconfiguration and microstructural embrittlement.

Wang et al. [141] reported that after prolonged aging, EPDM exhibited an approximately 18% hardness increase accompanied by a 12% loss in elongation, reflecting the progressive buildup of oxidative crosslinks.

Song et al. [142] similarly demonstrated that thermo-oxidative aging in cable-joint insulation produced surface cracking, pore formation, and substantial declines in tensile behavior.

Additional dynamic mechanical studies revealed that high-temperature aging reduces both storage and loss moduli and alters viscoelastic relaxation behavior, weakening the elastomer's ability to dissipate mechanical energy under PEMFC operating loads [137]. Collectively, these findings clarify the importance of managing thermo-oxidative pathways, particularly for seals located near heat sources, where elevated temperatures can accelerate degradation even in the absence of strong acid exposure.

Tribological research has gained increasing prominence in sealing-material studies over the past decade. As many balance-of-plant housings, ducts, and valves are constructed from glass-fiber-reinforced polyamides such as PA66GF30, the

BUPT

interaction between elastomers and these counterfaces is increasingly recognized as a critical degradation pathway. Studies of the composite itself reveal that under dry sliding, glass fibers can be exposed and pulled from the matrix, generating micro-cutting surfaces that severely abrade contacting elastomers.

Li et al. [143] reported prominent fiber protrusion and groove formation on PA66GF30 under high sliding loads, while Kunishima et al. [144,145] showed that fiber–matrix debonding increases friction and wear, producing counterface textures capable of inducing significant surface damage in compliant sealing materials.

When elastomers interact with such surfaces, tribological wear is dominated by plowing, fatigue cracking, and debris formation. For EPDM, Karger-Kocsis et al. [146] quantified strong correlations between carbon black content and wear resistance, with specific wear rates decreasing from 2.3×10^{-6} mm³/N·m in unfilled EPDM to 1.2×10^{-6} mm³/N·m at 60 phr carbon black. Felhős and Karger-Kocsis [147] similarly observed a reduction in friction coefficient from 1.3 to 0.8 over the same filler range. These results demonstrate that tribological optimization is essential for ensuring seal longevity in polymer–composite interfaces where abrasive contact is inevitable.

Beyond traditional EPDM formulations, significant attention has shifted toward **sustainable and recyclable elastomer systems**. Recent developments include bio-based EPDM synthesized using renewable monomers and recycled fillers derived from end-of-life tires.

Studies assessing recycled carbon black (RCB) highlight challenges associated with inconsistent surface morphology, residual organic impurities, and reduced dispersion quality.

Rikmann et al. [148] reported that low-grade RCB frequently exhibits agglomeration and contains PAHs that impair reinforcement efficiency, while Billotte et al. [149] showed that RCB enhances UV resistance in HDPE composites but introduces variability in oxidative stability. Ghosh et al. [150] demonstrated that combining reinforcing-grade carbon black with devulcanized rubber can improve tensile strength by up to 15 %, but high filler loadings significantly reduce elongation and increase abrasion.

Parallel research on devulcanization technologies has advanced through continuous thermo-mechanical processing. Brunella et al. [151] achieved devulcanization degrees up to 93.9 % using twin-screw processing, although high levels of network breakdown risk excessive chain scission and loss of mechanical performance. These sustainability-oriented studies illustrate promising pathways for circular materials but also highlight that the chemical and mechanical robustness of these systems under PEMFC-specific acidic and thermal stresses remains largely uncharacterized.

While each of these research directions has greatly expanded the scientific understanding of elastomer behavior in demanding environments, the literature also reveals several persistent **gaps**.

One of the most significant limitations is the lack of integrated studies that simultaneously assess chemical, mechanical, and tribological degradation under realistic PEMFC operating conditions. Most investigations isolate a single degradation mode—acid exposure, thermal aging, or tribological stress—despite clear evidence that these mechanisms interact synergistically during real operation. Swelling from chemical attack alters modulus and enhances wear susceptibility; tribological abrasion exposes fresh polymer surfaces that are more chemically reactive; and thermal

BUPT

oxidation accelerates stress relaxation, compromising sealing pressure. Without integrated testing methodologies, it remains difficult to establish accurate lifetime predictions or to design formulations optimized for coupled degradation environments.

Another key research gap lies in the insufficient study of elastomer–composite tribology for balance-of-plant components. Although numerous studies have examined friction and wear against steel, real PEMFC components often interface elastomers with PA66GF, PA46, PPS, or PTFE-modified composites. Fiber liberation, micro-cutting, and polymer transfer films produce wear mechanisms distinct from metal–polymer interactions, yet very few studies examine long-term sliding or vibrational contact involving these materials.

A further limitation is the lack of systematic characterization of ionic and organic leachates released during elastomer degradation. Many studies monitor conductivity, mass uptake, or pH changes, but do not identify the specific chemical species responsible for membrane poisoning or catalyst degradation. Given the sensitivity of PEMFC cooling circuits and membrane environments to trace contaminants, the absence of molecular-level leaching data restricts the ability to evaluate downstream impacts.

Sustainable EPDM and TPV materials also remain insufficiently studied under PEMFC-relevant conditions. While recycled fillers, bio-based monomers, and devulcanized elastomers offer promising environmental advantages, their performance under combined acidic, thermal, and mechanical stresses is largely untested. Variability in recycled filler morphology and incomplete network recovery during devulcanization raise questions regarding long-term reliability that the current literature has yet to address.

Finally, predictive modeling tools for elastomer lifetime—including time–temperature superposition models, Arrhenius-based degradation kinetics, and finite element methods—remain disconnected from experimental chemical- and tribological-aging data. Without validated multiphysics models capable of linking chemical degradation, stress relaxation, and wear evolution, seal designers must rely on empirical safety margins rather than mechanistic predictions.

In summary, recent literature has greatly deepened the understanding of the chemical, thermal, and tribological degradation pathways of sealing elastomers in PEMFC environments. Significant progress has been made in characterizing the effects of acid exposure, thermo-oxidative aging, filler morphology, and crosslink chemistry on the stability of EPDM and related materials. However, the absence of integrated aging frameworks, the limited study of elastomer–composite tribology, the insufficient identification of leachates, and the lack of durability data for sustainable elastomer systems highlight important research gaps. Addressing these gaps is essential for advancing the development of sealing materials that meet the stringent durability demands of modern PEMFC technology.

BUPT

3 SCOPE AND OBJECTIVES

3.1 Scope

The main goal of the present doctoral research was to study the behavior of sustainable elastomeric materials, with a particular focus on Ethylene Propylene Diene Monomer (EPDM) and Thermoplastic Vulcanizates (TPV) variants, under the specific conditions required for sealing the peripheral components of Proton Exchange Membrane Fuel Cell (PEMFC) systems.

Considering the stringent requirements for durability and environmental sustainability in hydrogen mobility, the study aims to investigate how the structure, composition, surface coatings, and the nature of reinforcing fillers—specifically circular and recycled carbon blacks—influence the mechanical integrity, tribological performance, and chemical stability of the seals when subjected to accelerated thermal and chemical aging.

The present work deals with the development of a comprehensive characterization framework that moves beyond standard datasheets to assess material behavior in simulated fuel cell environments. By evaluating the trade-offs between sustainability (using recycled feedstocks) and performance (maintaining low leaching and high sealing force), this research seeks to validate eco-friendly elastomeric formulations that can withstand the acidic and dynamic conditions of the cathodic air circuit.

3.2 Objectives

To fulfill the aim of this work and to provide a scientifically grounded selection methodology for next-generation PEMFC sealing materials, the following specific objectives have been defined:

Comparative analysis of elastomeric sealing materials for PEMFCs:
A critical review of the state of the art regarding materials currently employed for sealing in PEMFC applications, identifying performance limitations and the potential for integrating sustainable alternatives.

Characterization of the mechanical behavior under aging:
Evaluation of the changes in critical mechanical properties (tensile strength, elongation, hardness, and compression set) of EPDM and TPV materials induced by accelerated thermal and acidic aging protocols, simulating the long-term service environment of the stack periphery.

Evaluation of tribological performance:
Assessment of the coefficient of friction and specific wear rates of EPDM and TPV gaskets in dry sliding contact against glass-fiber reinforced polyamide (PA66GF30), utilizing pin-on-disk configurations to simulate the dynamic mechanical stresses encountered in air control valves.

BUPT

Assessment of chemical stability and leaching potential:

Investigation of the chemical stability and the potential leaching of organic and ionic compounds from ECO-EPDM elastomers containing circular (CCB) or recycled (RCB) carbon fillers. This involves the use of advanced analytical techniques, such as High-Performance Liquid Chromatography (HPLC-DAD), electrical conductivity measurements, and SEM-EDS, to estimate the risk of membrane contamination and catalyst poisoning.

Calibration of hyperelastic material models for FEA:

Utilization of experimental stress-strain data and tribological results to calibrate constitutive hyperelastic material models (e.g., Arruda-Boyce) and their subsequent integration into Finite Element Analysis (FEA) simulations. This objective aims to accurately predict sealing force retention and contact mechanics under realistic assembly and operating conditions.

Correlation of mechanical, tribological, and chemical results:

Integration of the experimental data obtained from mechanical, tribological, and chemical investigations to establish a holistic performance profile. This final correlation aims to identify the most sustainable and robust material formulation capable of meeting the rigorous demands of gaskets used on the cathode side of PEMFC systems.

BUPT

4 METHODOLOGY AND EQUIPMENT

This chapter details the experimental framework employed to evaluate the durability and performance of elastomeric materials intended for PEMFC peripheral components. The investigation encompasses a diverse range of polymer families, including Thermoplastic Styrenic Elastomers (TPS), standard EPDM and TPV grades, and sustainable "Eco" variants reinforced with circular (CCB) or recycled (RCB) carbon black. To replicate the aggressive service conditions of the cathodic air loop, these materials were subjected to accelerated aging protocols, specifically involving extended thermal exposure and immersion in sulfuric acid solutions.

The subsequent characterization utilized a multi-disciplinary approach, combining mechanical testing (tensile, hardness, compression set) with advanced physicochemical analyses to track degradation mechanisms and structural evolution.

Due to the distinct functional roles of the materials investigated—ranging from static gaskets to dynamic valve seals—the experimental matrix was tailored to address specific performance criteria for each material subclass. Figure 4.1 provides a comprehensive flowchart visualizing this methodology, mapping each material group to its corresponding aging conditions and characterization tests. As illustrated in the diagram, while fundamental mechanical and morphological assessments were applied across most categories, specialized testing streams were established for targeted objectives. For instance, tribological pin-on-disk testing was conducted exclusively on low-friction (LF) formulations to evaluate wear resistance, whereas advanced chemical stability analyses, such as High-Performance Liquid Chromatography (HPLC) and SEM-EDS, were reserved for the sustainable CCB and RCB variants to rigorously quantify their leaching potential and risk of membrane contamination.

BUPT

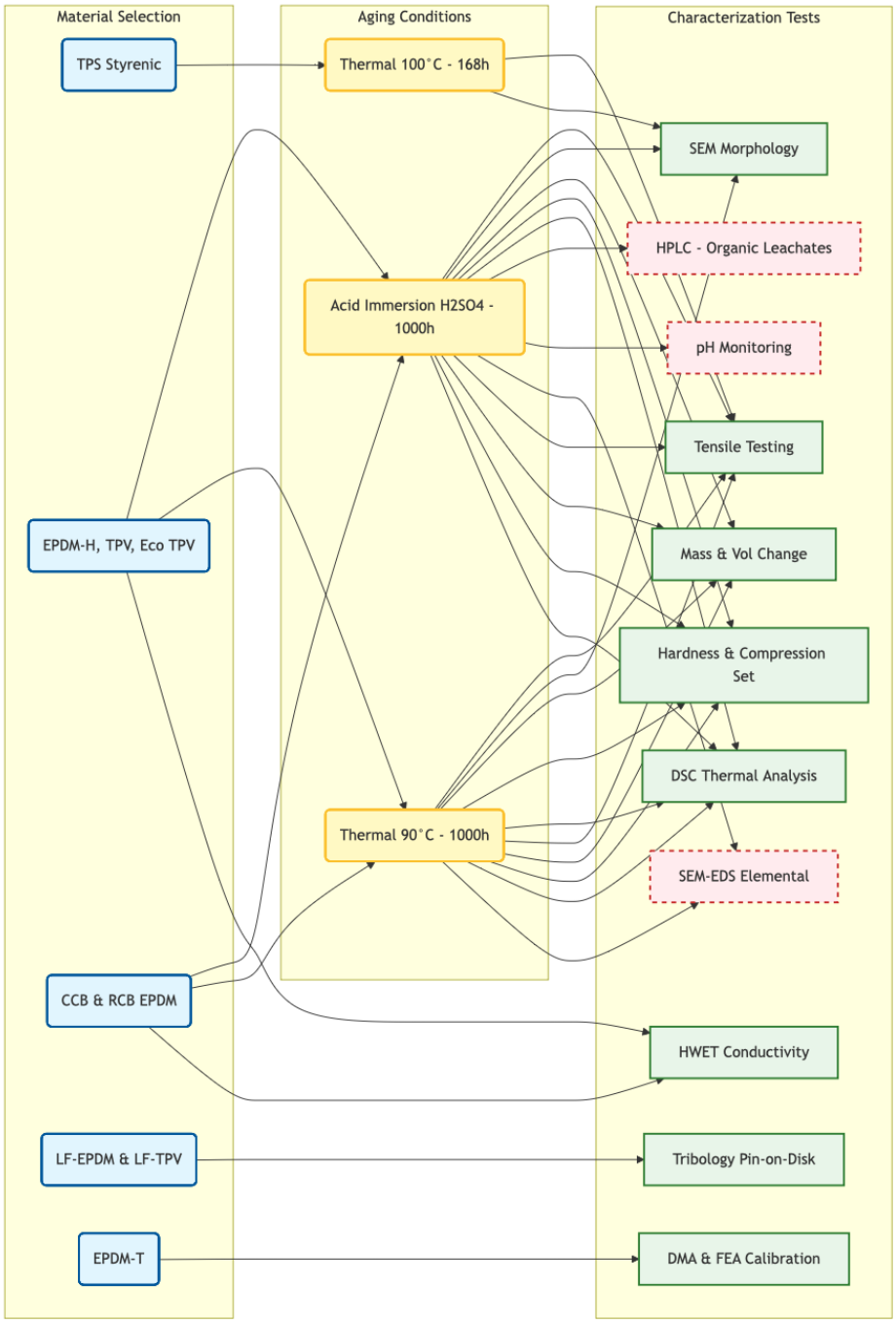


Figure 4.1. Flow-chart of the experimental program of the thesis.

BUPT

4.1 Materials

4.1.1 Thermoplastic Styrenic Elastomer (TPS) – Heat Aging Study

Thermoplastic elastomers (TPEs) are polymeric materials that combine the elastic behavior of crosslinked rubbers with the melt processability of thermoplastics [1]. In the heat aging study, the investigated material was a thermoplastic styrenic elastomer (TPS), a TPE grade with rubber-like flexibility and elasticity.

Dumbbell-shaped (DB) tensile specimens were manufactured from TPS provided by Kraiburg. The geometry followed ISO 37 (Figure 4.2) recommendations for dumbbell specimens, with dimensions corresponding to the standard type 2.

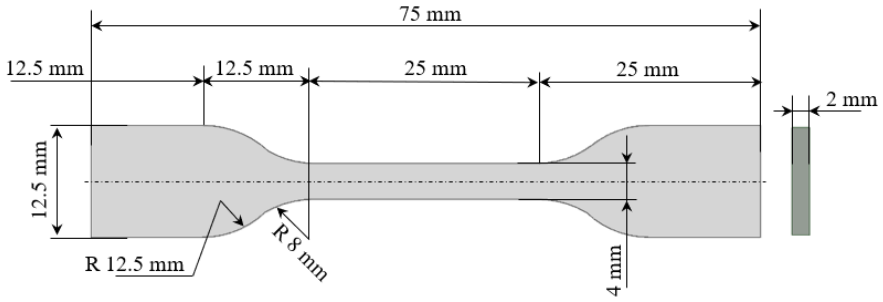


Figure 4.2. ISO 37 Type to Dumbell geometry and dimensions

4.1.2 EPDM-H, TPV and Eco TPV – Chemical and Thermal Aging

Thermoplastic vulcanizate (TPV) and Eco Thermoplastic Vulcanizate (Eco TPV) are composite elastomeric systems designed to combine rubber elasticity with the processing advantages of thermoplastics. Both are based on a blend of crosslinked EPDM rubber dispersed in a thermoplastic polypropylene (PP) matrix, providing mechanical robustness and thermal stability.

BUPT

Eco TPV contains at least 15% post-consumer recycled materials, lowering the overall carbon footprint compared to conventional EPDM or standard TPV while maintaining comparable performance.

The base EPDM rubber (EPDM-H) used in these systems is peroxidically cured and is known for high resistance to oxidation, weathering, heat, and ozone. Basic mechanical and thermal characteristics of EPDM, TPV and Eco TPV used for the aging studies are summarized in dedicated tables within the corresponding experimental chapters (e.g., tensile strength, elongation at break, hardness, compression set, and typical working temperature ranges).

4.1.3 Low-Friction EPDM and Low-Frtiction TPV for Tribological Tests

Tribological testing was performed on low-friction (LF) formulations of EPDM (LF EPDM) and TPV (LF TPV) developed for dynamic sealing applications in the automotive industry. The key material properties are summarized in Table 4-1.

Table 4-1. Comparison of mechanical and thermal properties of low-friction EPDM and TPV.

Property	**LF EPDM**	**LF TPV**
Hardness (Shore A)	62	80–87
Density (g/cm³)	1.06	0.96
Tensile strength (MPa)	19.4	10.4
Elongation at break (%)	330	530
Compression set (%)	11 (24 h at 125 °C)	36–52 (22–70 h at 70–125 °C)
Working temperature (°C)	−40 to +125 (typical)	−60 to +135 (typical continuous use)
Ozone and weather resistance	Excellent	Excellent
Typical uses	Seals, gaskets, vibration dampers, automotive	Seals, bellows, tubing, gaskets, automotive parts

Polyamide 66 reinforced with 30% glass fibers (PA66GF30) was used as the rigid counterpart in pin-on-disk tests, machined into 6 mm diameter balls. This combination replicates dynamic seal contact conditions between elastomeric materials and glass fiber-reinforced thermoplastics commonly used in automotive components.

BUPT

4.1.4 EPDM-T – Temperature Dependent Mechanical Characterization

For the comprehensive study of temperature-dependent stiffness, tensile behavior, and FEA calibration, a specific EPDM (EPDM-T) compound was investigated. Its formulation was:

- 60 wt.% EPDM (base elastomer),
- 32 wt.% carbon black (reinforcing filler),
- 3.4 wt.% zinc oxide (vulcanization activator, promoting crosslink density and thermal stability),
- 4.6 wt.% various additives and processing aids.

The compound was peroxide-cured to obtain the targeted crosslink structure and thermal resistance.

Dumbbell-shaped specimens were prepared according to ISO 37 type 2.

4.1.5 ECO EPDM with Circular and Recycled Carbon Black (CCB and RCB EPDM) – Chemical Stability & Leaching

Two peroxide-cured EPDM compounds were investigated in greater detail in the ECO EPDM studies:

- CCB EPDM: EPDM filled with circular carbon black obtained by advanced pyrolysis and refinement of end-of-life tires, designed to deliver more controlled particle morphology and improved circularity.
- RCB EPDM: EPDM filled with recycled carbon black recovered from waste tires using conventional pyrolytic recycling routes, typically associated with a broader particle size distribution and higher variability in surface residues.

Both compounds were manufactured by Arlanxeo (Geleen, The Netherlands) and supplied as vulcanized sheets with identical base EPDM polymers and crosslinking systems, isolating the effect of filler type. Representative initial mechanical and structural properties (reproduced from [22]) are listed in Table 4-2.

Table 4-2. Initial properties of ECO EPDM compounds CCB and RCB [22]

Property	**CCB EPDM**	**RCB EPDM**
Tensile strength (MPa)	15	12
Elongation at break (%)	271	262
Shore A hardness	77	75
Microhardness (IRHD)	47	45
Crosslinking system	Peroxide	Peroxide
Filler type	Circular carbon black	Recycled carbon black

BUPT

Specimens for tensile, swelling, hardness, microhardness, and leaching studies were die-cut from 2 mm thick sheets, with total exposed surface areas of 23.2 cm² in immersion-based tests where explicitly stated, with the tensile samples being according to ISO 37 type 2 [152].

4.2 Aging Protocols and Environmental Exposures

4.2.1 Thermal Aging of Thermoplastic Styrenic Elastomer

TPS samples were thermally aged according to ISO 188 [153]. Specimens were kept for 168 h at 100 °C in a thermal chamber (Figure 4.3). After aging, selected samples were used for tensile testing and for scanning electron microscopy to evaluate changes in surface morphology and microstructure.

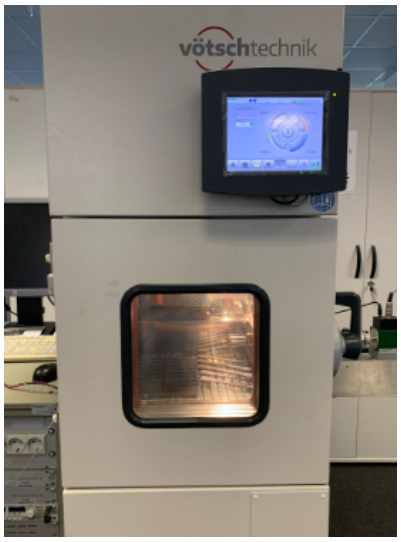


Figure 4.3. Thermal chamber

4.2.2 Chemical and Thermal Aging Protocols for EPDM-H, TPV, Eco TPV and ECO EPDM (CCB/RCB)

To reproduce the chemically aggressive and thermally demanding conditions relevant to proton-exchange-membrane fuel cell (PEMFC) environments, all elastomeric systems — EPDM, TPV, Eco TPV, and the sustainable ECO EPDM variants (CCB and RCB) — were subjected to controlled aging procedures involving both acidic immersion and elevated-temperature exposure. The chemical aging protocol consisted of full immersion of the specimens in aqueous sulfuric-acid solutions of predefined concentrations, maintained at 90 °C for an extended duration to induce accelerated degradation. Three media were selected to represent a spectrum of acidic severities typically encountered in PEMFC balance-of-plant components: strongly acidic (1 M H_2SO_4), moderately acidic (0.1 M H_2SO_4), and mildly acidic (0.001 M H_2SO_4). All samples were kept fully submerged for 1000 h under isothermal

BUPT

conditions. After completion of the immersion period, specimens were rinsed, dried, and stored prior to further characterization.

In parallel with the chemical-immersion procedure, thermal aging was performed to isolate the effects of elevated temperature from those induced by acidic environments. Samples were placed in a controlled hot-air oven at 90 °C for 1000 h under dry conditions, without any exposure to liquids. This method provided a direct assessment of heat-induced structural and mechanical changes across all materials.

Both the chemical and thermal aging routes were applied consistently to the conventional EPDM, TPV, and Eco TPV systems, as well as to the ECO EPDM materials filled with circular or recycled carbon black. The unified protocol enabled a direct comparison of degradation pathways, including the influence of filler type, polymer morphology, and environmental severity, while ensuring methodological coherence across all material systems investigated in this thesis.

4.3 pH Tracking and Chemical Analysis of Leachates

4.3.1 pH Measurements

In the ECO EPDM leaching study, the pH of acid solutions was monitored before and after aging:

- Instrument: Mettler Toledo FiveEasy™ Plus pH meter (Greifensee, Switzerland),
- Measurement temperature: 23 ± 1 °C,
- Solutions were analyzed immediately after sample removal to minimize environmental variations.

Initial pH values (~0.1, 0.84, and 2.24) were determined for 1 M, 0.1 M, and 0.001 M H_2SO_4 solutions, respectively; final pH values were compared to assess proton consumption and possible release of basic or acidic species from the elastomers.

4.3.2 HPLC Analysis of Organic Leachates

High-performance liquid chromatography (HPLC) was employed to analyze the organic compounds leached from CCB EPDM and RCB EPDM after immersion in sulfuric acid solutions of varying concentrations (1 M, 0.1 M, and 0.001 M H_2SO_4) at 90 °C for 1000 h. The analyses were performed using an Agilent 1260 Infinity II system equipped with a UV–Vis diode-array detector (DAD). The instrument was manufactured by Agilent Technologies in Santa Clara, California, with the HPLC production facility located in Waldbronn, Baden-Württemberg, Germany. Chromatographic separation was achieved using a Teknokroma C18 reversed-phase column supplied by Teknokroma Analítica S.A. (Barcelona, Spain), selected for its compatibility with non-volatile organic species typically released during elastomer degradation.

BUPT

Prior to analysis, all leachate solutions were filtered through 0.45 μm syringe filters to remove suspended particulates that could interfere with chromatographic performance. To ensure consistent detector response and avoid column overloading, each filtered sample underwent a dilution step in which 100 μL of the leachate was mixed with 900 μL of acetonitrile, yielding a final solution volume of 1 mL. This controlled dilution improved peak shape, stabilized the baseline, and ensured reliable quantification.

Chromatographic separation was performed using a mobile phase composed of acetonitrile and water, employing a gradient elution program followed by an isocratic segment to resolve compounds with differing polarity. The flow rate was maintained at 1.0 mL/min, and 20 μL of each prepared sample was injected into the column. The column temperature was held constant at 25 °C to ensure reproducibility across runs. The UV–Vis detector monitored the effluent at five wavelengths (220, 230, 240, 250, and 270 nm), enabling detection of a wide range of UV-active leachates, including low-molecular-weight organic acids, additives, or degradation products potentially released from the elastomer matrix or carbon black filler.

This HPLC protocol enabled qualitative identification and semi-quantitative comparison of organic compounds extracted from CCB EPDM and RCB EPDM under acidic conditions. The chromatographic data complemented the ion leaching results from hot-water extraction tests and the microstructural and elemental information obtained from SEM–EDS, providing an integrated understanding of the chemical stability and degradation pathways of ECO EPDM materials in fuel-cell-relevant environments.

BUPT

4.4 Mass and Volume Change Measurements

4.4.1 General Mass and Volume Change under Acidic Immersion

To quantify swelling, shrinkage, and mass change induced by acidic media, specimens of EPDM, TPV, and Eco TPV were weighed, and their volume determined before and after immersion.

- Before immersion, each sample was weighed in air and in water (in some studies in combination with a sinker) to obtain baseline mass and apparent mass in water.
- After 1000 h at 90 °C in the respective H_2SO_4 solutions (0.001 M, 0.1 M, 1 M), the same set of measurements was repeated.

The percentage mass change was calculated using:

$$\Delta m_{100} = \frac{m_i - m_0}{m_0} \times 100 \tag{19}$$

where
m_0 is the initial mass
m_i is the mass after immersion

When a sinker was used for hydrostatic weighing, the percentage volume change was calculated by:

$$\Delta V_{100} = \left(\frac{m_i - m_{i,w} + m_{s,w}}{m_0 - m_{0,w} + m_{s,w}} - 1 \right) \bullet 100 \tag{20}$$

where m_0 is the initial mass of the test piece, m_i is the mass of the test piece after immersion, $m_{0,w}$ is the initial mass of the test piece plus sinker in water, $m_{i,w}$ is the mass of the test piece plus sinker after immersion in water, and $m_{s,w}$ is the mass of the sinker in water.

This formulation allowed precise determination of swelling or shrinkage based on buoyancy, while the inclusion of the sinker ensured stability and repeatability for small or buoyant samples.

4.4.2 Mass and Volume Change for ECO EPDM without Sinker

In the ECO EPDM chemical stability study, a simplified hydrostatic weighing protocol without a sinker was used. Specimens were weighed in air and in water before and after aging. The volume change equation:

$$\Delta V_{100} = \left(\frac{m_i - m_{i,w}}{m_0 - m_{0,w}} - 1 \right) \times 100 \tag{21}$$

This approach provided sufficient sensitivity for relatively large EPDM specimens and allowed tracking of swelling/shrinkage due to long-term immersion in acidic solutions without using auxiliary hardware.

BUPT

4.5 Hot Water Extraction and Ion Leaching Tests

General Hot Water Extraction Test (HWET) for EPDM and TPV-Based Materials

The hot water extraction test (HWET) was used to evaluate ion leaching and chemical stability under hot, neutral aqueous conditions. The procedure used:

- Non-contaminating borosilicate glass bottles as containers,
- Deionized water with initial conductivity < 1.0 μS/cm,
- A portable conductivity tester to measure conductivity before and after exposure.

Specimens were used in their original state. Their mass was recorded before immersion. Samples were placed in vessels filled with deionized water, gently agitated for 1 minute to homogenize the solution, and the initial conductivity was measured at 23 °C. The containers were then sealed and incubated at 80 °C.

Conductivity measurements were taken at multiple time intervals (e.g., 0 h, 24 h, up to 168 h). After exposure, specimens were removed, gently dried and their mass re-measured. For a material to pass the test, the final conductivity had to remain below 5 μS/cm, in line with criteria used for fuel cell cooling circuits [10]. This procedure quantified the ion leaching tendency and chemical stability of EPDM, TPV, and Eco TPV formulations.

Hot Water Extraction and Conductivity in ECO EPDM Leaching Study

In the ECO EPDM leaching study, HWET was implemented with additional instrumentation details and slightly different conditions:

- CCB and RCB EPDM specimens with total surface area of 23.2 cm^2 were immersed in 100 mL deionized water,
- The water was maintained at 80 °C for 168 h,
- Conductivity was measured before and after immersion using a HI98308 PWT tester (Hanna Instruments, Woonsocket, RI, USA) with a working range of 0.0–99.9 μS/cm and resolution of 0.1 μS/cm.

This setup enabled quantitative comparison of ionic leaching from circular vs recycled carbon black-filled EPDM under neutral hot water conditions.

BUPT

4.6 Thermal Analysis

4.6.1 Thermogravimetric Analysis (TGA) and Differential Scanning Calorimetry (DSC)

Thermogravimetric analysis (TG) of TPS was carried out using an STA 449 F1 instrument in nitrogen atmosphere:

- N_2 flow rate: 250 mL/min,
- Temperature range: 30–900 °C,
- Heating rate: 20 K/min,
- Sample mass: 28.2 ± 2 mg.

Differential scanning calorimetry (DSC) was performed on the same STA 449 F1 equipment to investigate thermal transitions:

- Heating cycle: from 30 °C to 900 °C at 20 K/min,
- Cooling cycle: from 910 °C to −25 °C,
- Sample mass: 28.2 ± 2 mg,
- Nitrogen atmosphere, flow rate: 250 mL/min.

These measurements provided information on thermal stability and phase transitions of TPS.

DSC Analysis of EPDM-H, TPV, Eco TPV, and ECO EPDM (CCB and RCB)

Differential Scanning Calorimetry (DSC) was used to evaluate the thermal transitions and degradation-induced changes across all elastomer families investigated in this thesis, namely EPDM-H, TPV, Eco TPV, and the sustainable ECO EPDM formulations containing circular (CCB) and recycled (RCB) carbon black. All measurements were performed using the same instrument, a Discovery DSC 25P (TA Instruments, New Castle, DE, USA), to ensure complete methodological consistency between the different material systems.

For the sulfuric acid–immersion study on EPDM-H, TPV, and Eco TPV, DSC scans were carried out under nitrogen purge conditions, using a purge flow of 40 mL/min, with the samples heated from −60 °C up to 200 °C at a heating rate of 10 K/min. This thermal program enabled the identification of the glass transition temperature (Tg) and any potential melting or crystallization events that may arise from thermally or chemically induced structural changes.

The same DSC program and operating parameters were applied to the ECO EPDM (CCB and RCB) samples. Fresh, thermally aged, and acid-aged specimens were analyzed to capture potential shifts in Tg or modifications in endothermic features caused by filler–matrix interactions, oxidative degradation, or migration of low-molecular-weight components.

BUPT

4.7 Mechanical Testing

4.7.1 Tensile Testing Procedures

Tensile testing was performed on all elastomer and polymer samples using standardized dumb-bell specimens (ISO 37 Type 2) and universal testing machines, under controlled environmental conditions. Prior to testing, specimens were cut from sheet materials using a precision die cutter and conditioned at 23 °C and 50 % relative humidity (RH) for at least 24 h, where applicable.

For Thermoplastic -Sulfur (TPS), tests were carried out on a Zick Rockwell 005 machine at room temperature. A preload of 1 N was applied before each test. Three crosshead speeds were employed — 5 mm/min, 50 mm/min, and 500 mm/min — to investigate the influence of strain rate. For each speed, five specimens were tested in both virgin and aged conditions (30 specimens in total), and stress–strain data were collected to assess the effects of heat aging and strain rate on tensile properties.

For EPDM-H, TPV, and Eco TPV, tensile tests were conducted on an Instron universal testing machine equipped with mechanical grips and a video extensometer to ensure accurate strain measurement and minimize slippage. Testing was done at a crosshead speed of 500 mm/min and under standard laboratory conditions (23 °C, 50 % RH). The measured parameters included tensile strength, elongation at break, and tensile stress at defined strains (e.g., 100 % elongation).

For EPDM-T (used in stiffness and finite-element calibration studies), tensile tests were performed at multiple temperatures: −40 °C, 23 °C, 80 °C, and 125 °C, using ISO 37 Type 2 dumbbells. An Instron tensile machine was employed, with constant crosshead speed of 500 mm/min, and ambient humidity maintained at approximately 53 %. A video extensometer recorded strain, enabling accurate stress–strain curves for each temperature condition — critical for temperature-dependent constitutive modeling.

Finally, for the "eco" variants of EPDM (both CCB EPDM and RCB EPDM), specimens were cut from 2 mm-thick vulcanized sheets as ISO 37 Type 2 dumbbells. Tensile tests were conducted on an Instron universal testing machine with video extensometry at 500 mm/min under standard lab conditions (23 °C, 50 % RH). At least three replicates per condition (fresh, thermally aged, and chemically aged at various acid concentrations) were tested. The resulting stress–strain curves were used to derive tensile strength and elongation at break for each state.

All test data — stress–strain curves, tensile strength, elongation at break, and stress at defined strains — were analyzed to assess the effects of material type, strain rate, temperature, aging (thermal and chemical), and formulation (virgin vs eco-variant), ensuring a comprehensive comparison across all elastomer types and conditions.

BUPT

4.7.2 Compression Set Measurements

Compression set tests were conducted to evaluate the ability of the elastomeric materials to recover after long-term compression at elevated temperatures. Procedures followed ISO 815-1A [154] , using Type B specimens with:

- Thickness: 6.3 mm,
- Diameter: 13 mm.

Specimens were compressed by a defined deflection and maintained at 125 °C for 72 h. After the specified time, the samples were allowed to recover at room temperature, and the final thickness was measured.

The compression set (CS) was calculated as:

$$CS(\%) = \frac{h_0 - h_1}{h_0 - h_s} \times 100 \tag{22}$$

where
h_0 is the initial thickness,
h_1 is the thickness after recovery,
h_s is the height of the spacer used during compression.

4.7.3 Hardness and Microhardness Testing

Shore A hardness and IRHD microhardness were measured for all EPDM and TPV-based materials, including CCB and RCB ECO EPDM.

- Shore A hardness: evaluated according to ISO 48-4 [155].
- Microhardness (IRHD): measured following ISO 48-2 [156].

Multiple readings were taken and averaged for each material and aging condition to assess changes in surface stiffness and crosslink density.

BUPT

4.8 Dynamic Mechanical Analysis (DMA)

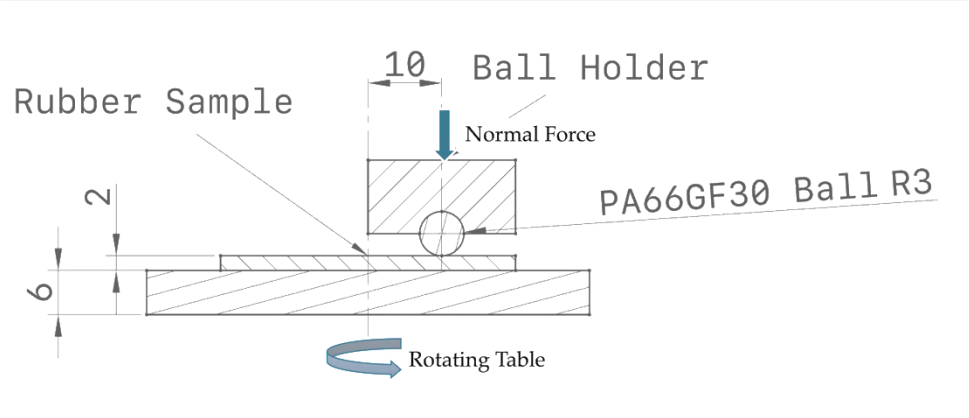
Dynamic mechanical analysis of the EPDM compound was performed in a single cantilever configuration:

- Frequency: 1 Hz,
- Displacement amplitude: 50 μm,
- Heating rate: 5 K/min,
- Temperature range: 20–160 °C.

The DMA provided temperature-dependent storage modulus, loss modulus, and damping (tan δ), characterizing the viscoelastic behavior and glass transition-related phenomena of the EPDM.

4.9 Tribological Testing

Tribological measurements were performed using a TR-20 Micro Pin-on-Disk Tribometer (DUCOM Instruments, Bangalore, India), configured in ball-on-disk mode to reproduce frictional interactions representative of elastomer–composite sealing contacts. A schematic of the experimental configuration is provided in **Error! Reference source not found.**.



In this arrangement, the rotating disk consisted of EPDM or TPV elastomer sheets with a thickness of 2 mm, which were bonded to a metallic substrate and mounted onto the tribometer stage. The stationary counterbody was a 6 mm diameter PA66GF30 ball (polyamide 66 reinforced with 30 wt.% glass fibers), supplied by RGPBALLS S.r.l., Cinisello Balsamo, Italy. This material pairing reflects the type of contact encountered in dynamic automotive sealing systems, where elastomers slide against glass fiber-reinforced thermoplastics under fluctuating mechanical loads.

Normal loading was applied vertically through a calibrated dead-weight system coupled to a pivoting lever arm, ensuring stable and repeatable loading during each test. The frictional force was measured continuously using a strain-gauge-based force sensor integrated into the loading arm. This setup enabled real-time computation of the coefficient of friction (CoF) throughout the test duration.

All experiments were carried out under dry, unlubricated conditions at 23 °C, with each run lasting 30 minutes. The rotational speeds were set to 92, 183, and 286

BUPT

RPM, corresponding to linear sliding speeds of approximately 0.05, 0.10, and 0.15 m/s, respectively, for a 10 mm-diameter wear track. Normal loads of 1 N, 3 N, and 6 N were selected to span a representative range of contact pressures experienced by elastomeric seals in service.

Before each test, the elastomer disk was cleaned using isopropanol to remove dust and surface contaminants. After testing, specimens were removed and weighed using a high-precision analytical balance (accuracy ±0.00001 g) to quantify mass loss.

Wear track morphology was assessed using a Leica DMS1000 digital microscope (Leica Microsystems, Wetzlar, Germany). Micrographs were acquired under controlled illumination and magnification, and wear track dimensions were extracted using the system's integrated image-analysis software. The inner and outer diameters of each wear scar were used to calculate the worn surface area. Surface features such as tearing, polishing, abrasion, and debris accumulation were also evaluated. The measurement uncertainty for wear area quantification was estimated at ±3%, based on repeated measurements and the resolution limits of the DMS1000 optical system.

4.10 Microscopy and Surface/Elemental Analysis

4.10.1 SEM of TPS Before and After Thermal Aging

To visualize microstructural changes due to thermal aging, TPS specimens (unaged and aged) were examined using a FEI INSPECT S scanning electron microscope (SEM):

- Operating mode: low vacuum,
- Detector: Secondary Electrons (SE), Large Field Detector (LFD),
- Accelerating voltage: 2.00 kV,
- Spot size: 3.0,
- Working distance (WD): 9.9–10.3 mm depending on specimen,
- Magnifications: 1200× and 2500×.

These conditions allowed detailed comparison of surface features before and after 168 h at 100 °C.

4.10.2 SEM of EPDM-H, TPV and Eco TPV after Acid and Heat Aging

For the sulfuric acid–immersion study, SEM analysis was performed on EPDM, TPV and Eco TPV samples using a VEGA TESCAN microscope:

- Samples were sputter-coated with a thin layer of gold to enhance electrical conductivity and image resolution,
- Operation under high vacuum conditions,
- Accelerating voltage: 20.0 kV,
- Working distance: 12.42–15.34 mm,
- Magnifications:

BUPT

- Low magnification: 366×, 373×, 380× (large-scale surface features),
- High magnification: 738×, 778×, 791×, 806× (finer microstructural details).

This combination enabled a multiscale assessment of surface damage, filler dispersion, cracking, and degradation-induced roughening.

4.10.3 SEM–EDS of ECO EPDM (CCB and RCB)

To investigate degradation mechanisms and filler-dependent differences in ECO EPDM, SEM coupled with energy-dispersive X-ray spectroscopy (SEM–EDS) was carried out on:

- Fresh samples,
- Thermally aged samples (90 °C, 1000 h),
- Acid-aged samples (1 M H_2SO_4, 90 °C, 1000 h).

The instrument used was a Thermo Fisher Axia ChemiSEM system (Thermo Fisher Scientific, Waltham, MA, USA):

- Samples mounted on aluminum stubs with conductive carbon adhesive and sputter-coated with gold,
- Detector: CBS,
- Accelerating voltage: 10.00 kV,
- Working distance: ~10.2 mm,
- Magnifications: 500× and 1000×,
- Horizontal field width (HFW) at 1000×: ~414 µm.

EDS acquisition parameters:

- Accelerating voltage: 10.00 kV,
- Acquisition time: 379 s,
- Average count rate: ~1140 cps,
- Total counts: > 430,000,
- Mapping resolution: 768 × 512 pixels.

Quantitative EDS data were reported as atomic and weight percentages for key elements:

- Carbon (C),
- Oxygen (O),
- Sulfur (S),
- Magnesium (Mg),

and, in extended analyses, also:

- Silicon (Si),
- Zinc (Zn).

Changes in oxygen and sulfur content were used to infer oxidation and acid uptake, while Mg, Si, and Zn were tracked as indicators of filler-related species or residues associated with recycled content. Correlating SEM morphology with EDS mapping provided insight into the degradation pathways and stability differences between CCB and RCB EPDM.

BUPT

5 RESULTS

5.1 Thermoplastic Styrenic Elastomer (TPS): Thermal Aging and Mechanical–Thermal Behavior [157]

It is important to distinguish the specific role of the TPS investigation within the broader scope of this thesis. Unlike the EPDM and TPV grades analyzed in subsequent sections, which are candidates for direct contact with acidic condensates in the cathodic loop, the TPS material is evaluated here primarily as a baseline for thermoplastic behavior under thermal stress. Consequently, the characterization of TPS focuses exclusively on heat aging (100 ◦C) and mechanical response at varying strain rates. The deep chemical stability analyses—specifically High-Performance Liquid Chromatography (HPLC) and Hot Water Extraction Tests (HWET)—were not performed on the TPS samples. These advanced leaching protocols were reserved for the complex EPDM and Eco-TPV matrices (discussed in Section 5.2), where the presence of recycled fillers (CCB/RCB) introduces a specific risk of releasing unknown organic or ionic contaminants that could poison the fuel cell membrane.

5.1.1 Tensile Behavior Before and After Thermal Aging

The tensile behavior of the TPS specimens was evaluated in [157] by extracting stress–strain data for each combination of loading speed and material condition. Figure 5.1 illustrates the resulting curves for both virgin and heat-aged specimens across the applied test speeds of 5, 50, and 500 mm min^{-1}. In all cases, aging resulted in an increase in tensile strength accompanied by a reduction in elongation at break, a trend consistent with previously reported thermo-oxidative stiffening phenomena in styrenic block copolymers. The increase in strength is associated with post-aging physical or chemical crosslinking, while the reduced ductility reflects microstructural embrittlement and decreased segmental mobility within the elastomeric mid-blocks.

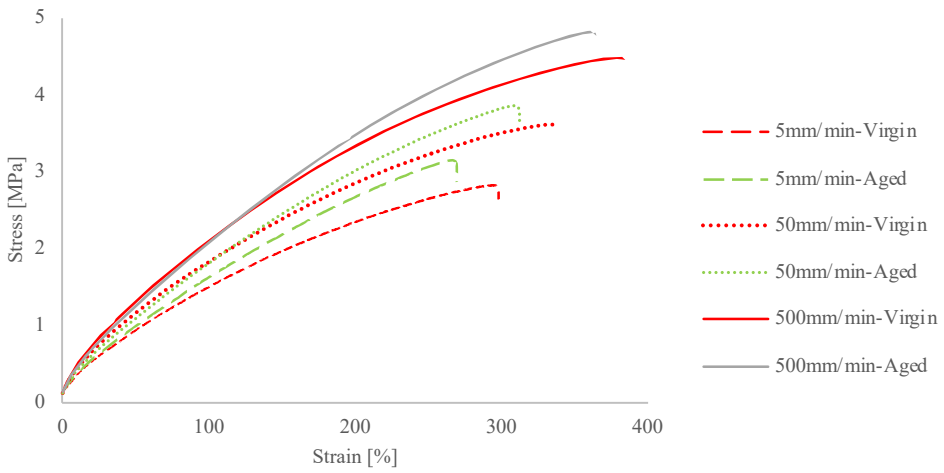


Figure 5.1. TPS tensile response dependence on load speed and sample state

BUPT

5.1 - Thermoplastic Styrenic Elastomer (TPS): Thermal Aging and Mechanical–Thermal Behavior [157] 65

Stress was calculated from the applied force using $\sigma = F/A_0$, where A_0 is the initial cross-sectional area of the sample. The ultimate tensile strength (UTS), defined as the maximum stress prior to failure, exhibited a clear rate-dependent increase for both virgin and aged materials. At the lowest loading speed of 5 mm min^{-1}, the aged specimens reached a UTS of 3.17 MPa, representing a 14 % increase compared to the corresponding virgin specimens. At 50 mm min^{-1}, the aged material exhibited a tensile strength 12.6 % higher than the unaged material, while at 500 mm min^{-1} the increase remained significant at 9.1 %. These trends indicate that the aged TPS specimens exhibit greater resistance to deformation at all strain rates, although this comes at the cost of lower failure strain.

BUPT

The full set of tensile results is summarized in Table 5-1. and graphically represented in Figure 5.2.

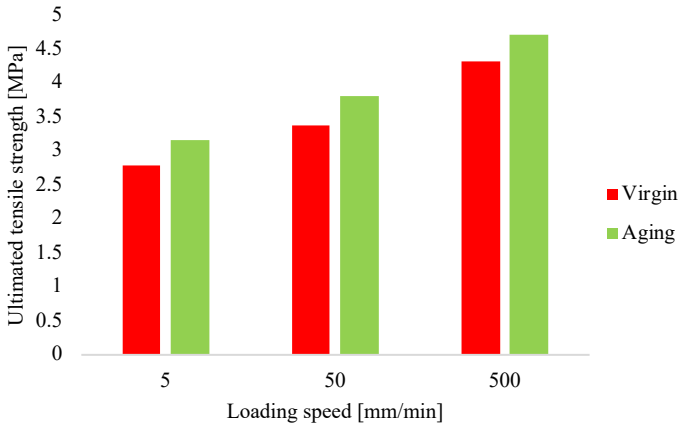


Figure 5.2. Ultimate tensile strenght dependence on the loading speed

Table 5-1. Results of tensile testing in tabular form

Sample state	Loading speed [mm min^{-1}]	Ultimate Tensile Strength [MPa]	Standard deviation for Ultimate Tensile Strength [MPa]	Elongation at break [%]	Standard deviation for Elongation at break [%]
Virgin (unaged)	500	4.32	0.127	381	17.536
Aged	500	4.72	0.106	366	25.074
Virgin (unaged)	50	3.38	0.176	334	43.260
Aged	50	3.8	0.052	312	15.249
Virgin (unaged)	5	2.78	0.042	298	25.434
Aged	5	3.17	0.012	269	21.014

. For each loading speed, the aged material shows higher UTS and lower elongation at break relative to virgin specimens, with standard deviations reflecting consistent reproducibility across tests. At 500 mm min^{-1}, the virgin TPS exhibited a UTS of 4.32 MPa and an elongation of 381 %, whereas the aged sample reached 4.72 MPa with a reduced elongation of 366 %. Similar patterns were observed at intermediate and low loading speeds, confirming that aging systematically shifts the material response toward a stiffer and less extensible regime. These results align with the known sensitivity of TPS to thermo-oxidative hardening, as documented in earlier investigations.

BUPT

5.1.2 Thermal Stability (TGA)

Figure 5.3 presents the thermogravimetric response of the TPV samples, revealing the sequential degradation of the material's constituent phases. The primary polymer matrix, accounting for approximately 70 % of the total mass, undergoes complete thermal decomposition by around 470 °C. A second degradation event appears near 780 °C, corresponding to the breakdown of the elastomeric component, which represents roughly 10 % of the mass. The remaining residue, approximately 20 %, corresponds to carbon black.

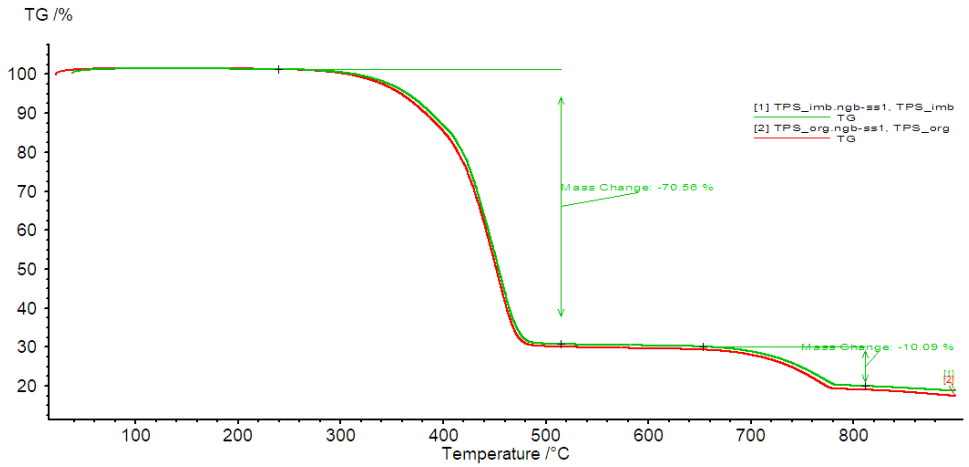


Figure 5.3. TGA curve of both aged and virgin samples of TPS

5.1.3 Thermal Transitions (DSC)

Figure 5.4 represents the DSC curves for virgin (green) and aged material (red) and they show no visible structural difference between aged and virgin samples. Thermoplastic matrix melting starting point identified at around 140°C.

Ageing leads to changes in crystalline structure in addition to oxidative damage. A significant reduction in molecular weight due to oxidative chain scission would cause a reduction in melting temperature. However, it is apparent that ageing does not reduce melting temperature; indeed, a slight increase is observed. This could be due to crosslinking effects resulting from oxidative damage.

BUPT

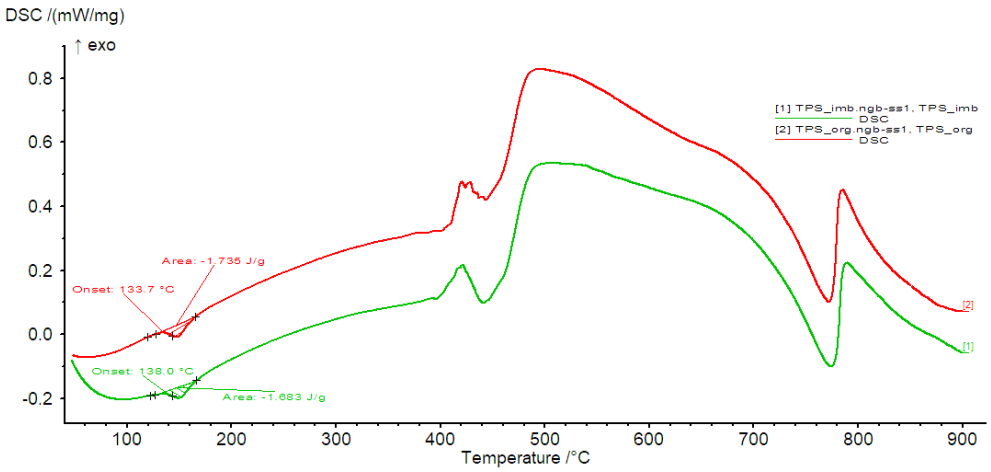


Figure 5.4. DSC curve of both aged and virgin samples of TPS

5.1.4 Surface Degradation After Aging (SEM)

Microscopic observations of the aged materials have been investigated using scanning electron microscopy (SEM) in order to confirm the mechanical degradation previously discerned. It was noticed (as it can be seen in Figure 5.5) that the number of these voids increased in the aged samples. The surface morphology of TPS aged at 100 °C for 168h shows cracks indicating higher kinetics of degradation for severe conditions.

BUPT

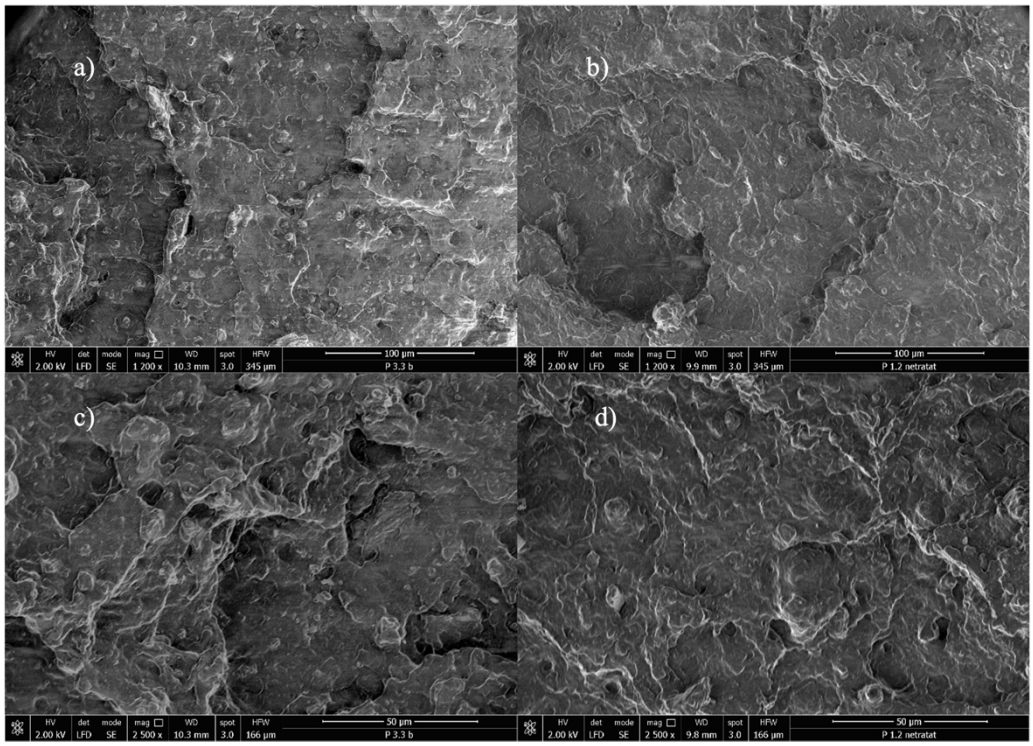


Figure 5.5. SE micrograph of TPS/SEBS a) aged, magnitude 1200x; b) unaged, magnitude 1200x; c) aged, magnitude 2500x; d) unaged, magnitude 2500x

5.2 Chemical and Thermal Stability of Elastomeric Materials (EPDM-H, CCB EPDM, RCB EPDM, TPV and Eco TPV)

The thermal and chemical aging performed on the studied materials are fully described in chapter 4.2.2. These results were published in [19,20,22,23].

5.2.1 Swelling Behavior Under Acidic Environments

Mass and volume change

Table 5-2 summarizes the weight change (WEC) and volume change (VC) of EPDM-H, TPV, and ECO TPV after immersion in H_2SO_4 solutions of 0.001 M, 0.1 M, and 1 M for 1000 h at 90 °C. The results show that the materials exhibit both positive and negative volume changes depending on the acid concentration. At the lowest concentration (0.001 M), EPDM-H displays a slight volume reduction of –1.048 %, while TPV exhibits a similar contraction of –0.298 %. Such negative values indicate that, under mildly acidic conditions, certain formulations may undergo densification rather than swelling. This behaviour may arise from network tightening due to

additional crosslinking reactions or from the loss of low-molecular-weight

Table 5-2. Weight and volume change results

	EPDM		TPV		ECO TPV	
Solution	**WEC [%] (σ)**	**VC [%] (σ)**	**WEC [%] (σ)**	**VC [%] (σ)**	**WEC [%] (σ)**	**VC [%] (σ)**
0.001M	0.533 (0.022)	-1.048 (0.232)	0.753 (0.071)	-0.298 (0.561)	0.948 (0.230)	0.205 (0.795)
0.1M	1.436 (0.035)	1.107 (0.062)	3.577 (0.065)	3.083 (0.250)	4.325 (0.037)	4.537 (0.236)
1M	1.882 (0.005)	1.637 (0.070)	5.224 (0.186)	4.866 (0.483)	6.145 (0.50)	6.501 (0.600)

after immersion in solution for 1000h at 90°C. The standard deviation σ is written in parentheses.

constituents, both of which can lead to a more compact polymer structure.

As the acidity increases, all materials transition to positive WEC and VC values, reflecting swelling, fluid uptake, and the onset of chemical degradation processes. ECO TPV demonstrates the highest susceptibility to acid-induced changes, reaching 6.145 % WEC and 6.501 % VC in the 1 M solution, signalling substantial degradation of both the elastomeric and thermoplastic phases. TPV also shows considerable mass and volume increases at high acidity, with maximum values of 5.224 % and 4.866 %, respectively. In contrast, EPDM-H exhibits the greatest chemical stability of the three materials, with comparatively modest changes of 1.882 % in weight and 1.637 % in volume after exposure to 1 M H_2SO_4. These trends confirm the superior resistance of the EPDM-H network to acid-driven swelling and structural disruption.

Building on the swelling behaviour previously discussed for EPDM-H, the ECO EPDM formulations (CCB and RCB) exhibited the same overall trend of acid-concentration-dependent mass and volume changes, yet with markedly different magnitudes that reflect the influence of filler origin and microstructural uniformity. Both materials showed measurable swelling under all immersion conditions, with the extent of weight and volume increase rising as the acidity decreased. This behaviour, consistent with osmotic uptake phenomena in partially crosslinked elastomers, is illustrated in Figure 5.6.

Across all sulfuric acid concentrations, RCB EPDM displayed higher swelling than its CCB counterpart. At the highest acid concentration (1 M H_2SO_4), CCB EPDM

BUPT

exhibited an average weight increase of 1.82 % and a volume change of 0.97 %, whereas RCB EPDM reached 2.95 % and 1.63 %, respectively. These differences became more pronounced at 0.1 M, where CCB EPDM showed increases of 3.61 % (weight) and 3.06 % (volume), while RCB EPDM rose significantly to 6.30 % and 4.53 %. At the lowest concentration, 0.001 M H_2SO_4, the trend remained consistent: RCB EPDM swelled more extensively, with 6.50 % weight and 4.90 % volume increase, compared to 4.75 % and 4.15 % for CCB EPDM.

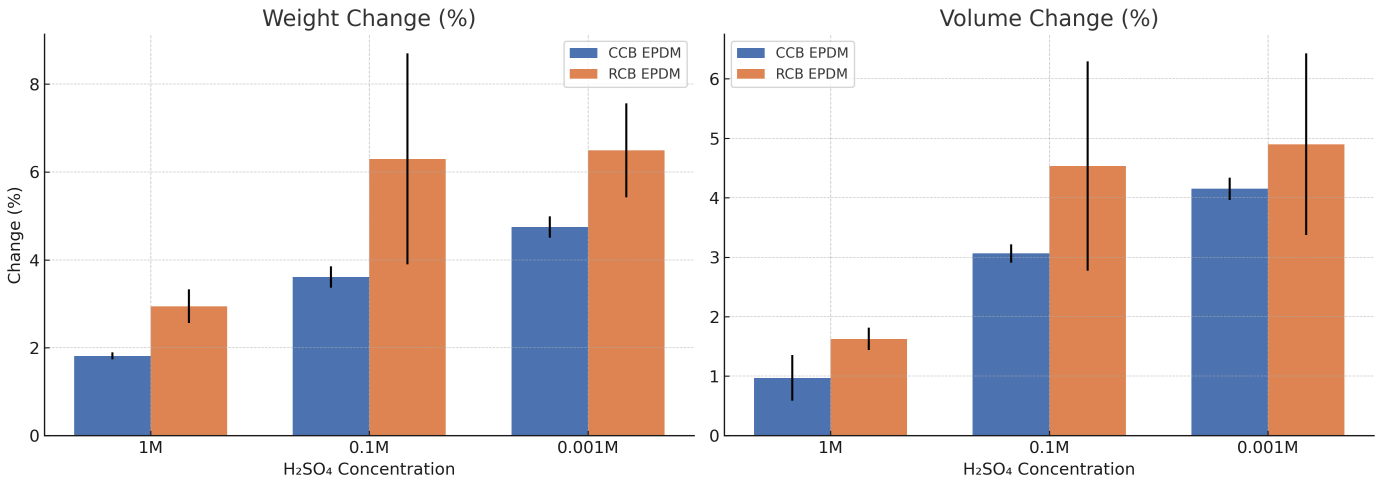


Figure 5.6. Weight and volume change of CCB EPDM and RCB EPDM

The consistently higher uptake observed in RCB EPDM suggests that the recycled carbon black introduces a more open, heterogeneous, or polar filler structure, facilitating deeper penetration of water and ions into the elastomeric network. The particularly high swelling at 0.1 M indicates that moderately acidic conditions may accentuate these microstructural pathways, possibly due to increased filler dispersion variability or the presence of residual porosity inherent to recycled filler systems. In contrast, CCB EPDM demonstrates more stable behaviour, with smoother, more linear increases in swelling, consistent with a more uniform filler morphology and stronger matrix–filler interactions that limit fluid ingress. The larger standard deviations associated with RCB EPDM, especially at intermediate acid strength, further underscore its microstructural inconsistency and reduced network integrity relative to the circular carbon black formulation.

Discussion of Swelling Behaviour Under Acidic Environments

The swelling behaviour of EPDM-H, TPV, ECO TPV, and the two ECO EPDM formulations (CCB and RCB) reveals clear material-dependent differences driven by acid concentration, filler characteristics, and polymer–filler interactions. Across all systems, sulfuric acid immersion at 90 °C for 1000 h produced measurable changes in weight and volume, but the extent of these changes varied significantly.

BUPT

EPDM-H showed the highest chemical stability, with minimal swelling even at 1 M H_2SO_4 (WEC 1.882 %, VC 1.637 %). At the lowest acid concentration (0.001 M), EPDM-H and TPV both exhibited slight negative volume changes, suggesting network densification through additional crosslinking or loss of volatile constituents. As acidity increased, all three materials (EPDM-H, TPV, ECO TPV) transitioned to positive WEC and VC values. ECO TPV consistently showed the greatest susceptibility to acid-induced degradation, reaching 6.145 % WEC and 6.501 % VC at 1 M—reflecting the vulnerability of its PP-rich thermoplastic phase to hydrolysis and oxidation. TPV exhibited intermediate behaviour, with noticeable swelling but less severe than ECO TPV.

The ECO EPDM materials followed the same acidity-dependent trend but with systematically higher swelling in RCB EPDM compared to CCB EPDM. At 1 M H_2SO_4, their swelling remained moderate (CCB: 1.82 % / 0.97 %; RCB: 2.95 % / 1.63 %), but the differences intensified at 0.1 M, where RCB EPDM reached 6.30 % WEC and 4.53 % VC—nearly double the corresponding values of CCB EPDM. Even at 0.001 M, RCB continued to swell more (6.50 % vs. 4.75 % WEC).

This consistent gap between the two ECO EPDM systems highlights the importance of filler morphology. Recycled carbon black introduces greater heterogeneity, higher porosity, and more polar oxygen-containing functionalities, which collectively enhance fluid uptake and diffusion pathways [126,158,159]. Circular carbon black, with its more uniform particle size distribution and better filler–rubber compatibility, restricts water and proton ingress, yielding smoother, more predictable swelling behaviour. The pronounced swelling of RCB EPDM at 0.1 M suggests that moderately acidic conditions best exploit the microstructural weaknesses of the recycled filler system. The higher standard deviations observed in RCB EPDM further confirm its less consistent network structure.

Overall, the swelling results establish three clear conclusions.

First, EPDM-based materials outperform TPV and ECO TPV in chemical stability, retaining low swelling even under aggressive conditions.

Second, TPV and especially ECO TPV are significantly more susceptible to acid-induced structural changes, reflecting the limitations of their thermoplastic phase.

Third, filler origin is decisive within ECO EPDM, with CCB EPDM demonstrating superior resistance to acid-driven swelling compared to RCB EPDM. These findings align with known mechanisms of sulfuric-acid degradation in unsaturated elastomers, driven by chain scission, oxidation, and filler-controlled diffusion pathways [136,139,160].

5.2.2 pH Evolution of Aging Media

The pH evolution of the sulfuric acid solutions was analyzed to assess the extent of chemical interaction between the elastomeric materials and their acidic environment during 1000 h of immersion at 90 °C. Measurements were performed for three concentrations of H_2SO_4 :0.001 M, 0.1 M, and 1 M. The solutions exhibited initial pH values of 2.24, 0.84, and 0.10. The final pH values reflect the degree of leaching, neutralization, or acid retention occurring during exposure, providing indirect insight into degradation dynamics and additive migration.

For EPDM-H, TPV, and ECO TPV, the initial and final pH values are summarized in Table 5-3. ECO TPV caused a slight increase in pH across all solutions after immersion, with values rising to 2.42 in the 0.001 M solution, 1.10 in the 0.1 M

BUPT

solution, and 0.37 in the 1 M medium. These modest increases indicate limited neutralization, consistent with a moderate level of ionic or basic species leaching from the material. TPV exhibited a similarly mild interaction: the 0.001 M solution experienced a small decrease in pH to 2.20, whereas the 0.1 M and 1 M solutions

Table 5-3. pH change for ECO TPV, EPDM H and TPV

Solution	Initial	after ECO TPV immersion (% increase)	after TPV immersion (% increase)	after EPDM immersion (% increase)
0.001M	2.24	2.42 (8%)	2.2 (-1.8%)	2.46 (9.9%)
0.1M	0.84	1.1 (31%)	1.12 (33.3%)	1.13 (34.5%)
1M	0.1	0.37 (270%)	0.36 (260%)	0.36 (260%)

[a] Samples aged in solutions at 90°C for 1000 h

increased slightly to 1.12 and 0.36, respectively. Among the three materials, EPDM-H induced the highest pH increases, with final values of 2.46 (0.001 M), 1.13 (0.1 M), and 0.36 (1 M), suggesting the presence of basic additives or degradation by-products released during immersion.

The notable pH increases in the 1 M solutions for all three materials—ECO TPV, TPV, and EPDM-H—reflect a dilution effect caused by the extraction of neutral or weakly basic constituents from the polymer matrices, which partially neutralize the strong acid [161]. These species likely originate from processing additives, stabilizers, or residual crosslinking agents that migrate into the aqueous phase during high-temperature immersion.

A similar evaluation was performed for the ECO EPDM formulations containing circular (CCB) and recycled (RCB) carbon black fillers. The initial pH values matched those described above (0.10, 0.84, and 2.24 for 1 M, 0.1 M, and 0.001 M H_2SO_4, respectively). After 1000 h of immersion, however, the two formulations produced distinctly different pH responses, which are detailed in Table 5-4. CCB EPDM caused a decrease in pH across all acid concentrations, reaching values of 0.00 (1 M), 0.47 (0.1 M), and 1.41 (0.001 M). This downward trend suggests either a net uptake of acid into the polymer matrix or a release of acidic groups from within the material, leading to increased proton concentration in the surrounding solution.

BUPT

Table 5-4. Initial and final pH values of sulfuric acid solutions (1 M, 0.1 M, 0.001 M) after 1000 h of immersion at 90 °C for CCB and RCB EPDM materials, along with the corresponding pH change (ΔpH), reproduced from [20]

Material Type	Acid Concentration	Initial pH	Final pH	ΔpH (Change %)
CCB EPDM	1 M	0.10	0.00	−0.10 (−100%)
CCB EPDM	0.1 M	0.84	0.47	−0.37 (−44.0%)
CCB EPDM	0.001 M	2.24	1.41	−0.83 (−37.1%)
RCB EPDM	1 M	0.10	0.32	+0.22 (+220.0%)
RCB EPDM	0.1 M	0.84	1.00	+0.16 (+19.0%)
RCB EPDM	0.001 M	2.24	2.51	+0.27 (+12.1%)

In contrast, RCB EPDM consistently increased the pH of the aging media. The 1 M solution rose from 0.10 to 0.32 (+220%), while the 0.1 M solution increased from 0.84 to 1.00 (+19.0%). Even in the weakest acid solution (0.001 M), the pH increased from 2.24 to 2.51 (+12.1%). These positive ΔpH values indicate the leaching of basic or buffering compounds, which neutralize a portion of the acid. This behaviour is consistent with the more heterogeneous surface chemistry of recycled carbon black, which may contain ash, metal oxides, or other alkaline residues originating from its recovery process.

The contrasting behaviours of CCB and RCB EPDM—pH decrease versus pH increase under identical conditions—highlight the strong influence of filler origin on chemical stability and leachate composition. CCB EPDM's pH-reducing effect aligns with a tighter filler–polymer interface and fewer alkaline impurities, whereas the alkalinity drift observed for RCB EPDM is consistent with the migration of residual basic species embedded within the recycled filler structure, as also suggested by its higher swelling and ionic release trends.

BUPT

5.2.3 Ionic Leaching Behavior (Hot Water Extraction Test)

The hot water extraction test (HWET) provides insight into the mobility of ionic species released from the elastomeric materials when exposed to neutral aqueous conditions. Electrical conductivity was monitored over 168 h to quantify the leaching of water-soluble compounds and to assess chemical stability under moisture-rich environments relevant to PEMFC operation.

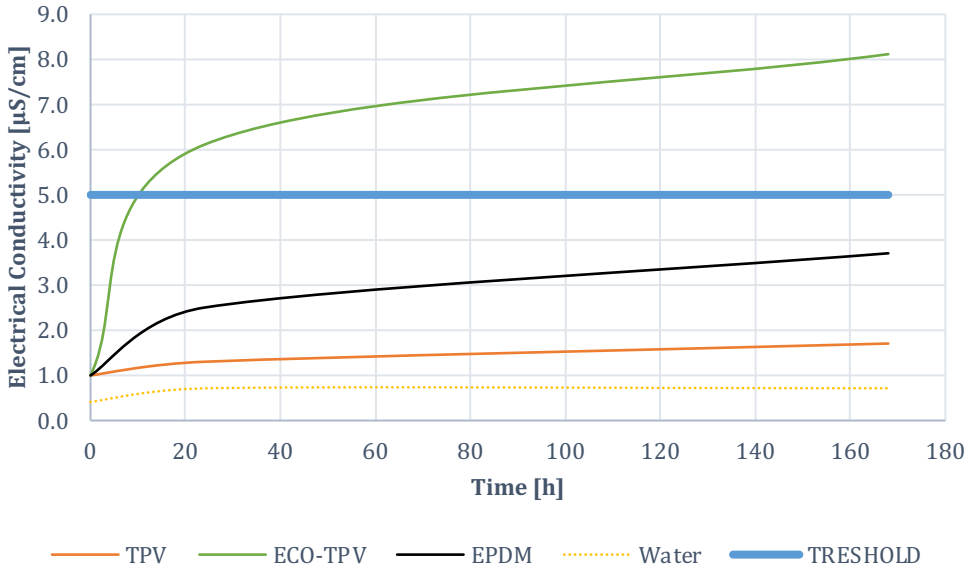


Figure 5.7. HWET result for EPDM-H, TPV and ECO-TPV

Figure 5.7 shows the evolution of conductivity for EPDM-H, TPV, ECO-TPV, and deionized water, the latter serving as the baseline reference. All materials exhibited an upward trend in conductivity during immersion at 80 °C, but the rate and magnitude of change varied significantly among the three systems. ECO-TPV showed the highest conductivity values throughout the experiment, surpassing the 5.0 µS/cm threshold within the first 20 h and continuing to rise toward approximately 8.0 µS/cm by 168 h. This elevated response indicates a greater susceptibility to ionic release, likely driven by the presence of more polar or ionizable domains in its hybrid thermoplastic–elastomeric architecture [162]. Such behavior aligns with established observations that materials containing polar fillers or additives exhibit enhanced ion mobility under hydrothermal conditions [163].

EPDM-H and TPV displayed more moderate conductivity profiles. EPDM-H crossed the 5 µS/cm threshold at approximately the 100-hour mark, signaling a significant release of extractable ionic species as immersion progressed. TPV remained below the threshold for the entire duration, despite showing a gradual increase in conductivity, indicating comparatively lower levels of leachable components. These differences reinforce the role of polymer polarity, filler–matrix compatibility, and crosslink density in controlling leaching behavior during prolonged water exposure.

BUPT

Complementary HWET analyses were performed on the two ECO EPDM formulations containing circular (CCB) and recycled (RCB) carbon black to evaluate the influence of filler origin on ionic mobility. The initial conductivity of the deionized water solutions was low (0.4 μS/cm for CCB and 0.6 μS/cm for RCB), confirming minimal background contamination. Upon immersion, both materials exhibited steady increases in conductivity (Figure 5.8), but the RCB formulation showed a markedly more rapid and intense response. After 168 h, the conductivity reached 5.5 μS/cm for CCB EPDM, while RCB EPDM attained 7.1 μS/cm, indicating significantly higher ionic release from the recycled-filler system.

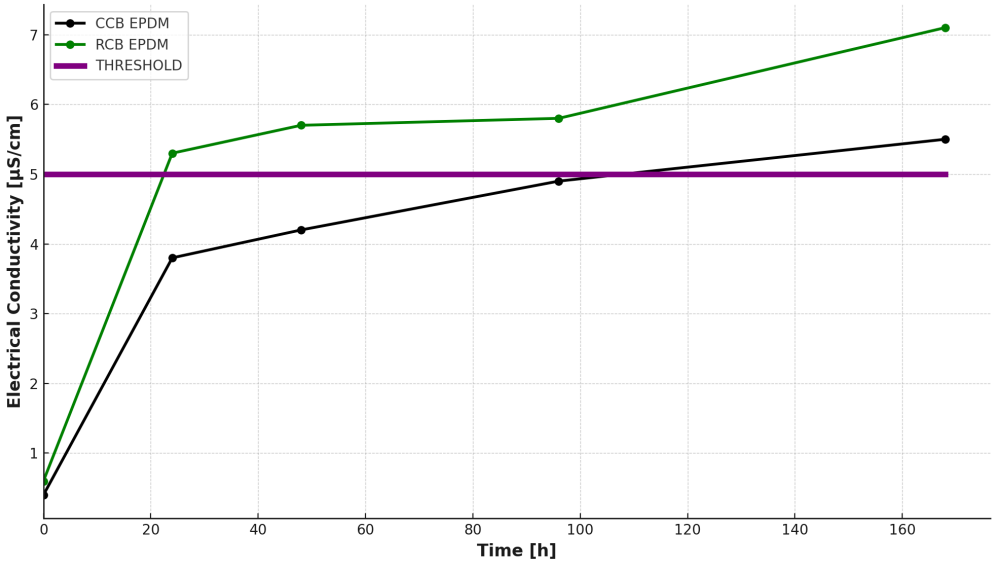


Figure 5.8. HWET result for CCB EPDM and RCB EPDM

The divergence in early-stage behavior is particularly notable. RCB EPDM exceeded the 5 μS/cm threshold [73] within the first 48 h, whereas CCB EPDM required 96 h to reach the same level. This accelerated rise in conductivity suggests that RCB EPDM contains a higher concentration of extractable ionic or polar constituents, likely arising from inherent impurities, ash content, or surface-active residues associated with recycled carbon black. These components are prone to migration under hydrothermal conditions, thereby increasing ionic leaching.

The HWET findings carry important implications for PEMFC sealing applications. Elevated ionic release may promote contamination of the membrane electrode assembly (MEA), alter local acid–base equilibration, or contribute to corrosion of adjacent metallic components. The faster and higher ionic mobility observed in RCB EPDM highlights its lower chemical stability relative to CCB EPDM, a conclusion that aligns closely with trends identified in swelling behavior and pH evolution. Collectively, these results confirm that RCB-filled EPDM is more reactive and permeable in aqueous environments, while CCB-filled EPDM maintains a more controlled leaching profile consistent with superior long-term chemical resilience.

BUPT

Discussion — Hot Water Extraction

The hot water extraction tests provide clear evidence that ionic leaching strongly depends on both the elastomer family and the filler system. ECO-TPV consistently exhibited the highest conductivity values, surpassing the 5 µS/cm threshold within the first 20 hours, confirming that its hybrid PP–rubber morphology and more polar additive profile favour rapid ionic mobility under hydrothermal conditions. EPDM-H showed moderate ionic release, crossing the threshold at around 100 hours, whereas TPV remained below it throughout the test, reflecting its lower content of extractable polar species. The ECO EPDM formulations revealed even more pronounced filler-driven effects: RCB EPDM displayed a substantially faster and higher conductivity rise than CCB EPDM, reaching 7.1 µS/cm at 168 hours and exceeding the 5 µS/cm limit within 48 hours, compared to 96 hours for CCB. This behaviour is consistent with the presence of residual impurities, ash, and surface-active functional groups commonly associated with recycled carbon black, which promote ion migration into the extraction medium. In contrast, CCB EPDM maintained slower, more controlled leaching, indicative of a cleaner, more uniform filler morphology. The collective results demonstrate that recycled-filler elastomers not only release more ionic species but also do so earlier during exposure, which may pose risks for PEMFC operation through membrane contamination, altered local pH environments, or corrosion of metallic components. Conversely, EPDM-H and especially CCB-based EPDM offer comparatively stable hydrothermal behaviour, reinforcing their suitability for long-term PEMFC sealing applications.

5.2.4 Thermal Behavior After Aging (DSC)

Differential scanning calorimetry was employed to evaluate the thermal transitions and potential degradation of the elastomeric systems after long-term exposure to acidic and thermal environments. Figure 5.10, Figure 5.9 and Figure 5.11 presens the DSC curves of TPV, ECO TPV, and EPDM-H in three conditions: as-delivered (AD, green), aged for 1000 h in 1 M H_2SO_4 (blue), and heat-aged for 1000 h at 90 °C (red). The TPV samples show a clear thermal transition in the AD state, followed by a slight shift after acid exposure and a more pronounced shift after thermal aging, indicating changes in crystallinity and possible matrix rearrangement. ECO TPV displays even more substantial modifications in its DSC profiles, with the most significant deviations occurring in the heat-aged samples, suggesting notable thermally driven degradation of both the PP matrix and the elastomeric phase. By contrast, EPDM-H exhibits minimal differences among AD, acid-aged, and heat-aged curves, reflecting its inherently stable saturated backbone and superior resistance to oxidative and acid-catalysed degradation.

This behaviour contrasts with the ECO EPDM systems examined in the dedicated chemical-aging study. Representative thermograms for CCB and RCB EPDM are shown in Figure 5.12. For both materials, the primary thermal event is the glass transition temperature (Tg), located between −45 °C and −50 °C. The fresh CCB EPDM shows a Tg of approximately −49.1 °C, which remains essentially unchanged after 1000 h in 1 M H_2SO_4 (−48.9 °C). The close overlap of the fresh and aged curves indicates that neither plasticization nor significant chain scission occurred, and the filler–matrix network retained its integrity under acidic exposure. In contrast, RCB EPDM shows a small downward Tg shift from −47.3 °C to −48.5 °C after aging. Although subtle, this shift suggests a slight increase in chain mobility, potentially arising from minor polymer chain scission or migration of low-molecular-weight

BUPT

residues—an interpretation consistent with the higher ionic leaching and greater pH drift observed for RCB in the HWET and pH tracking results.

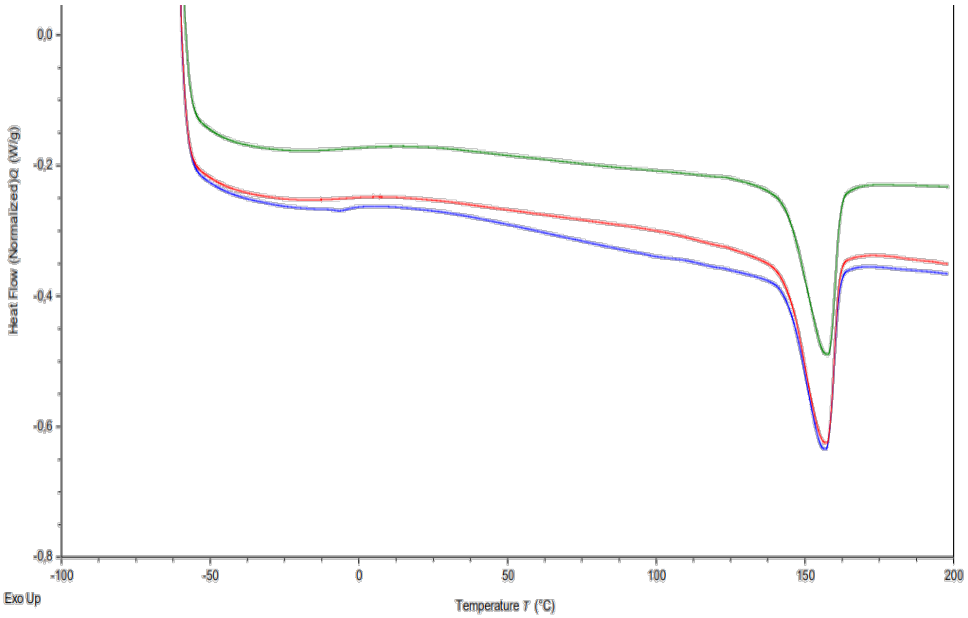


Figure 5.10. DSC curves for TPV

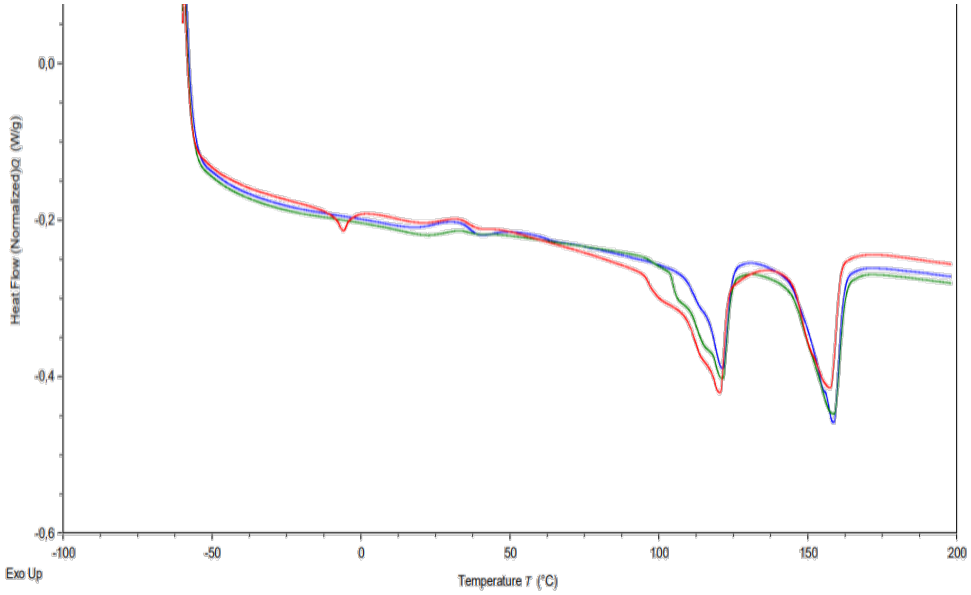


Figure 5.9. DSC curves for ECO TPV

BUPT

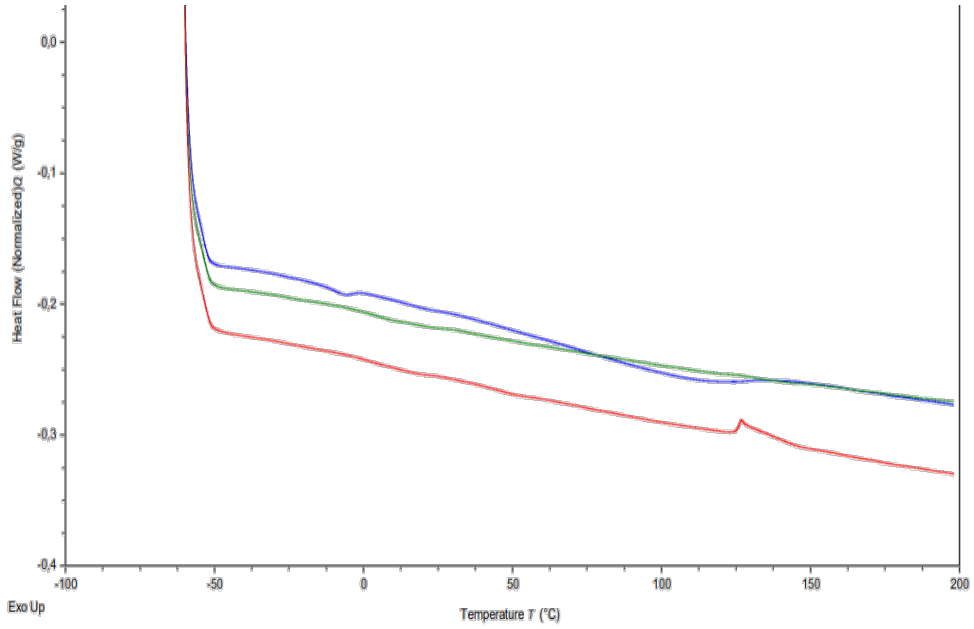


Figure 5.11. DSC curves for EPDM-H

All EPDM-based materials (EPDM-H, CCB EPDM, and RCB EPDM) exhibited secondary endothermic features between 20 °C and 50 °C. These events are typically associated with the melting of paraffinic waxes, processing aids, or low-molecular-weight fractions commonly used in rubber compounding [6]. Although these transitions do not indicate major phase changes, their slight shifts after aging may suggest minor additive redistribution or surface-active component migration—effects more evident in RCB EPDM due to its more heterogeneous filler architecture.

Taken together, the DSC results clearly distinguish the thermal stabilities of the studied elastomers. EPDM-H and CCB EPDM retain stable Tg positions and consistent thermograms across all aging conditions, confirming their strong resistance to thermochemical degradation. RCB EPDM shows small but meaningful deviations associated with filler-related microstructural variability and increased susceptibility to acid-catalysed changes. TPV and ECO TPV exhibit the largest thermal shifts, particularly in heat-aged states, reflecting the higher reactivity and reduced structural resilience of their thermoplastic matrix components. Overall, the DSC data reinforce the superior thermomechanical stability of EPDM-based systems—especially those reinforced with circular carbon black—under representative fuel-cell-like chemical and thermal stress.

BUPT

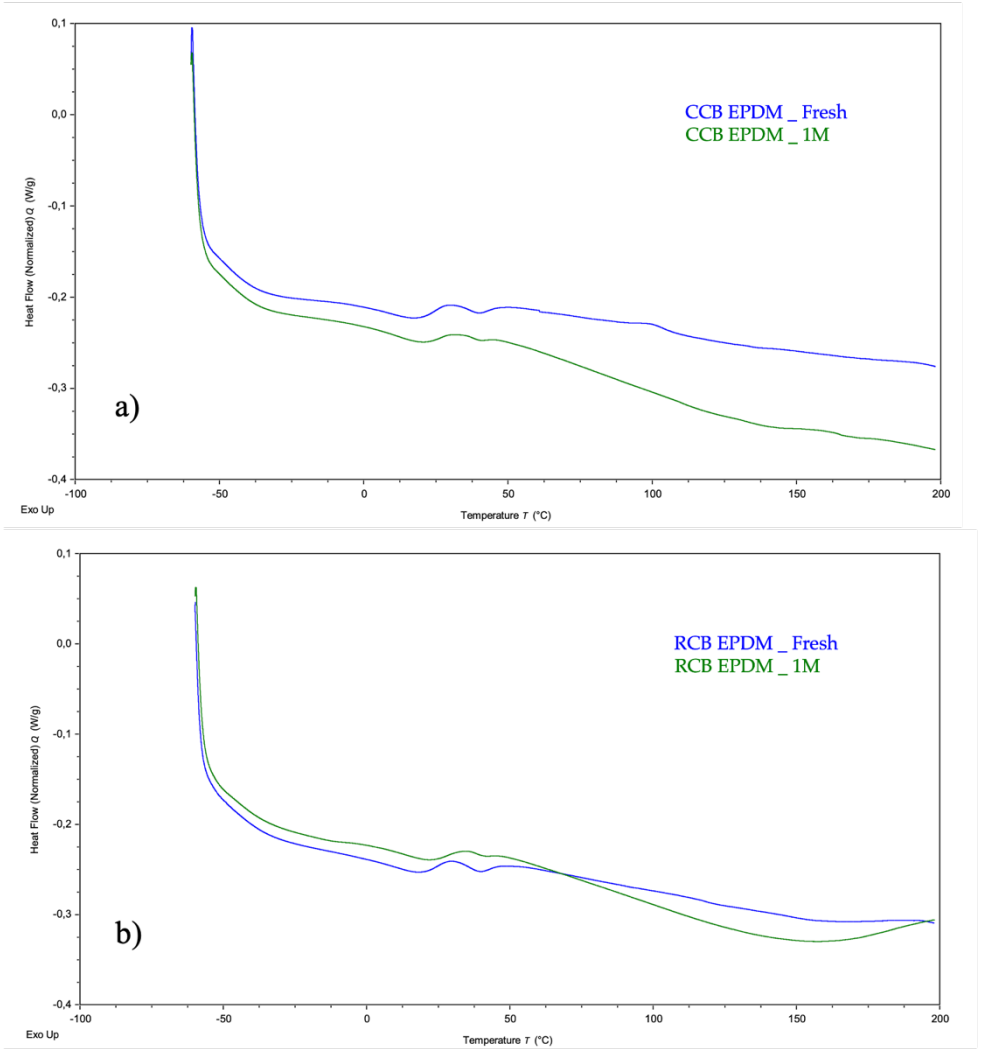


Figure 5.12. DSC thermograms of CCB EPDM (a) and RCB EPDM (b) before and after chemical aging in 1 M H_2SO_4 at 90 °C for 1000 h

5.2.5 Organic Leachate Profiles (HPLC-DAD) — ECO EPDM

High-performance liquid chromatography coupled with diode-array detection (HPLC-DAD) was used exclusively for the ECO EPDM materials—namely the CCB- and RCB-filled formulations—to characterize the organic species released into sulfuric acid solutions after long-term exposure. The analysis was performed at 230 nm, a wavelength commonly selected for detecting unsaturated, aromatic, or partially oxidized organic moieties in elastomer leachates. Both EPDM variants were immersed in H_2SO_4 solutions of 0.001 M, 0.1 M, and 1 M at 90 °C for 1000 h, after which the

BUPT

resulting aqueous phases were analyzed to quantify the extent of organic migration and to compare formulation-dependent degradation behavior.

Figure 5.13 presents the HPLC-DAD chromatograms at 230 nm for the leachates corresponding to each acid concentration: (a) 0.001 M, (b) 0.1 M, and (c) 1 M H_2SO_4. Solid curves represent CCB EPDM, whereas dashed curves represent RCB EPDM. Across all conditions, both the number and intensity of chromatographic peaks differed substantially between the two materials, demonstrating strong filler-dependent effects on leachable species release.

At 0.001 M H_2SO_4 (Figure 5.13a), RCB EPDM exhibited a larger total chromatographic area and more intense peaks than the CCB formulation. The most prominent RCB peaks occurred at retention times (RT) 4.651 min (482.73 mAU·min), 5.131 min (751.70 mAU·min), and 6.357 min (602.13 mAU·min). Although the CCB material displayed peaks at similar retention times—4.661 min (431.85 mAU·min), 5.135 min (742.46 mAU·min), and 6.137 min (262.46 mAU·min)—their cumulative intensities were lower, indicating reduced leaching of UV-active organics.

At 0.1 M H_2SO_4 (Figure 5.13b), both materials showed higher overall peak intensities relative to the 0.001 M case. RCB EPDM again produced the strongest signals, including peaks at RT 4.658 min (1358.91 mAU·min) and 5.138 min (833.13 mAU·min). CCB EPDM also showed increased leaching, with notable peaks at RT 4.652 min (850.26 mAU·min) and 5.134 min (603.79 mAU·min), but the total leachate intensity remained lower than RCB.

A markedly different trend emerged at 1 M H_2SO_4 (Figure 5.13c). Here, the CCB formulation produced the highest peak areas, particularly at RT 4.685 min (1235.30 mAU·min) and 5.262 min (1158.85 mAU·min), giving a total area of 2980.14 mAU·min—substantially exceeding the RCB value of 1910.97 mAU·min. In the RCB samples, the major peaks at RT 4.683 min (922.12 mAU·min) and 5.250 min (757.07 mAU·min) were lower in intensity compared to the CCB material. This inversion suggests that, under strongly acidic conditions, the more uniform CCB filler network may become susceptible to accelerated additive or oligomer migration.

An important observation is the decline in total peak area for RCB EPDM at 1 M H_2SO_4 compared to 0.001 M and 0.1 M. Several mechanisms may explain this counterintuitive effect. First, severe acid exposure may fragment extractable organics into low-molecular-weight species that are not UV-active at 230 nm or fall below the DAD detection threshold. Second, strong acid environments may promote matrix densification or the formation of a passivated surface layer, reducing further leachate transport. Such behaviour has been reported in degradation studies of filled elastomers, where higher chemical aggressiveness does not necessarily yield higher extractable content due to secondary degradation phenomena and matrix collapse [7,8]. These findings highlight the complexity of leaching mechanisms in carbon-black-reinforced elastomers and underscore the need for higher-resolution analytical techniques such as HPLC–MS or GC–MS for structural identification of the degradation products [4,9].

BUPT

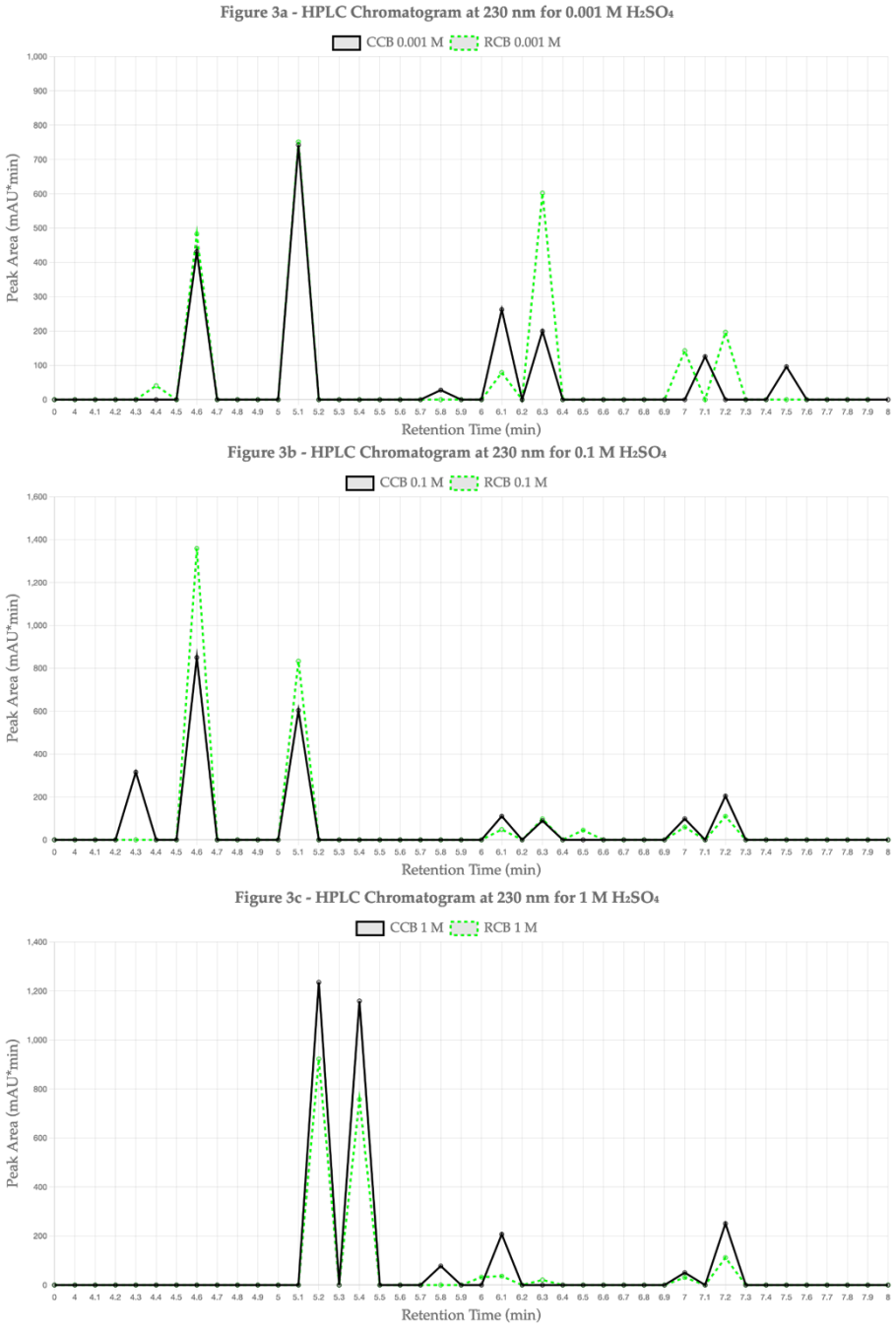


Figure 5.13. HPLC chromatograms at 230 nm for CCB and RCB EPDM samples extracted in (a) 0.001 M H_2SO_4, (b) 0.1 M H_2SO_4, and (c) 1 M H_2SO_4 for 1000 hours at 90 °C. Solid black lines represent CCB, and dashed green lines represent RCB [23]

BUPT

Table 5-5 summarizes the HPLC-DAD results, listing total peak areas and the number of peaks exceeding 100 mAU·min for each material and acid concentration. The data confirm that RCB EPDM releases more organic compounds under mild to moderate acidity, whereas CCB EPDM leaches more heavily under strongly acidic environments. This behaviour reflects fundamental differences in filler morphology, surface activity, and residual contaminant content.

Table 5-5. HPLC-DAD Results (230 nm). extracted in 0.001 M H_2SO_4, 0.1 M H_2SO_4, and 1 M H_2SO_4 for 1000 hours at 90 °C, taken from [23]

Material	Acid Concentration	Total Area (mAU*min)	% Change vs. CCB	Number of Peaks > 100 mAU*min
CCB EPDM	0.001 M	1872.06	–	5
RCB EPDM	0.001 M	2295.08	+22.6%	5
CCB EPDM	0.1 M	2271.69	–	6
RCB EPDM	0.1 M	2529.74	+11.4%	3
CCB EPDM	1 M	2980.14	–	4
RCB EPDM	1 M	1910.97	-35.9%	3

[23] provides a visual comparison of the total peak area across acid concentrations, reinforcing the inversion trend: greater RCB leaching at 0.001-0.1 M and greater CCB leaching at 1 M.

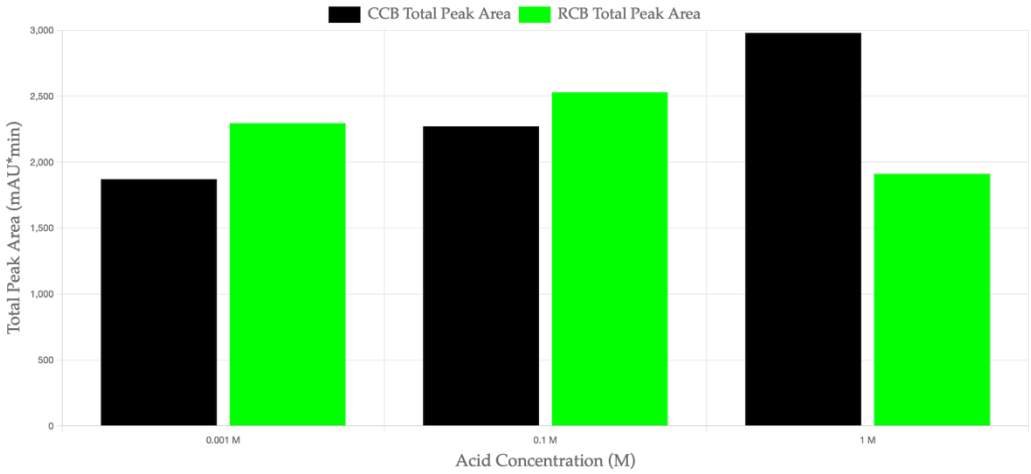


Figure 5.14. Total peak area (mAU·min) of leachates from CCB and RCB EPDM samples in sulfuric acid solutions of varying concentrations (0.001 M, 0.1 M, and 1 M for 1000 hours at 90 °C) as in

Together, the HPLC-DAD results demonstrate that filler origin plays a decisive role in controlling the migration of organic species from ECO EPDM materials under acidic exposure. RCB, due to its more heterogeneous recycled-filler surface chemistry,

BUPT

is more prone to organic release in milder acids, while CCB becomes more reactive under high-acidity conditions. These findings complement the swelling, pH drift, and HWET conductivity results and provide a molecular-level perspective on how filler structure influences chemical stability in fuel-cell-relevant acidic environments.

5.2.6 Tensile Behavior After Chemical and Thermal Aging

The tensile behavior of all investigated elastomeric systems—EPDM-H, TPV, ECO TPV, and the two ECO EPDM grades (CCB and RCB)—was evaluated under as-delivered and aged conditions (chemical and thermal). The results for EPDM-H, TPV, and ECO TPV are summarized in Table 5-6. Tensile testing results and illustrated in Figure 5.16, Figure 5.15, Figure 5.17 and Figure 5.18, while the ECO EPDM tensile response is presented in Figure 5.19 and Figure 5.20.

Table 5-6. Tensile testing results for EPDM-H, TPV and ECO-TPV

MATERIAL	EPDM				
Sample State	AD[a]	HE[b]	1M[c]	0.1M[d]	0.001M[e]
Tensile Strength (MPa)	18.84	16.7	17.8	18.1	17.95
Elongation at break (%)	187	163	180	182	183
Modulus at 100% elongation (MPa)	9.05	9.2	8.57	8.86	8.47
MATERIAL	TPV				
Tensile Strength (MPa)	10.449	10	10.58	10.3	9.34
Elongation at break (%)	500	472	511	501	487
Modulus at 100% elongation (MPa)	4.937	5.109	4.917	4.651	4.481
MATERIAL	ECO TPV				
Tensile Strength (MPa)	7.85	7.32	7.35	7	7.148
Elongation at break (%)	519	467	479	481	473
Modulus at 100% elongation (MPa)	3.77	3.87	3.76	3.43	3.503

[a] Samples as delivered; [b]Heat aged at 90°C for 1000 hours samples; [c]samples aged in 1M H_2SO_4 at 90°C for 1000 h; [d]samples aged in 0.1M H_2SO_4 at 90°C for 1000 h; [e]samples aged in 0.001M H_2SO_4 at 90°C for 1000 h

BUPT

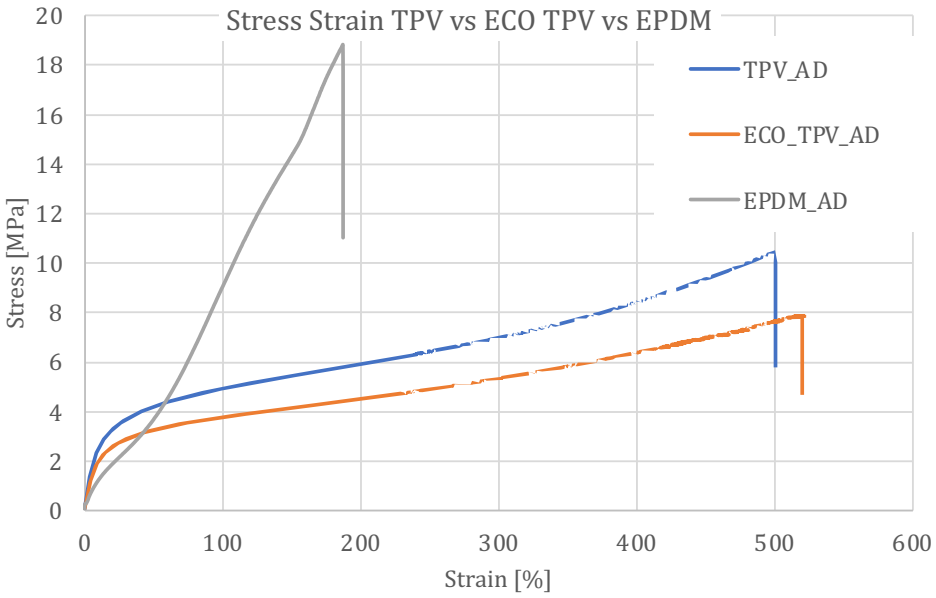


Figure 5.16. Stress-strain curves for as delivered (AD) samples of TPV, ECO TPV and EPDM-H [19]

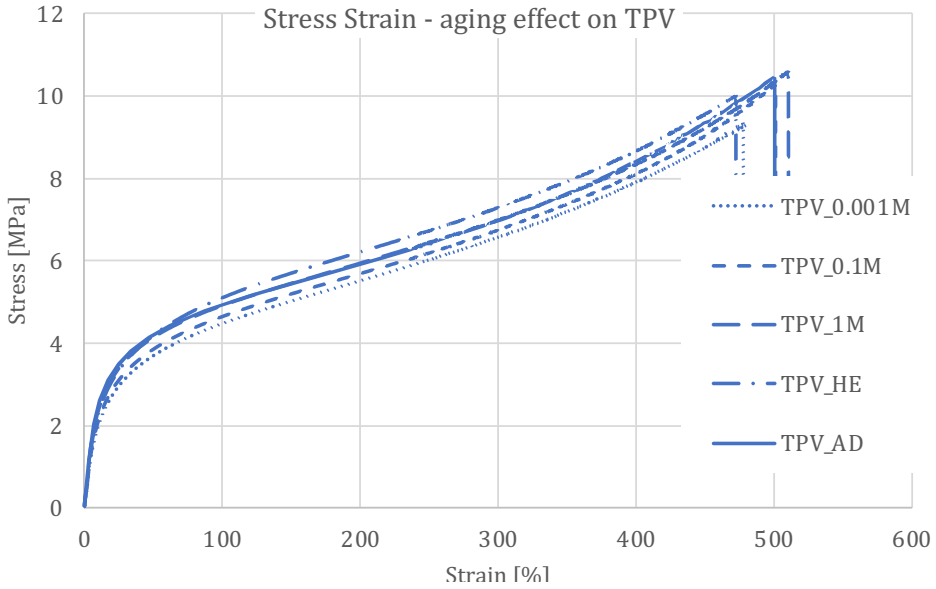


Figure 5.15. Stress-Strain behavior of TPV samples under different aging conditions. [19]

BUPT

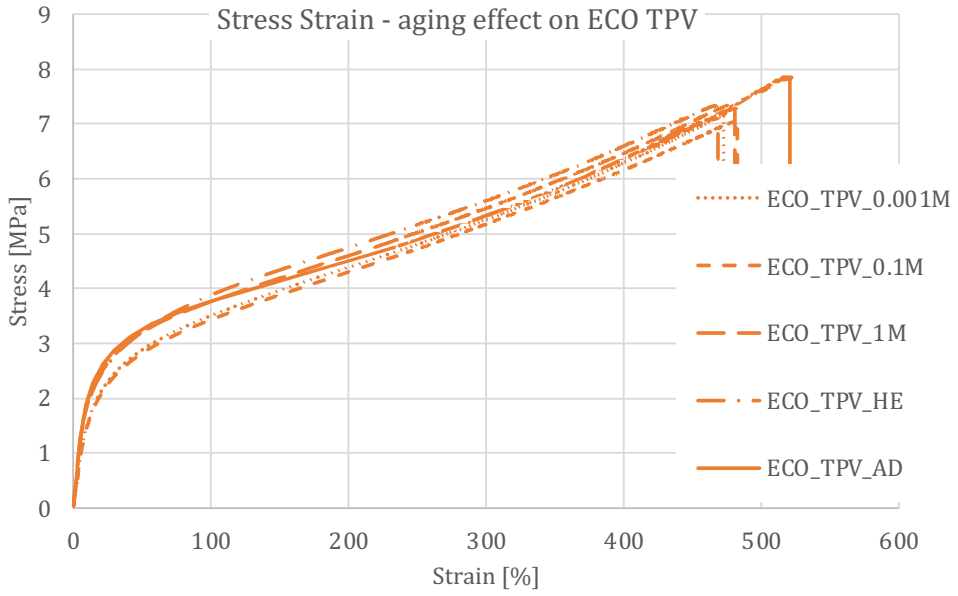


Figure 5.17. Stress Strain curves of ECO TPV under different aging conditions [19]

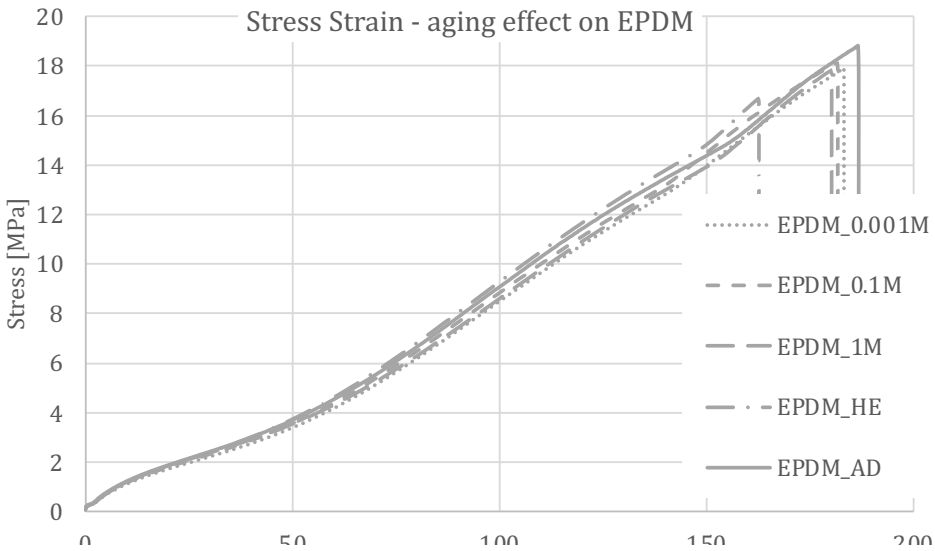


Figure 5.18. Stress Strain curves for EPDM-H under different aging conditions [19]

BUPT

For EPDM-H, tensile strength values ranged from 16.7 MPa to 18.84 MPa across the different aging treatments, with the highest strength observed in the as-delivered (AD) state (18.84 MPa) and the lowest recorded after heat aging (HE) at 90 °C for 1000 h (16.7 MPa). Correspondingly, elongation at break decreased from 187% in the AD state to 163% after thermal exposure. Despite these reductions, the modulus at 100% elongation remained relatively stable between 8.47 and 9.2 MPa, indicating that the overall stiffness of the EPDM-H network was only marginally affected. The stress–strain curves in Figure 5.18 show the sharp peak and robust resistance to deformation characteristic of EPDM-H, reflecting its saturated backbone and stable crosslink density.

For TPV, tensile strengths were between 9.34 and 10.58 MPa, with the highest values measured in the AD state. Elongation at break ranged from 470% to 500%, demonstrating the intrinsically high ductility of the PP–EPDM blend structure. Although aging in sulfuric acid (1 M, 0.1 M, and 0.001 M) and thermal aging produced slight decreases in tensile strength (Figure 5.15), elongation remained remarkably consistent, indicating that TPV's flexibility is retained even under chemically aggressive conditions. Modulus values showed limited fluctuation (4.481–5.109 MPa), suggesting minor alterations in crystallinity or crosslink density. Overall, TPV maintained a balanced mechanical response, though with moderate sensitivity to acid-induced chain relaxation or PP-phase softening.

In the case of ECO TPV, tensile strength decreased from 7.85 MPa in the AD state to approximately 7.14 MPa after chemical aging, while elongation at break varied between 467% and 519%. As shown in Figure 5.17, chemical exposure—especially in higher acid concentrations—reduced strength but did not significantly impact ductility, which remained stable across all conditions. The modulus at 100% elongation was the lowest among the three base materials, ranging from 3.43 to 3.87 MPa, consistent with ECO TPV's softer, more compliant morphology. These results indicate that while the "Eco" variant sacrifices some mechanical strength, it displays more uniform behavior under aging, suggesting comparatively improved resistance to chemical degradation of its PP and EPDM phases.

Figure 5.18 provides the corresponding stress–strain curves for EPDM-H in its aged conditions. Even after prolonged exposure to sulfuric acid or elevated temperatures, EPDM-H retained its characteristic high tensile strength and robust deformation behavior. Only samples aged in stronger acidic media exhibited modest reductions, confirming EPDM-H's well-documented chemical resilience.

The tensile properties of the two ECO EPDM systems—CCB EPDM and RCB EPDM—were assessed in fresh, thermally aged, and chemically aged states. Figure 5.19 presents the representative stress–strain curves averaged across replicates.

In the fresh state, RCB EPDM exhibited ~12 % higher tensile strength than CCB EPDM but ~25 % lower elongation at break, indicating a stiffer yet more brittle network. This behavior is consistent with the more variable morphology and higher aggregate rigidity typically associated with recycled carbon black. After thermal aging at 90 °C, both materials showed loss of strength and ductility; however, RCB EPDM experienced a much stronger degradation, with elongation decreasing by more than 40 %, whereas CCB EPDM retained over 70 % of its original ductility.

Chemical aging led to concentration-dependent degradation. In 1 M H_2SO_4, CCB EPDM preserved approximately 83 % of its original strength, whereas RCB EPDM declined to ~68 %, accompanied by a 30–35 % reduction in elongation. At 0.1 M, the

BUPT

performance divergence widened substantially: RCB EPDM lost nearly 45 % of its tensile strength and exhibited brittle failure, while CCB EPDM showed only moderate strength loss (~20 %) and maintained smoother stress–strain transitions. At 0.001 M, mechanical degradation was limited, but RCB EPDM still showed noticeable softening and increased variability, while CCB EPDM preserved more than 90 % of its tensile performance.

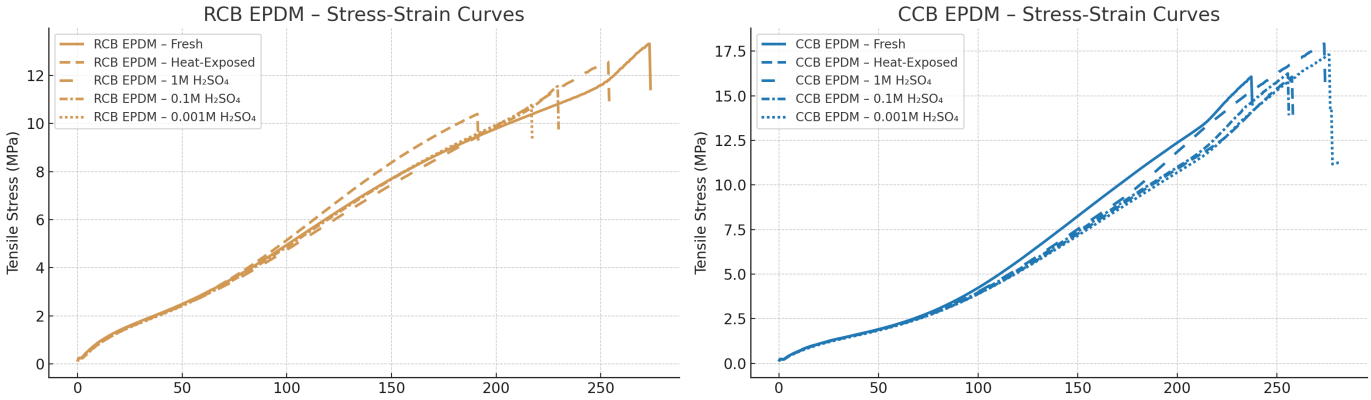


Figure 5.19. Stress-Strain respons of RCB EPDM (left) and CCB EPDM (right), in fresh, heat-aged and acid-aged conditions [22]

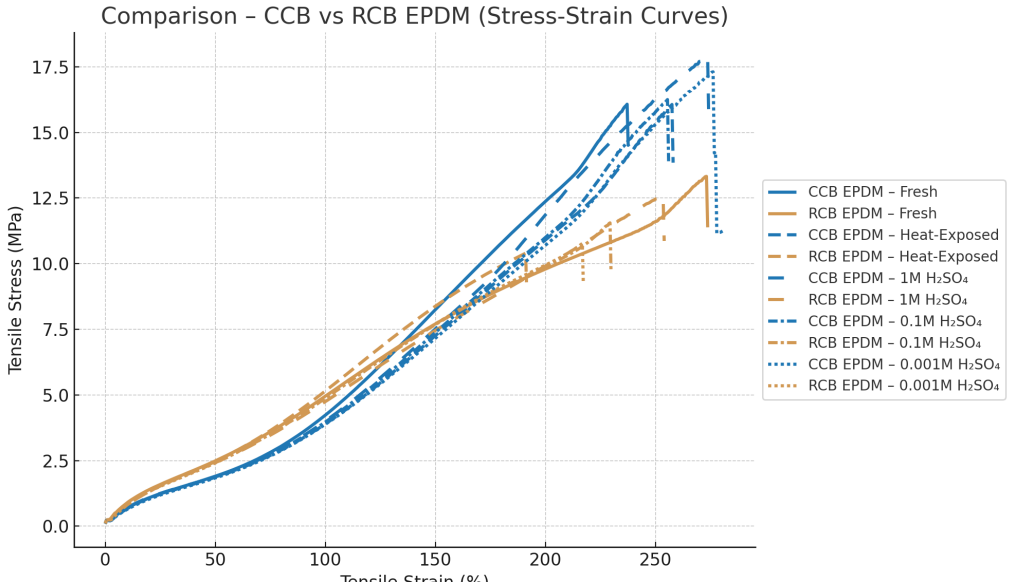


Figure 5.20. Comparative stress-strain behavior of CCB EPDM and RCB EPDM in fresh, heat-aged and acid-aged states [22]

BUPT

Figure 5.20 clearly illustrates the different degradation pathways: CCB EPDM retains a consistent curve shape and gradual failure mode across all environments, whereas RCB EPDM develops steeper initial slopes, abrupt fracture points, and pronounced scatter in the aged conditions.

Standard deviations highlight these distinctions. CCB EPDM showed low variability (0.15–0.3 MPa in the elastic region, <8 % in elongation at break), indicating a stable and uniform filler–matrix network. RCB EPDM exhibited significantly higher scatter under chemical aging (>0.5 MPa variation, large spread in failure strain), further validating the presence of microstructural inconsistencies and increased susceptibility to acid-driven embrittlement.

Discussion of Tensile Behavior Under Acid Exposure

The tensile results clearly demonstrate that the mechanical integrity of the elastomers is strongly dependent on both the polymer system and the severity of the acidic environment. EPDM-H showed the highest resistance to tensile degradation, maintaining tensile strengths between 16.7 and 18.84 MPa and preserving most of its elongation, even after immersion in 1 M H_2SO_4 for 1000 h. The modest decrease in tensile strength and elongation—particularly in the heat-aged and highly acidic conditions—indicates that the EPDM network experiences limited chain scission or crosslink destabilization under acid attack. Its stress–strain curves retained a characteristic steep rise and smooth failure transition, underscoring the robustness of its saturated backbone and peroxide-cured network. By contrast, TPV and ECO TPV exhibit noticeably greater sensitivity to acidic aging. Although their elongation at break remained high (≈470–500% for TPV and 467–519% for ECO TPV), their tensile strength decreased gradually with increasing acid concentration. This suggests selective degradation of the polypropylene continuous phase, which compromises load-bearing capacity while the elastomeric domains still provide extensibility. ECO TPV, starting from the lowest baseline strength, demonstrated the greatest fractional loss under acid exposure, especially at 1 M H_2SO_4, confirming that its modified formulation sacrifices some mechanical durability in exchange for improved environmental sustainability.

In the case of the ECO EPDM formulations, tensile behavior under acid aging revealed substantial formulation-dependent differences. Although RCB EPDM exhibited slightly higher initial tensile strength than CCB EPDM, it also suffered more severe performance losses under both thermal and chemical aging. After immersion in 1 M H_2SO_4, RCB EPDM lost approximately one-third of its initial tensile strength and experienced a 30–35% reduction in elongation, whereas CCB EPDM retained roughly 83% of its original strength and preserved much smoother stress–strain transitions. At intermediate acid concentrations (0.1 M), this divergence became even more pronounced: RCB EPDM displayed brittle, abrupt failure and large variability between replicates, while CCB EPDM showed only moderate softening. These behaviors reflect fundamental differences in filler morphology and matrix–filler interaction: the recycled carbon black in RCB EPDM introduces greater structural heterogeneity, allowing deeper acid ingress and promoting local chain scission, whereas the circular carbon black in CCB EPDM provides a more uniform reinforcing network that stabilizes the material under prolonged acidic attack. Together, these results highlight that while all EPDM-based materials outperform TPV systems in mechanical retention, the choice of filler—recycled versus circular carbon black—plays a decisive role in determining

BUPT

the tensile durability of sustainable EPDM compounds in fuel-cell-relevant acidic environments.

5.2.7 Hardness and Microhardness Changes

Figure 5.21 presents the evolution of Shore A hardness and micro-hardness (mIRHD) for EPDM-H, TPV, and ECO TPV in the as-delivered (AD) state and after immersion in sulfuric acid solutions of varying concentrations (0.001 M, 0.1 M, and 1 M) for 1000 h at 90 °C. Clear differences in the aging response emerge across the three materials. TPV retains the highest hardness among all samples, with less than a 5 % decrease in Shore A hardness under any conditioning environment and mIRHD values remaining above 88, demonstrating strong resistance to both chemical attack and thermal degradation. EPDM-H shows moderate changes, with a Shore A decrease of approximately 7–10 % and mIRHD values stabilizing in the 80–85 range, confirming partial but controlled softening under acidic exposure. By contrast, ECO TPV undergoes the largest hardness reduction, with Shore A values dropping by as much as 15–20 % and mIRHD falling to approximately 78–80, particularly in the higher-acidity media. These reductions reflect more significant matrix softening and structural relaxation in ECO TPV compared to TPV and EPDM-H.

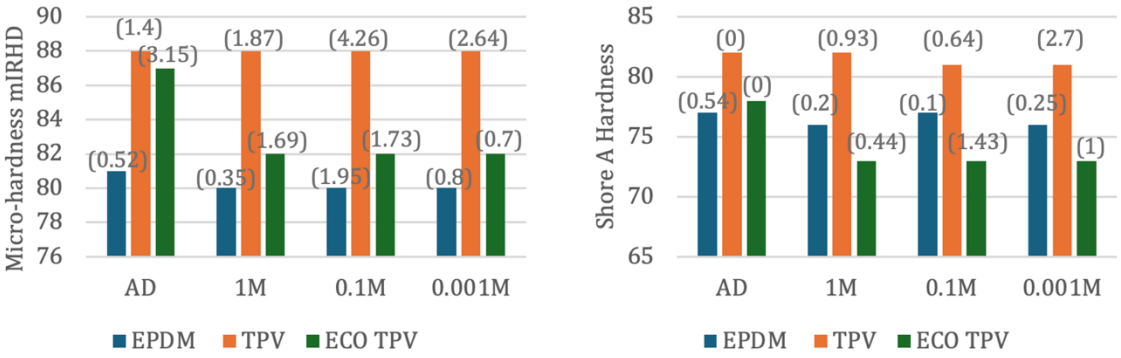


Figure 5.21. Shore A Hardness change of the samples (left) and micro-hardness mIRHD (right). The standard deviation σ is written in parentheses. Taken from [20]

A more detailed assessment of the two sustainable EPDM formulations is provided in Figure 5.22, which highlights the Shore A and IRHD micro-hardness changes for CCB EPDM and RCB EPDM after immersion in sulfuric acid and after thermal exposure. In the fresh state, RCB EPDM exhibits higher absolute hardness values—approximately 72 Shore A and 76 IRHD—relative to CCB EPDM, which measures around 63 Shore A and 71 IRHD. This initial difference reflects the intrinsically stiffer and more rigid network structure associated with recycled carbon black. After exposure to 1 M H_2SO_4, both materials softened slightly in IRHD while maintaining relatively stable Shore A values. CCB EPDM increased modestly to 67 Shore A and 73.5 IRHD, whereas RCB EPDM displayed stable Shore A hardness (~72) and a slight IRHD increase (76.5). Interestingly, CCB EPDM maintained stable Shore A hardness across all acid concentrations, while RCB EPDM showed a minor dip at 0.1 M H_2SO_4, indicating a slightly higher susceptibility to acid-induced surface softening.

BUPT

Following heat aging at 90 °C for 1000 h, both EPDM grades exhibited partial hardness recovery: CCB EPDM increased to approximately 69 Shore A and 72 IRHD, while RCB EPDM reached 73 Shore A and 75.5 IRHD, suggesting thermally induced re-ordering or post-curing effects in both materials.

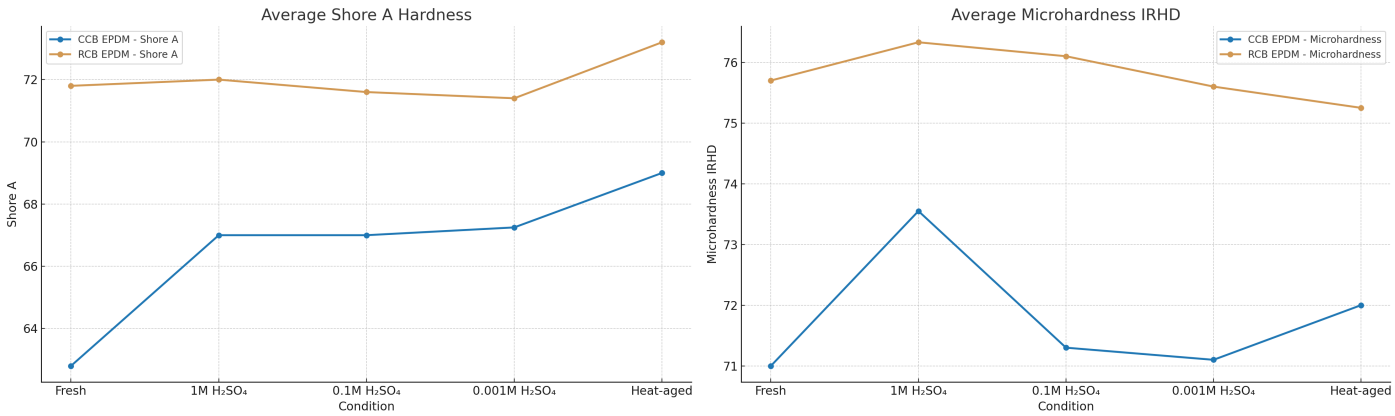


Figure 5.22. Average Shore A hardness (left) and IRHD microhardness (right) of CCB EPDM and RCB EPDM under fresh, heat-aged, and acid-aged conditions (1 M, 0.1 M, and 0.001 M H_2SO_4, 90 °C, 1000 h) [22]

5.2.8 Compression Set

Figure 5.23 presents the compression set values of EPDM-H, TPV, and ECO TPV after prolonged deformation under standardized conditions. Among the three materials, EPDM-H exhibits the lowest compression set, confirming its excellent ability to recover its original shape after sustained compressive loading. This behavior is fully consistent with the tensile test results, where EPDM-H also demonstrated the highest tensile strength and elongation at break. Together, these findings indicate a highly elastic, stable, and resilient network structure capable of maintaining sealing force even after long-term mechanical stress.

In contrast, ECO TPV records the highest compression set, revealing a substantially reduced recovery capability. This outcome aligns with its lower tensile strength and elongation values, suggesting that its thermoplastic–elastomeric microstructure undergoes a greater degree of permanent deformation. TPV shows intermediate compression set values, reflecting a balanced performance between EPDM-H and ECO TPV. Its moderate behavior matches its mechanical profile, where TPV maintains good elasticity but is more prone to permanent deformation compared to EPDM-H.

Overall, the compression set analysis further reinforces the superior elastic recovery and long-term sealing stability of EPDM-H, the moderate recovery behavior of TPV, and the lower deformation resilience of ECO TPV.

BUPT

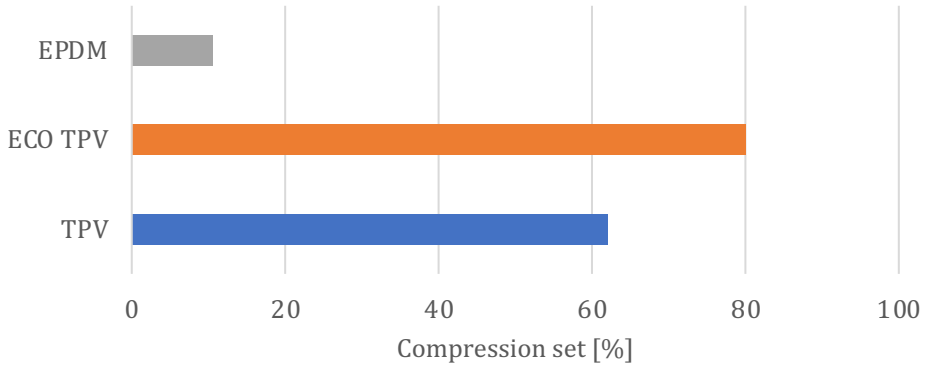


Figure 5.23. Compression set values for EPDM-H, TPV and ECO-TPV, taken from [19]

5.2.9 Microstructural and Chemical Surface Evolution (SEM / SEM-EDS)

Figure 5.24 presents SEM micrographs of EPDM-H, TPV, and ECO TPV in the as-delivered (AD), acid-aged, and heat-aged states, offering direct visual evidence of surface degradation mechanisms across the different material classes. In the AD condition, all three materials exhibit relatively smooth, defect-free surfaces with well-distributed filler domains and minimal microstructural irregularities. This baseline appearance reflects intact polymer–filler networks and confirms that no pre-existing degradation features were present prior to aging.

Following immersion in H_2SO_4 for 1000 h at 90 °C, all materials exhibit clear signs of chemical attack, though the severity varies strongly with formulation. ECO TPV shows the most pronounced changes, with visible micro-cracks, surface roughening, and localized erosion zones. These features are indicative of acid-induced degradation of both the thermoplastic and elastomeric phases, consistent with the material's higher swelling, conductivity, and hardness loss. TPV also exhibits notable deterioration, including shallow cracking and surface waviness, reflecting partial softening of the PP-rich matrix and disruption of the EPDM dispersed phase. EPDM-H displays the mildest changes, with only a modest increase in roughness and small isolated micro-fissures, further supporting its superior chemical stability demonstrated in swelling, pH, and mechanical tests.

A similar trend is observed in the heat-aged samples. Prolonged thermal exposure leads to surface embrittlement, crack formation, and minor delamination across all materials. ECO TPV again shows the most severe thermal degradation, while TPV undergoes moderate surface stiffening and fissuring. EPDM-H remains the most resistant, exhibiting only slight texture changes and limited micro-crack development, consistent with its stable hardness and mechanical retention.

BUPT

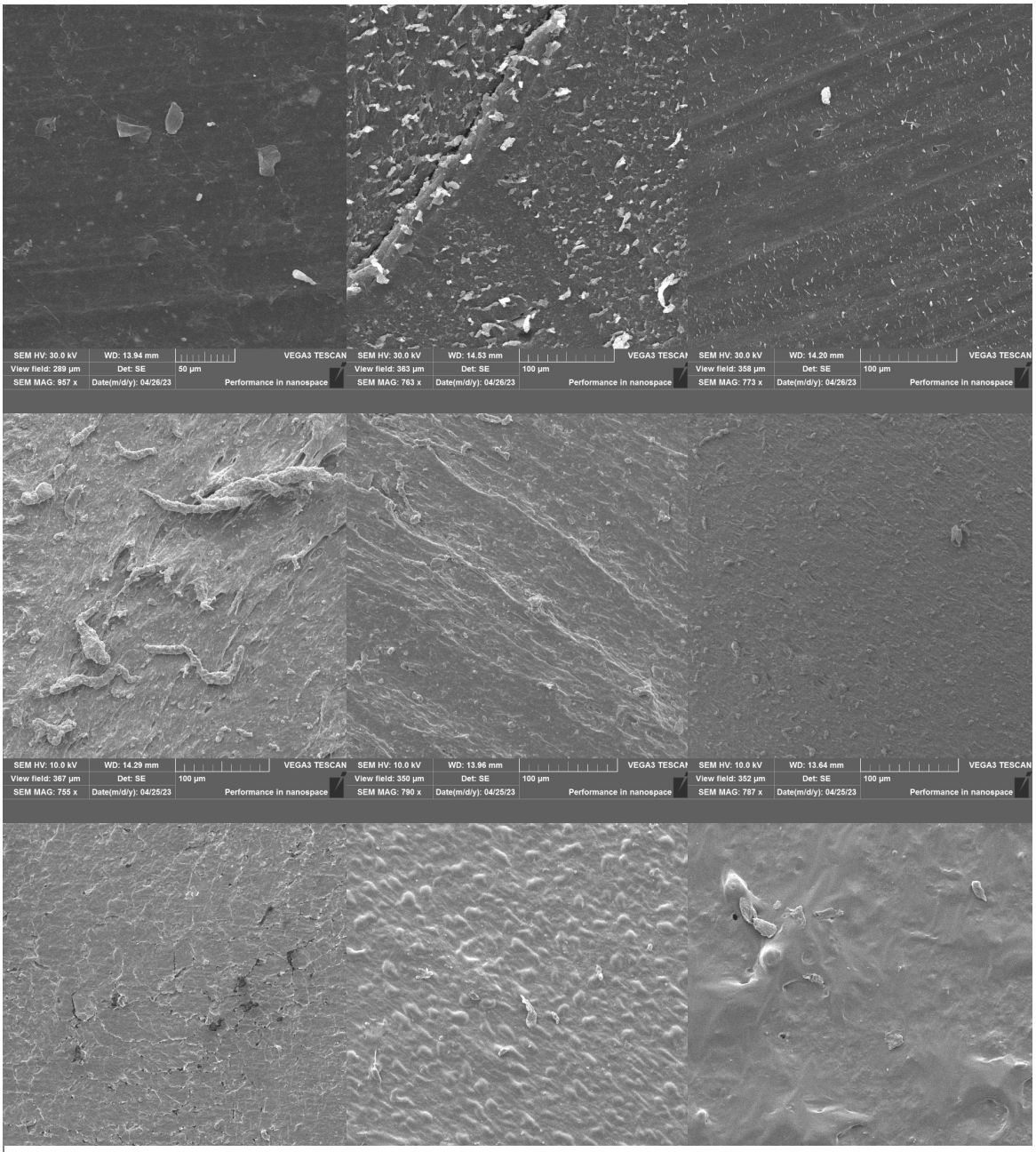


Figure 5.24. SEM images showing the surface of the studied samples. First row: EPDM AD (left), EPDM Heat Aged (center), EPDM aged in 1M (right); second row: TPV AD (left), TPV Heat Aged (center), TPV aged in 1M (right); third row: ECO TPV AD (left), ECO TPV, taken from [20]

BUPT

Complementing these observations, Figure 5.25 provides high-magnification SEM images of CCB and RCB ECO EPDM, revealing critical filler-dependent differences. Fresh CCB EPDM displays a smooth surface with uniform filler dispersion, whereas fresh RCB EPDM shows a visibly more open and heterogeneous filler structure, including discrete pores and loosely packed carbon black clusters. After exposure to 1 M H_2SO_4, both materials develop roughened surfaces, but the severity differs markedly: CCB EPDM exhibits only minor increases in roughness, while RCB EPDM shows extensive cracking, porous regions, and matrix erosion, consistent with its higher swelling, higher ionic release, and lower mechanical retention. These features reflect the known variability and impurity content of recycled carbon black, which promote acid ingress and accelerate degradation pathways [22].

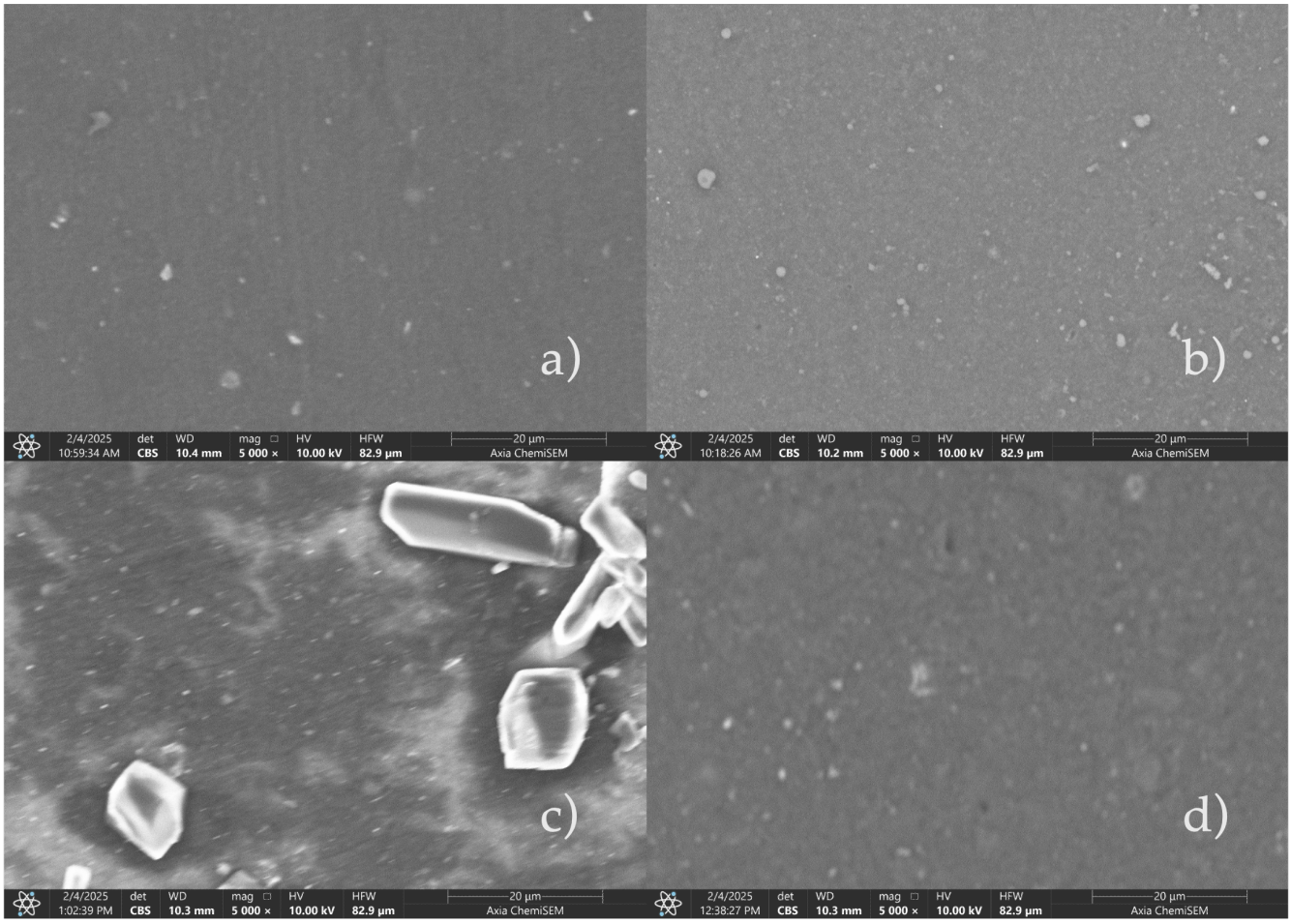


Figure 5.25. SEM micrographs of CCB and RCB EPDM samples at 5000x magnification. (a) Fresh CCB EPDM, showing a smooth surface with minimal irregularities. (b) Fresh RCB EPDM, with more visible filler particles and irregular distribution. (c) RCB EPDM after exposure to 1 M H_2SO_4 for 1000 hours, showing significant surface degradation with cracks and porous regions. (d) CCB EPDM after 1000 hours in 1 M H_2SO_4 [23]

BUPT

SEM and energy-dispersive X-ray spectroscopy (EDS) were also employed to examine surface morphology and elemental composition across fresh, heat-aged, and acid-aged ECO EPDM samples (Figure 5.26 and Figure 5.27). In the fresh state, both CCB and RCB EPDM show smooth and uniform surfaces; however, RCB EPDM reveals clear micro-porosity (labeled "a") and regions demonstrating an open filler structure ("b"), characterized by loosely aggregated carbon black particles and visible inter-particle gaps. Areas of early matrix erosion ("c") appear in fresh RCB EPDM as well, suggesting intrinsic microstructural heterogeneity. These features, absent or less severe in CCB EPDM, may facilitate fluid ingress and accelerate chemical degradation under acidic conditions.

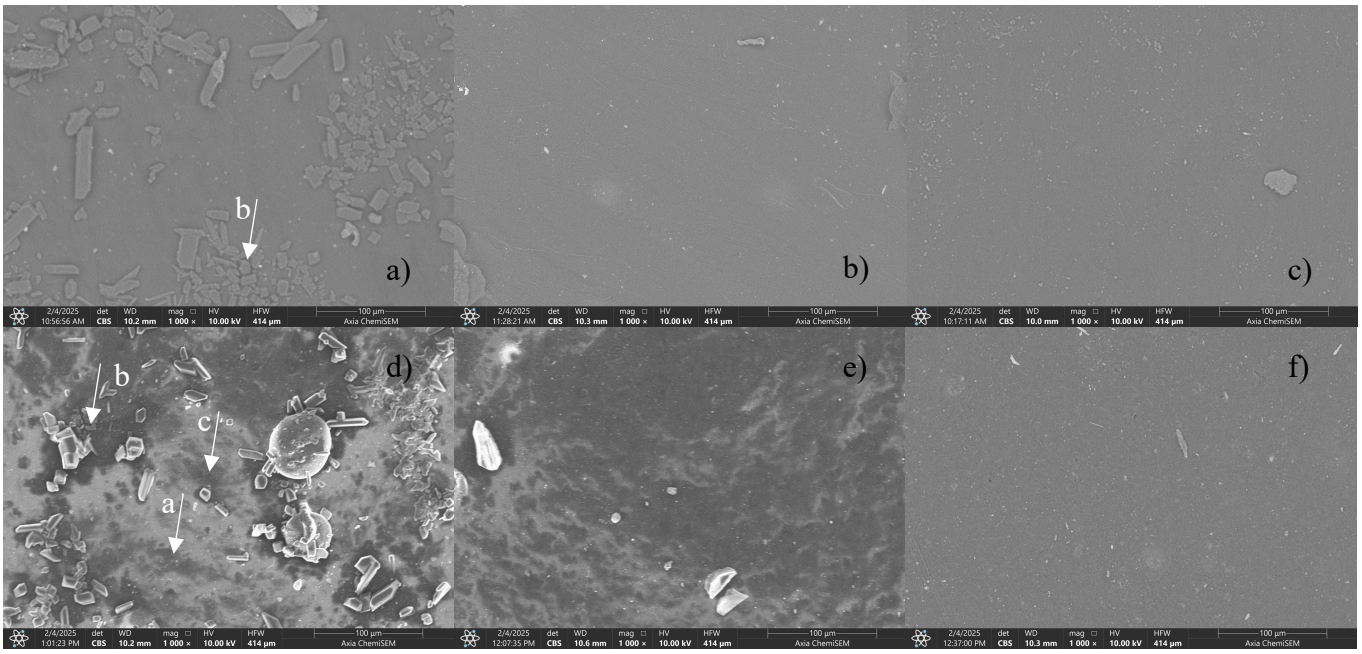


Figure 5.26. SEM micrographs of CCB EPDM (top row: a–c) and RCB EPDM (bottom row: d–f) at 1000× magnification under different conditions: (a, d) fresh samples, (b, e) heat-exposed (HE) samples, and (c, f) samples aged in 1 M H_2SO_4 solution. From [22]

EDS analysis confirms high carbon content in both materials—approximately 90.8 at.% for CCB and 85.1 at.% for RCB—along with low oxygen levels and trace elements including Mg, Si, S (in CCB), and Zn (in RCB). The detection of Zn and Si in RCB reflects the recycled filler origin, while slightly elevated oxygen in fresh RCB indicates residual surface oxidation or contamination from prior usage.

Following heat aging (Figure 5.26b,e), both materials exhibit mild surface roughening with no major crack propagation or filler extraction. EDS data show minor compositional changes, including increased carbon and reduced oxygen in both materials (e.g., CCB: 93.2 at.% C and 5.0 at.% O; RCB: 87.7 at.% C and 8.9 at.% O). Trace sulfur and calcium appear in heat-aged RCB EPDM, suggesting minor additive migration or thermo-oxidative transformation.

BUPT

After immersion in 1 M H_2SO_4 (Figure 5.26c,f), both formulations demonstrate substantial degradation. CCB EPDM presents rough, irregular surfaces with microvoids and signs of matrix erosion. Its EDS profile reveals sharp reductions in carbon (to 83.8 at.%) and increases in oxygen (12.8 at.%) and sulfur (2.9 at.%), indicating oxidative attack and sulfur incorporation from the acid. RCB EPDM, however, exhibits even more severe deterioration: carbon content drops further to 79.4 at.%, with oxygen rising to 16.0 at.% and sulfur to 2.6 at.%. The presence of Zn and Si persists in aged RCB, and both materials show slight decreases in magnesium. These chemical signatures confirm acid-driven oxidation and filler–matrix degradation, with RCB EPDM experiencing the strongest compositional and structural breakdown.

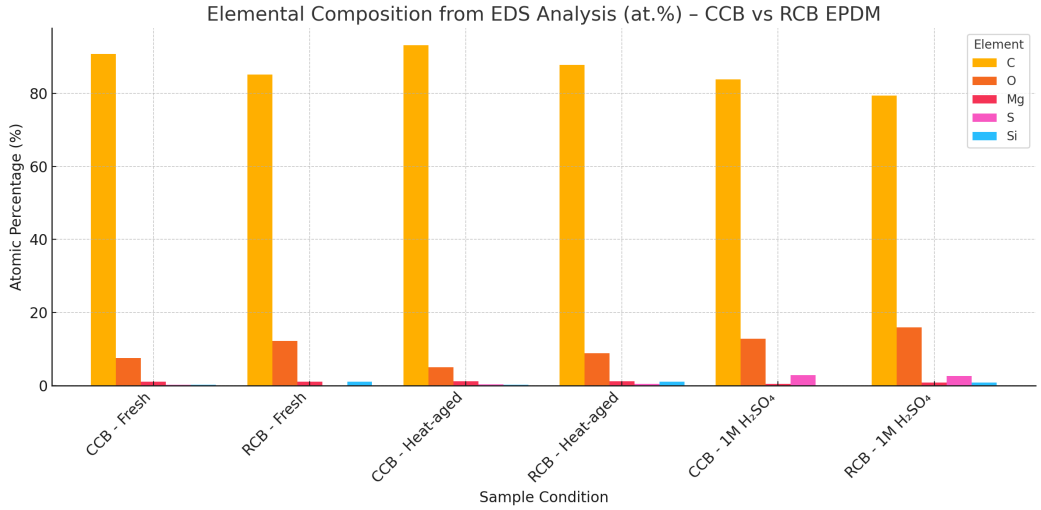


Figure 5.27. Elemental Composition of RCB and CCB EPDM samples from EDS analisys, from [22]

It is important to note that EDS provides semi-quantitative data, and values should be interpreted as indicative of relative changes rather than absolute composition.

Discussion

The SEM findings deepen and visually validate the degradation mechanisms inferred from the swelling, pH, conductivity, hardness, and tensile results. Materials that exhibited higher ionic release, larger swelling ratios, and greater reductions in mechanical integrity—namely ECO TPV and RCB EPDM—also displayed the most severe microstructural deterioration, including crack networks, porous domains, and surface erosion. These features indicate advanced chemical attack along polymer–filler interfaces, confirming that heterogeneous filler structures, as seen in RCB EPDM, create preferential pathways for acid penetration and subsequent matrix breakdown. In contrast, the relatively smooth and minimally altered surfaces of EPDM-H and CCB

BUPT

EPDM align with their low swelling, stable hardness, and superior tensile retention, demonstrating that uniform filler dispersion and a more cohesive polymer network limit both fluid ingress and acid-driven oxidative scission. The microcracking observed in TPV and ECO TPV further supports the vulnerability of their thermoplastic phases, where PP-rich domains undergo localized embrittlement and degradation under acidic and thermal stress. Collectively, the SEM observations provide the morphological evidence that ties all previous trends together, clearly distinguishing robust elastomer–filler systems from those prone to rapid chemical deterioration under PEMFC-like environments.

5.3 Temperature-Dependent Mechanical Behavior of EPDM-T [18]

5.3.1 Temperature-Dependent Tensile Behavior

The temperature-dependent tensile response of EPDM-T is presented in Figure 5.28 and reveals a non-monotonic evolution of stiffness and ductility across the investigated thermal range. At −40 °C, the material exhibits its highest stiffness and lowest elongation, indicative of a glassy, brittle regime dominated by restricted segmental mobility. As the temperature increases to 23 °C, EPDM-T transitions to a more compliant state, displaying moderate stiffness and balanced mechanical behavior. This regime represents the normal operational window in which the polymer network exhibits both acceptable strength and elasticity. At 80 °C, the expected softening becomes evident, with reduced stiffness linked to thermally activated chain mobility and partial relaxation of the crosslinked network.

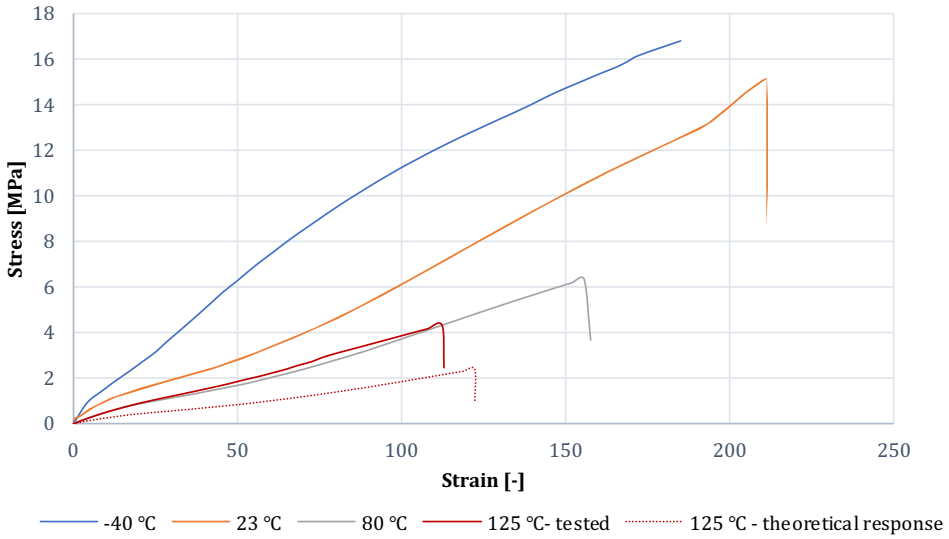


Figure 5.28. Tensile test behavior of EPDM-T at various temperatures [18]

BUPT

An unexpected trend arises at 125 °C, where EPDM-T stiffness increases again, surpassing the values observed at 80 °C. This deviation from conventional elastomeric thermal softening behavior likely reflects the influence of the compound formulation, particularly the high carbon black loading. Carbon black is a well-documented reinforcing filler that improves tensile strength, modulus, and resistance to deformation through both physical reinforcement and improved heat dissipation [164]. The 30 wt.% carbon black present in the studied formulation improves thermal conductivity, limiting localized thermal softening and stabilizing the polymer network at elevated temperatures. The additional 5 wt.% zinc oxide also contributes to crosslinking efficiency by acting as an activator, though its reinforcing effect is secondary to that of carbon black [165]. Together, these factors produce the anomalous stiffening observed at 125 °C, illustrating the complex interplay between filler reinforcement, thermal energy, and polymer network dynamics in highly filled EPDM.

5.3.2 Dynamic Mechanical Analysis

Figure 5.29 presents the results of the dynamic mechanical analysis (DMA), capturing the evolution of storage modulus (elastic response), loss modulus (viscous dissipation), stiffness, and tan δ across temperatures from 20 °C to 160 °C. The storage modulus increases steadily with temperature, which is atypical for elastomers and again reflects the strong reinforcing contribution of carbon black to the stiffness of the material. The stiffness curve follows a similar upward trajectory, reinforcing the interpretation that high filler loading leads to structural stabilization rather than thermally driven softening.

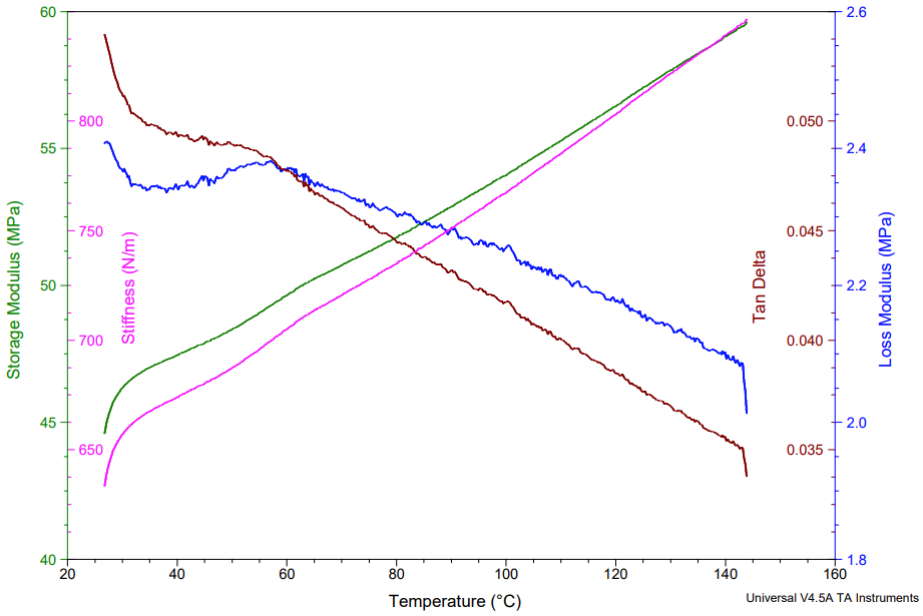


Figure 5.29. DMA result of the studied EPDM-T [18]

BUPT

Simultaneously, the loss modulus decreases with increasing temperature, indicating a diminishing capacity of the material to dissipate energy as heat. The accompanying decline in tan δ suggests reduced damping efficiency at high temperatures, a trend significant for applications where vibrational or dynamic loading persists across thermal cycles. Together, these DMA results highlight that the examined EPDM compound demonstrates enhanced rigidity and reduced viscoelastic damping at elevated temperatures—behavior that deviates from typical rubbery materials but is consistent with heavily filled EPDM systems.

5.3.3 FEA Material Modelling

To accurately capture the hyperelastic behavior of the EPDM compound for finite element analysis, three constitutive models—Arruda-Boyce (AB), Yeoh 3D, and Mooney-Rivlin (MR) 5-parameter—were calibrated against the experimentally obtained stress–strain curves. The top row of Figure 5.30 illustrates the comparison between the experimental data (blue dotted lines) and the model fits (solid lines). Among the three models, the Arruda-Boyce formulation provides the closest match to the experimental uniaxial tensile response, preserving both the initial stiffness and the nonlinearity of the curve.

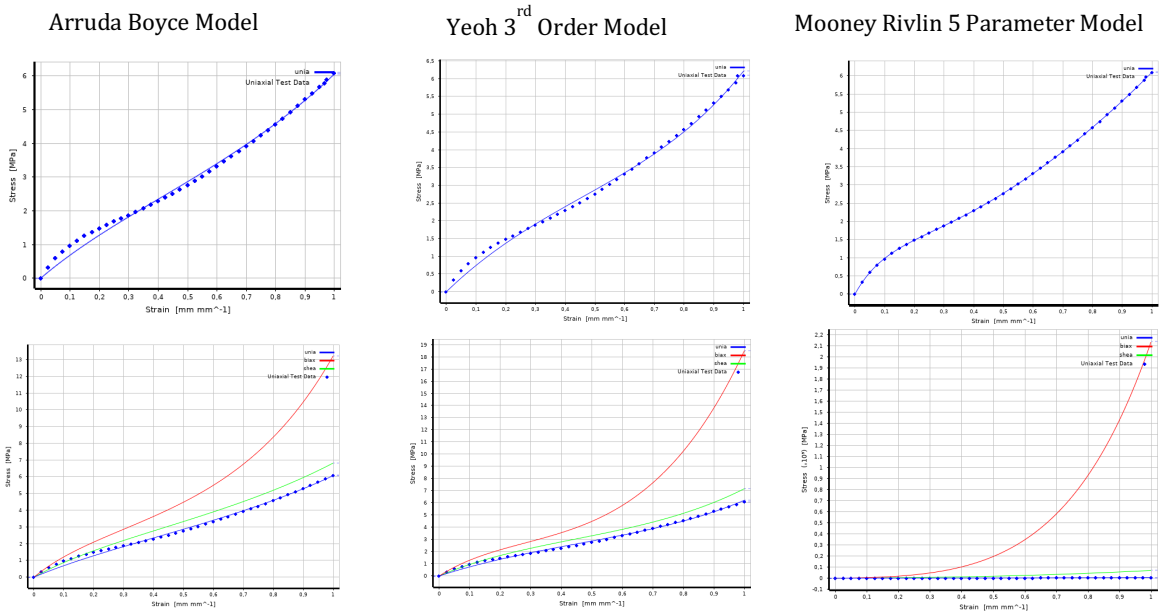


Figure 5.30. Tensile curve fitting with different material models

The Yeoh 3D and Mooney-Rivlin 5-parameter models are capable of approximating the uniaxial response, yet their greater rigidity becomes pronounced in the predicted biaxial behavior, shown in the bottom row of Figure 5.30. Both exhibit higher-than-expected stiffness and deviate from the known deformation characteristics of EPDM, making them less appropriate for the present application.

BUPT

The Arruda-Boyce model, in contrast, maintains a realistic biaxial representation with moderate rigidity and closer correspondence to expected physical behaviour. For this reason, the Arruda-Boyce model was selected as the most suitable candidate for subsequent FEA simulations, enabling accurate representation of the mechanical response across different deformation modes.

5.4 Tribological Behavior of LF-EPDM and LF-TPV Against PA66GF30 [21]

The tribological characteristics of LF EPDM and LF TPV in contact with a 30 wt.% glass-fiber-reinforced polyamide composite (PA66GF30) were evaluated under dry sliding conditions using a ball-on-disk configuration. The test matrix included three normal loads (1 N, 3 N, 6 N) and three linear speeds (0.048, 0.096, and 0.15 m/s), corresponding to rotational speeds of 92, 183, and 286 RPM. The results are presented in terms of the time-dependent coefficient of friction (CoF), mass loss, wear area and wear volume, and wear-track morphology. Together, these parameters allow a comprehensive assessment of frictional stability and wear resistance for both elastomers under increasingly severe tribological conditions.

5.4.1 Coefficient of Friction (CoF) Evolution

The smoothed CoF–time curves shown in Figure 5.31 (EPDM) and Figure 5.32 (TPV) exhibit the typical two-stage evolution of elastomer–polymer sliding contacts consisting of an initial transient regime lasting approximately 150–250 s, followed by a quasi-steady state. Distinct material-dependent behaviour was observed as a function of load and speed. At 1 N, EPDM displayed moderate initial friction values that increased sharply with sliding speed, stabilizing at approximately 0.54 at 0.048 m/s, 0.67 at 0.096 m/s, and 0.83 at 0.15 m/s. This trend reflects a shift from adhesive friction at low speed to deformation-controlled and thermally assisted sliding at higher velocities, where greater shear leads to increased frictional heating and micro-ploughing.

For TPV at 1 N, an inverse pattern was recorded. CoF values were high even at low speed, stabilizing above 0.9 across the speed range. The elevated friction is attributed to insufficient normal force to compress TPV's hybrid microstructure, resulting in a large real contact area dominated by adhesive interactions. Unlike EPDM, TPV did not show significant friction escalation with speed at 1 N.

At 3 N, EPDM's friction retained its monotonic dependence on speed, with steady-state values between 0.44 and 0.67. At 0.15 m/s, the CoF increased progressively over time, suggesting the onset of surface degradation or fatigue. TPV showed comparatively stable friction across all speeds at this load, with CoF values of approximately 0.41, 0.47, and 0.50—reflecting an interface less sensitive to velocity, due to TPV's ability to redistribute stresses within its thermoplastic–elastomeric network.

At 6 N, EPDM displayed persistent friction growth at higher speeds, reaching up to 0.68 at 0.15 m/s. This steady rise in friction throughout the test indicates progressive mechanical damage and viscoelastic instability. In contrast, TPV again exhibited a stable frictional response, with values ranging from 0.36 to 0.45 and minor decreasing trends in some curves, implying the development of a smoother tribological interface during sliding. The PV-based plot in Figure 8 shows that TPV

BUPT

maintains significantly lower average CoF values across the PV spectrum, especially at higher PV levels, confirming its inherently more stable frictional behaviour under high load and speed.

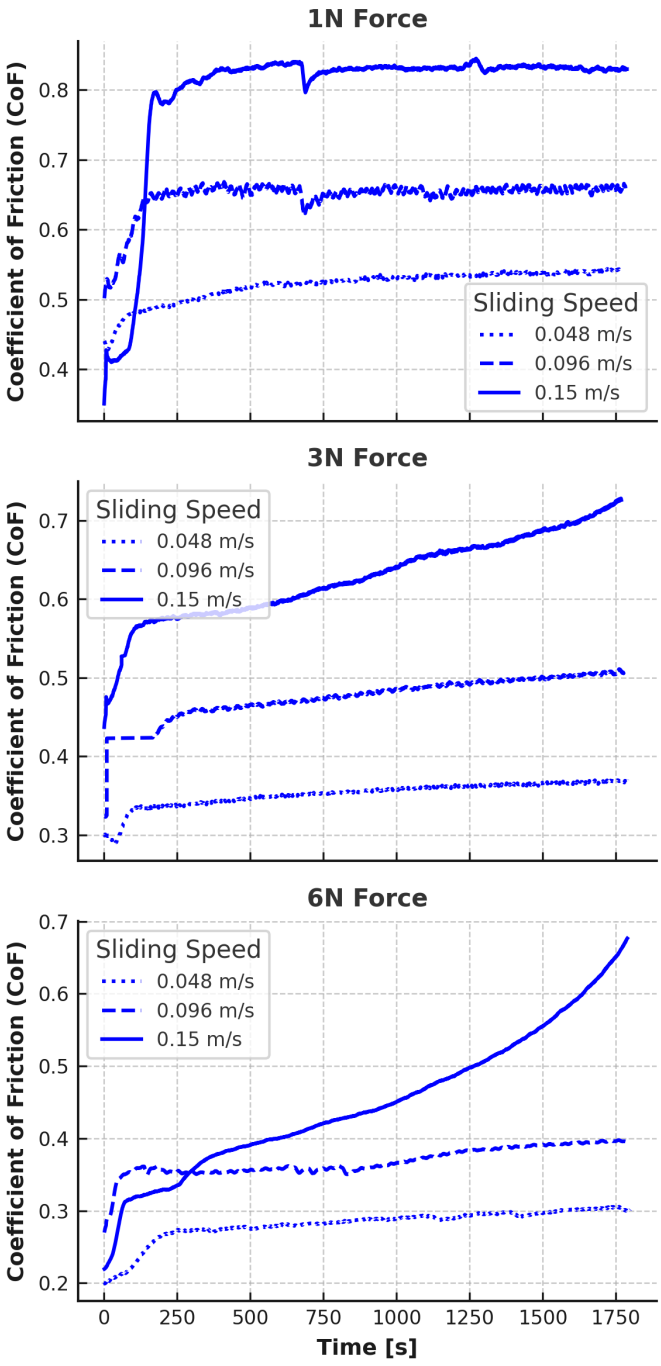


Figure 5.31. CoF vs Time for EPDM, grouped by force [21]

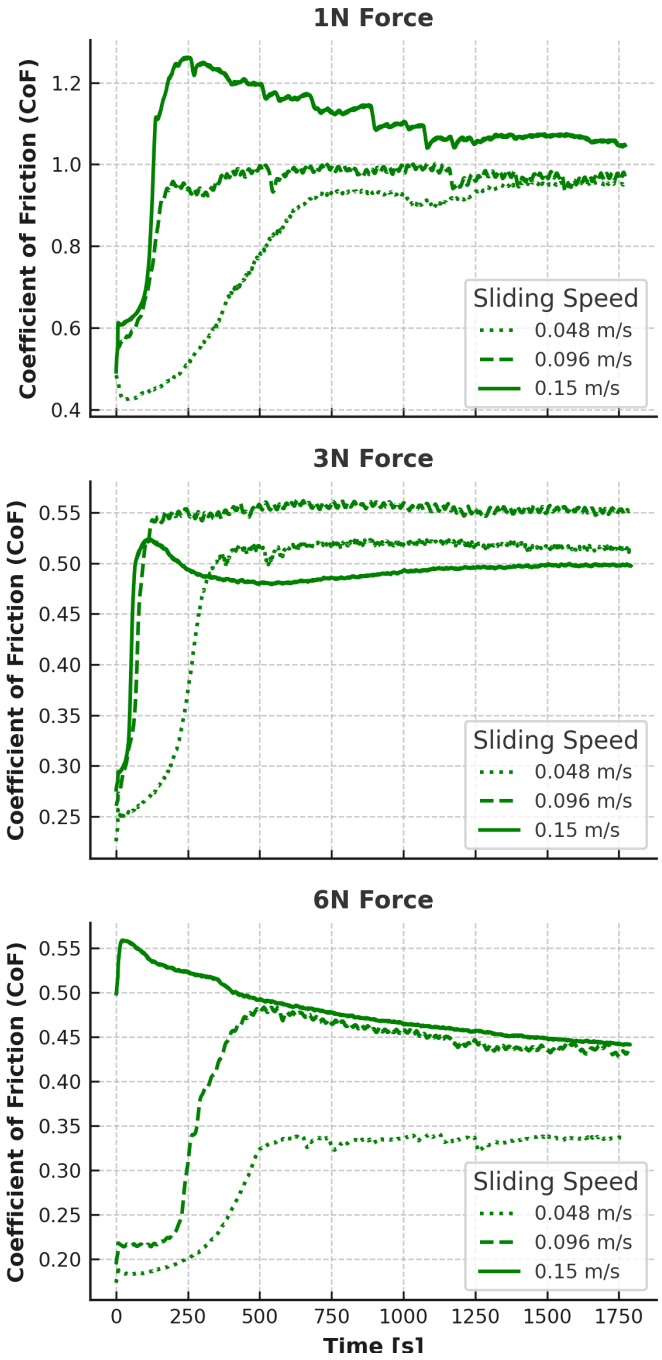


Figure 5.32. CoF vs Time for TPV, grouped by force [21]

BUPT

5.4.2 Mass Loss

Wear behavior was evaluated by calculating the percentage mass loss using the standard expression:

$$\Delta m(\%) = \left(\left(m_{initial} - m_{final} \right) / m_{initial} \right) \times 100 \quad (23)$$

EPDM (Figure 5.33) exhibited a clear increase in mass loss with both load and sliding speed. The baseline wear at 1 N and 0.048 m/s was approximately 0.016%. At 3 N, mass loss increased to values between 0.034% and 0.045% depending on speed. The most severe condition (6 N, 0.15 m/s) produced mass loss values near 0.060%, indicating significant material removal through combined abrasive, fatigue, and micro-cutting mechanisms. The nonlinear increase at high PV suggests that EPDM transitions into an unstable wear regime characterized by tearing and subsurface damage.

TPV (Figure 5.34) demonstrated much lower wear across all conditions. At 1 N, wear ranged from ~0.004% at 0.048 m/s to ~0.012% at 0.15 m/s. At 3 N, wear remained nearly constant (~0.010–0.011%) across speeds, indicating little sensitivity to velocity. Even at 6 N, the maximum wear observed was ~0.022% at 0.15 m/s, representing a roughly threefold reduction compared to EPDM under identical conditions. This behaviour reflects TPV's improved resistance to mechanical removal and its ability to maintain interface stability even under elevated loads and speeds. TPV remains consistently below EPDM in mass-loss performance across the entire PV range, converging only at the highest PV (0.9 N·m/s).

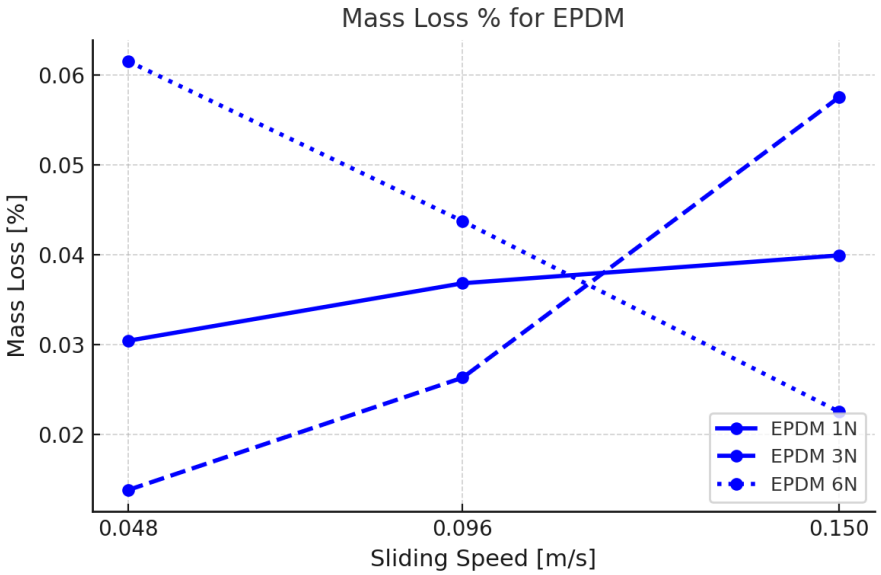


Figure 5.33. Mass Loss % vs sliding speed [m/s] for EPDM across the different forces

BUPT

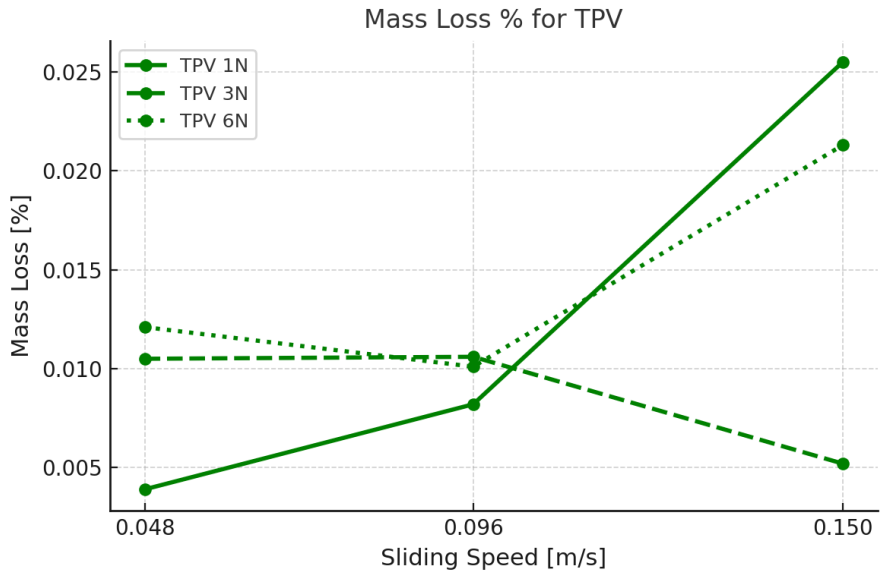


Figure 5.34. Mass Loss % vs sliding speed [m/s] for TPV across the different forces

5.4.3 Wear Area and Wear Volume

Wear areas were determined using calibrated optical microscopy and computed from the measured inner and outer track diameters using the standard ring-area relationship:

$$A = \pi \times \left(D_{outer}^2 - D_{inner}^2\right)/4 \quad (24)$$

EPDM showed clearly increasing wear area with both load and speed (Figure 5.35). At 1 N, wear areas ranged from ~50 mm² at 0.048 m/s to ~58 mm² at 0.096 m/s, with a minor drop at 0.15 m/s. At 3 N, areas increased from ~70 to ~77 mm², while at 6 N they spanned from ~74 to ~91 mm². TPV exhibited substantially smaller wear areas at 1 N and 3 N for all speeds. Only at 6 N and 0.15 m/s did TPV approach EPDM's wear area (87.7 vs. 91.6 mm²), corresponding to the region where material behaviour converges in wear volume and PV-based performance.

Wear volume was then calculated using the mean track diameter and track circumference:

$$D_{mean} = (D_{outer} + D_{inner})/2 \quad (25)$$

$$C = \pi \times D_{mean} \quad (26)$$

$$V = A \times C \quad (27)$$

BUPT

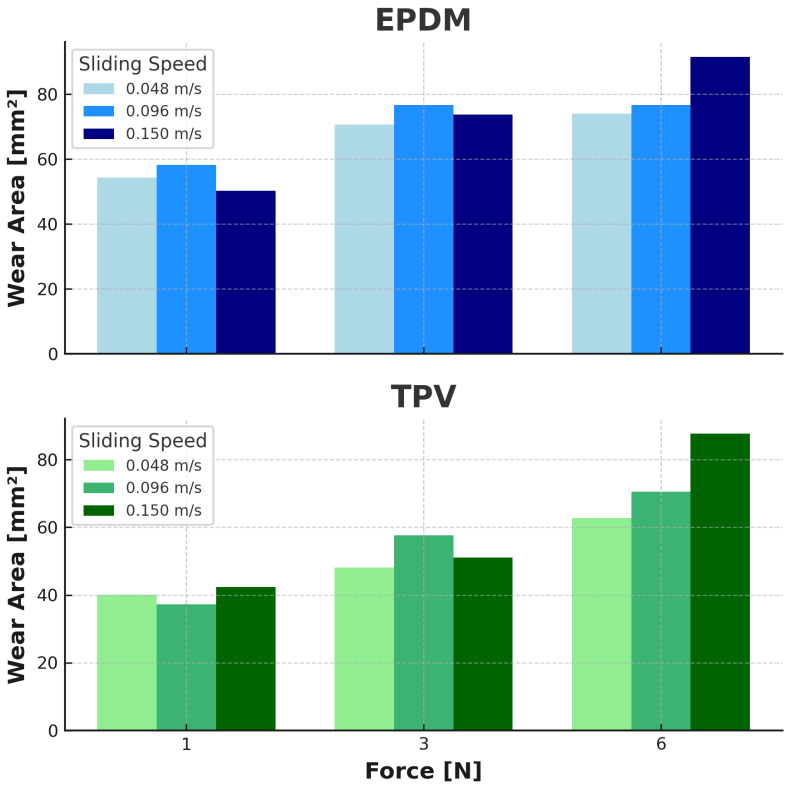


Figure 5.35. Wear area by Force and rotational speed for EPDM (top) and TPV (Bottom)

The wear-volume plot in Figure 5.36 reveals a strong PV dependence for EPDM, with wear volume rising steadily up to approximately 3412 mm³ at 0.9 N·m/s. TPV again demonstrated substantially lower wear volumes across most conditions, remaining below 2200 mm³ except at the highest PV where both materials converged. This pattern further highlights TPV's ability to maintain low material removal under most operating conditions, with divergence occurring only at extreme loads and speeds.

Wear-track morphology (Figure 5.37 and Figure 5.38) reinforces these quantitative findings. EPDM surfaces showed irregular, broad tracks with accumulated debris, edge tearing, and signs of micro-ploughing—features consistent with fatigue-assisted abrasive wear. TPV tracks were narrower and smoother, with evidence of progressive polishing rather than tearing, indicating effective stress distribution and reduced susceptibility to local damage.

BUPT

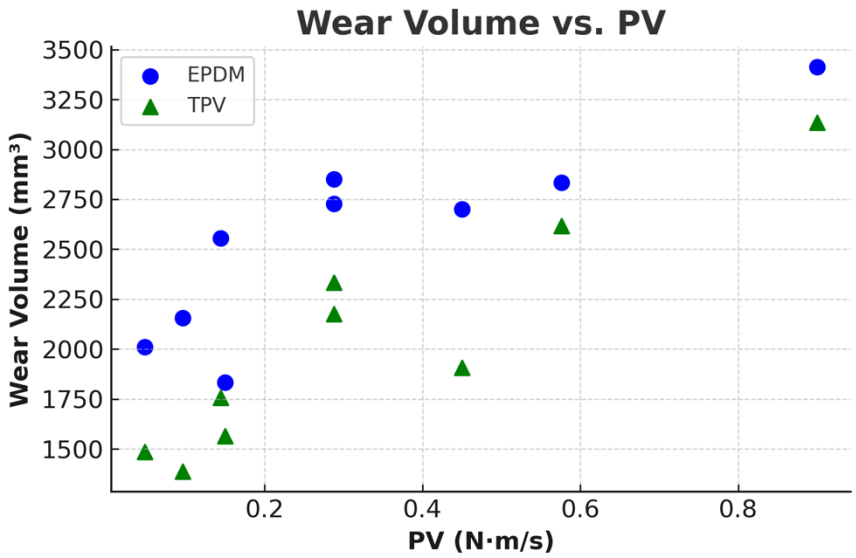


Figure 5.36. Wear volume of EPDM and TPV samples as function of PV parameter

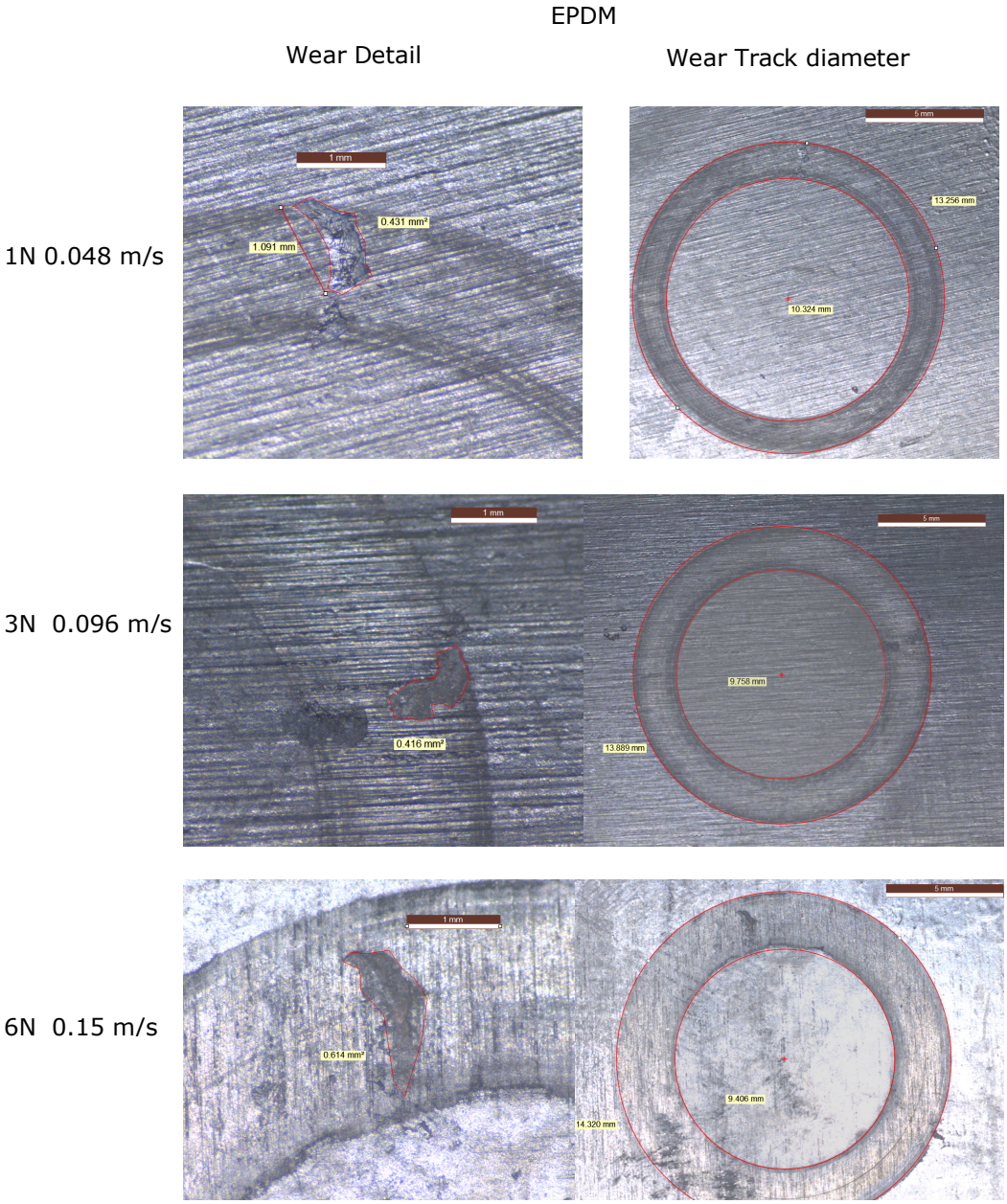


Figure 5.37. Digital microscopy images of localized wear defects (left) and corresponding full wear tracks (right) for EPDM samples tested under increasing normal loads and sliding speeds: 1 N at 0.15 m/s (top row), 3 N at 0.096 m/s (middle row), and 6 N at 0.048 m/s [21]

BUPT

5.4 - Tribological Behavior of LF-EPDM and LF-TPV Against PA66GF30 [21] 109

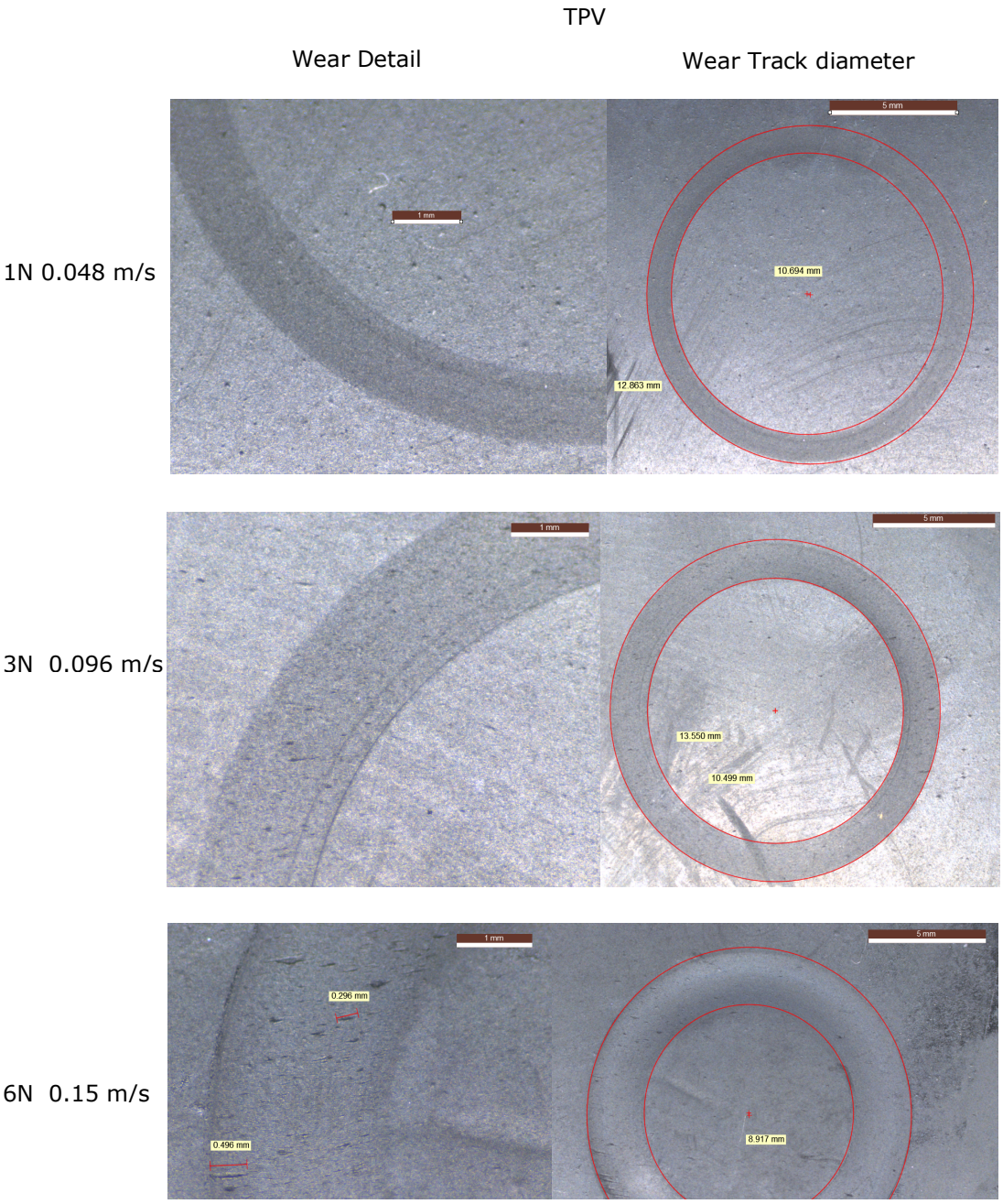


Figure 5.38. Digital microscopy images of localized wear defects (left) and corresponding full wear tracks (right) for TPV samples tested under increasing normal loads and sliding speeds: 1 N at 0.15 m/s (top row), 3 N at 0.096 m/s (middle row), and 6 N at 0.048 m/s [21]

BUPT

5.4.4 FEA calibration and Simulation of Friction

Finite element analysis (FEA) was used to replicate the tribological behavior of LF EPDM and LF TPV against PA66GF30 and to validate the experimentally measured frictional response. The simulation framework was designed in LS-DYNA and ANSYS Mechanical and relied on direct input of experimentally obtained tensile curves, Mooney–Rivlin hyperelastic calibration, realistic boundary conditions, and frictional contact definitions. The goal of the simulation was twofold: (i) to reproduce the CoF trends and contact-pressure evolution measured in the ball-on-disk tests, and (ii) to extend the analysis toward a real sealing application through a push-in simulation of an elastomeric lip under reciprocating displacement.

Material Model Calibration

The starting point of the simulation was the experimental stress–strain data obtained for EPDM and TPV. True modulus of elasticity was computed from the engineering curves, after which the data were entered into ANSYS "Engineering Data" as uniaxial test points. Curve fitting was performed using the Mooney–Rivlin 3-parameter model, which provided the most realistic biaxial response for the tribological contact. This calibration ensured that the numerical models captured the nonlinear elastic behavior observed experimentally.

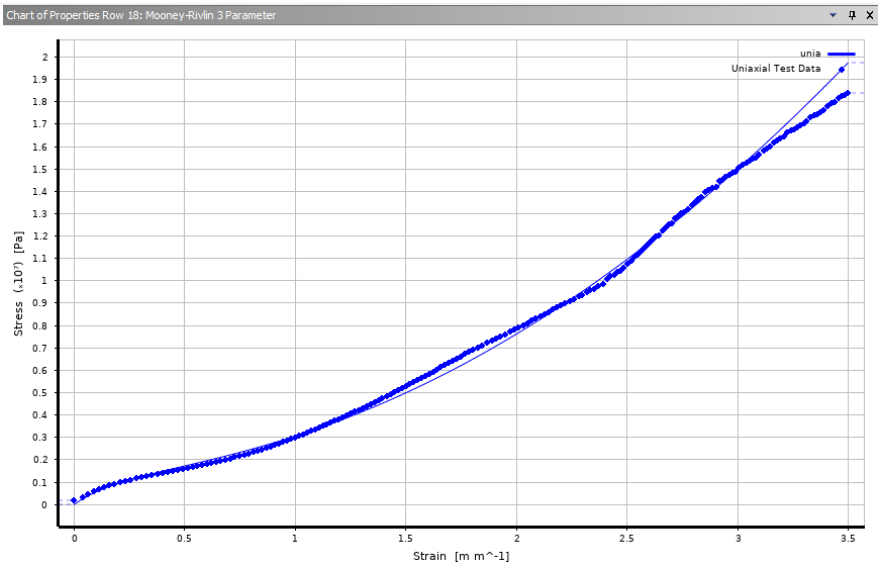


Figure 5.39. Mooney-Rivlin 3-parameter curve fitting for EPDM

Both C10–C01 combinations and D1 compressibility terms were optimized automatically. For TPV, density was also used as an input because of its thermoplastic-elastomeric hybrid structure. The PA66GF30 counterbody was modeled as a linear elastic material, consistent with its high stiffness and minimal deformation under the applied loads.

BUPT

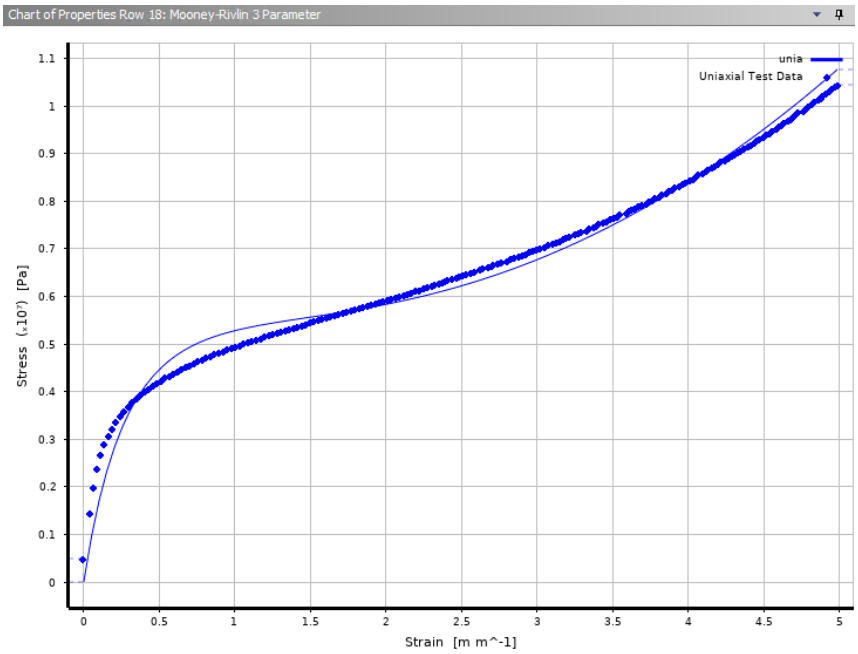


Figure 5.40. Mooney-Rivlin 3-parameter curve fitting for TPV

Geometry and Model Setup

The geometry (Figure 5.41) for the ball-on-disk simulation was created in SpaceClaim, consisting of a 6 mm PA66GF30 spherical counterbody and an elastomeric disk. Surface bodies were generated to apply boundary conditions without introducing artificial forces. The ball and disk were left as flexible bodies, while the tool components were defined as rigid, ensuring clean transfer of reaction forces and energy.

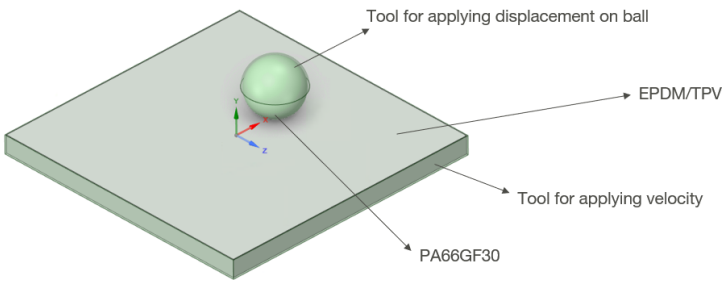


Figure 5.41. Geometry for ball-on-disk simulation

BUPT

A specific coordinate system was assigned to the plate to control boundary conditions and prevent numerical imbalance. Contact was defined exclusively through frictional contact interactions; the "Body Interaction" module was intentionally suppressed because simultaneous activation of both contact definitions may halve the normal reaction force and artificially reduce friction.

Meshing and Section Control

To minimize discontinuities in Courant time-step calculations, a uniform element size was used across all components. The PA66GF30 plate was meshed with tetrahedral elements to avoid hourglassing, while the ball and elastomer were meshed with deformable solid elements.

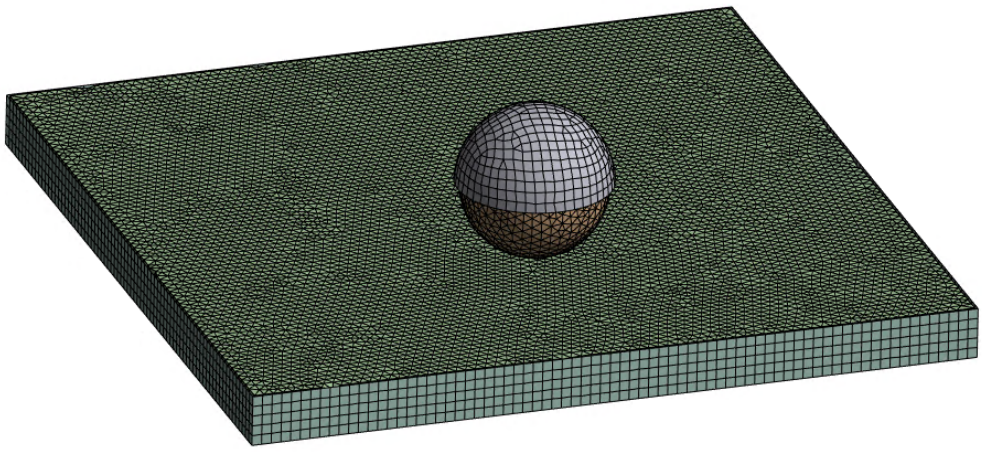


Figure 5.42. Ball-on-Disk simulation setup meshing

In LS-DYNA, the default 4-node tetrahedral section (elform = 10) was replaced by a one-point nodal pressure tetrahedron (elform = 13), which improved contact stability at the cost of approximately 20% additional computational effort.

Boundary Conditions and Test Replication

The test kinematics were reproduced by prescribing rotational motion to the disk, with angular velocity corresponding to 92, 183, and 286 rpm (≈0.048, 0.096, and 0.15 m/s). The normal force was applied to the ball through a gradual load ramp to reach 1 N, 3 N, or 6 N. This avoided artificial inertial spikes and produced a stable steady-state contact.

Friction was not input as a fixed value; instead, the solver computed it directly using:

$$\mu(t) = \frac{F_{shear}(t)}{F_{normal}(t)} \tag{28}$$

BUPT

The time-averaged CoF was then compared against the experimentally measured values.

Three representative experimental friction conditions were used as calibration targets:

TPV
- 1 N, 92 rpm → CoF ≈ 0.819
- 3 N, 183 rpm → CoF ≈ 0.546
- 6 N, 286 rpm → CoF ≈ 0.478

EPDM
- 1 N, 92 rpm → CoF ≈ 0.520
- 3 N, 183 rpm → CoF ≈ 0.471
- 6 N, 286 rpm → CoF ≈ 0.450

These values served as numerical benchmarks for both materials. The FEA results reproduced the observed trend: TPV consistently exhibited lower shear-force growth and more stable frictional behaviour, whereas EPDM showed steeper increases in friction with rising load and velocity. The match between simulation and experiment confirms that the calibrated hyperelastic models correctly capture deformation-controlled and adhesion-controlled friction mechanisms at the elastomer–composite interface.

5.4.5 Application-Level Push-In Simulation (Seal Actuation Case Study)

Load-Dependent Assignment of Friction for Application Simulation

A key methodological step in this study was ensuring that the friction coefficient used in the application-level sealing simulation was not arbitrarily chosen, but instead derived directly from experimental behaviour under equivalent loading. This closed-loop methodology proceeded as follows:

1. Resolve Interference Fit:

The push-in seal geometry (¼ symmetry) was fully assembled numerically, and the interference between the rubber lip and the metallic shaft was resolved. This simulation yielded the true sealing force acting normally at the interface.

2. Match Load to Experimental CoF:

The sealing force obtained in step 1 was compared with the loads used in the tribological tests (1 N, 3 N, 6 N).

The friction coefficient assigned to the application model was then the CoF measured experimentally at the closest corresponding load and sliding speed.

For example, if the interference simulation indicated a sealing force near 3 N, the model used the measured CoF from the 3 N, 183 rpm test.

3. Perform Push-In Simulation:

With the friction coefficient now physically grounded, the full push-in analysis was executed, generating insertion force curves, contact pressure distribution, and von Mises stress fields.

This methodology ensures that the sealing behaviour in the application model reflects realistic frictional interactions based strictly on validated experimental evidence.

Push-In Seal Simulation Results

The calibrated friction model was applied to a realistic sealing assembly consisting of a dynamic elastomeric lip inserted into a cylindrical metallic housing. Due to symmetry, only one quarter of the seal was modelled, reducing computational cost while preserving mechanical accuracy.

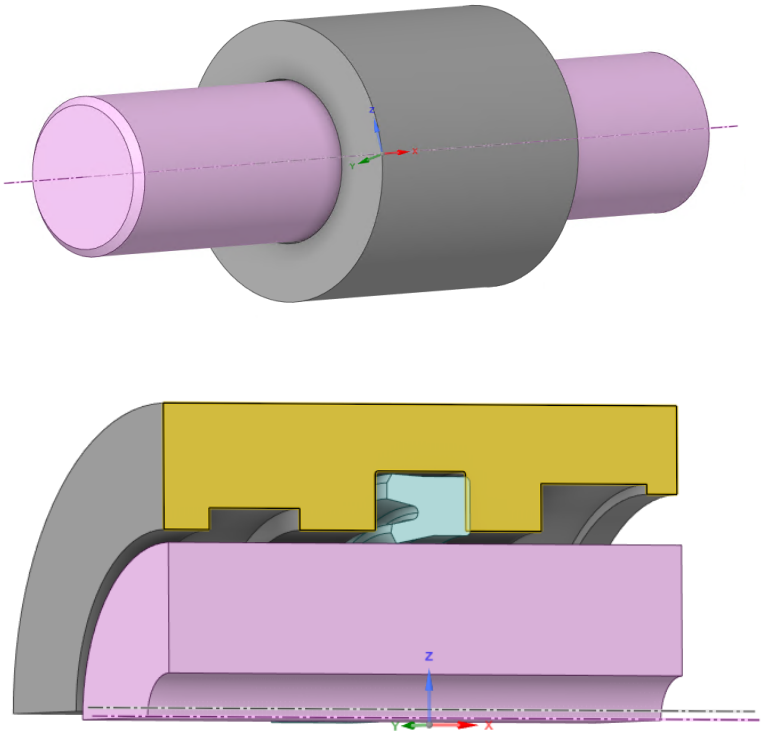


Figure 5.43. Application model

Two representative cases were extracted: a high-deformation EPDM case and a stabilised TPV case.

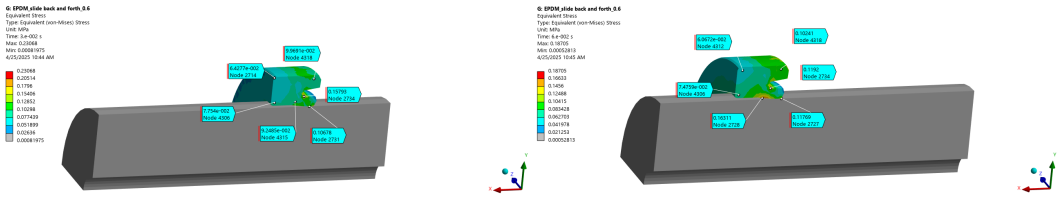


Figure 5.44. Far Left and Far Right position of the moving in simulation

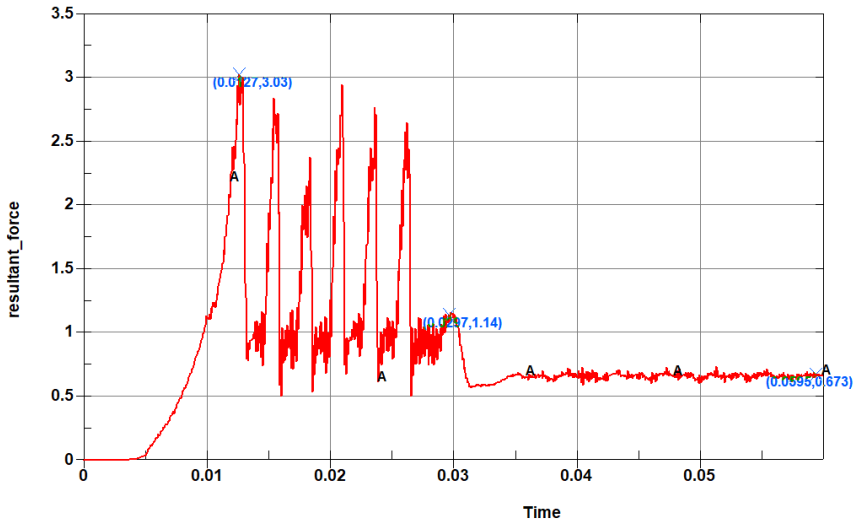


Figure 5.45. Resistance force–time response for EPDM with CoF = 0.6 under reciprocating motion

The simulated force curve (Figure 5.45) begins with a sharp rise as the seal starts moving, reaching a peak resistance of approximately 3.03 N at the onset of motion. Once reciprocation begins, the force oscillates between characteristic maxima and minima that correspond to the two stroke limits. At the far-left reversal, the resistance stabilizes around 1.14 N, while at the far-right reversal it decreases further to roughly 0.67 N. These cyclic variations reflect the alternating loading and unloading of the sealing lip during the forward–backward motion, with higher resistance at direction changes and lower resistance during steady sliding.

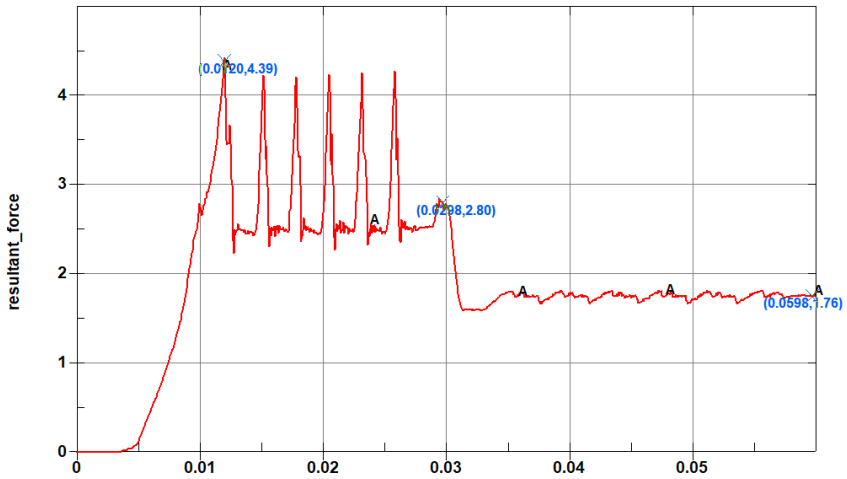


Figure 5.46. Resistance force–time response for TPV with CoF = 0.48 under reciprocating motion.

BUPT

The TPV simulation results (Figure 5.46) begins with a steep rise in resistance, peaking at approximately 4.39 N at the start of motion. Once reciprocating sliding is initiated, the force signal exhibits periodic oscillations characteristic of the forward–backward stroke. At the far-left reversal, resistance stabilizes near 2.80 N, while at the far-right reversal, the force drops to around 1.76 N. Compared to EPDM, the force variation is smoother and more uniform, reflecting TPV's more stable interfacial behavior and reduced shear sensitivity under alternating motion.

6 CONCLUSIONS

The original research described in the present work consists in a theoretical study on available literature data regarding elastomeric sealing materials, degradation mechanisms, and applications in hydrogen energy systems. The focus was directed to aspects concerning the characterization of sustainable elastomeric materials, the optimization of material selection for peripheral components in Proton Exchange Membrane Fuel Cell (PEMFC) systems, and the evaluation of their durability under simulated operating conditions.

In the current state of the art, sealing in PEMFC systems involves the use of specialized gaskets and O-rings made from synthetic rubbers, primarily EPDM, designed to withstand acidic environments, humid air, and temperature fluctuations. These seals are critical for preventing gas crossover and leakage, which are primary failure modes in fuel cell stacks. However, standard materials often rely on fossil-based feedstocks and virgin carbon black, contributing to a significant carbon footprint. Furthermore, the specific degradation behavior of thermoplastic vulcanizates (TPVs) and sustainable elastomers containing recycled fillers under the combined chemical, thermal, and tribological stresses of the cathodic air loop remains insufficiently characterized in existing literature.

Considering that EPDM is one of the most suitable materials for protection against environmental stressors due to its saturated backbone and chemical resistance, the main attention was focused on utilizing this polymer for its advantages, and simultaneously exploring sustainable alternatives to overcome environmental limitations.

The present work dealt with the comprehensive characterization of functional elastomeric materials based on EPDM, TPV, and Eco-friendly variants (utilizing circular and recycled carbon black) using standardized aging and tribological testing methods. EPDM and its sustainable counterparts provide the necessary elasticity and chemical inertness, improving the sealing reliability. Simultaneously, the TPV variants offer processing advantages and distinct tribological behaviors. Moreover, the integrated testing approach provides a holistic view of material degradation, linking microstructural changes to macroscopic performance loss.

This technique delivers a rigorous selection methodology for functional sealing materials and guarantees a better understanding of the lifespan of components in the cathodic air circuit.

BUPT

5.4 - Tribological Behavior of LF-EPDM and LF-TPV Against PA66GF30 [21] 117

The personal contributions in this study refer to:

- utilizing accelerated aging protocols (acidic immersion and thermal exposure) in order to evaluate the chemical stability of EPDM, ECO EPDM, TPV, and Eco-TPV functional materials;
- exploring the possibility of combining circular carbon black (CCB) and recycled carbon black (RCB) as reinforcing phases with EPDM rubber, to develop sustainable sealing solutions;
- development of a comprehensive dual-validation methodology that integrates chromatographic analysis (HPLC) with mechanical degradation tracking. This contribution overcomes the limitations of traditional separate testing by demonstrating how acidic aging simultaneously drives network embrittlement (mechanical failure) and the release of UV-active organic contaminants (chemical failure), providing a more accurate lifetime prediction for peripheral components.
- the successful employment of high-performance liquid chromatography (HPLC) and hot water extraction tests (HWET) to quantify organic and ionic leachates, assessing the risk of membrane contamination;
- comparative analysis of the tribological behavior of low-friction EPDM and TPV against glass-fiber reinforced polyamide (PA66GF30), a common housing material in balance-of-plant components;
- calibration of hyperelastic material models (Arruda-Boyce) for Finite Element Analysis (FEA) to predict sealing force and contact mechanics;
- investigations on the degradation mechanisms, as well as investigations on the influence of the acidic environment on the morphology of the elastomers;
- correlating mechanical, tribological, and chemical results to identify the most robust material for cathodic side applications.

In this regard, several aspects can be highlighted:

- A careful selection of the base polymers (EPDM vs. TPV) and filler systems (virgin, circular, and recycled) was performed to address the specific requirements of PEMFC peripheral sealing.
- EPDM-H was found to be the most chemically stable material, exhibiting the lowest volume change and mass uptake even after 1000 hours of immersion in 1 M sulfuric acid.
- The swelling behavior was strongly dependent on the material class; Eco TPV demonstrated the highest susceptibility to acid-induced swelling (over 6% mass increase), indicating the vulnerability of the thermoplastic phase to hydrolysis and oxidation.
- Circular Carbon Black (CCB)–filled EPDM demonstrated superior stability compared to Recycled Carbon Black (RCB)–filled EPDM. RCB variants showed significantly higher swelling and microstructural degradation, attributed to the higher heterogeneity and impurity content of the recycled filler.
- Leaching analysis via HPLC and conductivity measurements revealed that RCB EPDM releases significantly more ionic and organic species, particularly in the early stages of exposure. This indicates a higher risk for catalyst poisoning and membrane contamination compared to the cleaner CCB formulation.
- Mechanical testing confirmed that EPDM-H retains the highest tensile strength and elongation at break after aging, whereas TPV and Eco TPV experienced gradual strength loss due to degradation of the polypropylene matrix.

- Compression set results highlighted that EPDM-H offers the best elastic recovery, while Eco TPV exhibited the highest permanent deformation, raising concerns about long-term sealing force retention.
- Tribological investigations revealed a distinct trade-off: TPV maintained a more stable and lower coefficient of friction under high load and speed conditions, while EPDM exhibited friction escalation due to thermal softening and adhesive wear.
- Regarding wear volume, EPDM showed higher material loss at high PV factors, whereas TPV demonstrated superior wear resistance in dynamic sliding against PA66GF30, developing a smoother wear track.
- Microstructural analysis via SEM validated the mechanical findings. Acid-aged RCB EPDM and Eco TPV showed extensive surface cracking and erosion, whereas EPDM-H and CCB EPDM maintained relatively smooth and intact surfaces.
- The Arruda–Boyce hyperelastic model was identified as the most accurate constitutive model for simulating the mechanical response of these elastomers in finite-element analysis, providing a reliable tool for predictive seal design.
- The overall assessment suggests that although TPV offers tribological advantages for dynamic applications, EPDM—especially formulations using virgin or circular carbon black—remains the superior choice for static sealing in chemically aggressive PEMFC environments due to its unmatched chemical and thermal stability.

Using the described method, a comprehensive characterization of sustainable sealing materials has been achieved, highlighting the viability of circular economy materials like CCB EPDM while identifying the limitations of current recycled black (RCB) and thermoplastic vulcanizates (Eco TPV) in harsh acidic environments. Simultaneously, the optimization process has clarified the degradation mechanisms driven by acid concentration and temperature, providing a clear guideline for material selection. Moreover, significantly different leaching behaviors were found between circular and recycled fillers, emphasizing the need for high-purity feedstocks in fuel cell applications. Furthermore, with the calibration of material models, the behavior of these seals can be accurately predicted in digital simulations.

Accordingly, the present work highlights the crucial importance of selecting elastomeric formulations based not only on initial mechanical properties but on long-term chemical stability and leaching potential. At the same time, it proves the feasibility of using circular carbon black as a sustainable reinforcing filler that does not compromise the functional performance of EPDM gaskets.

Outlook

- The theoretical and experimental study realized in the context of this thesis highlights current tendencies in the development and manufacturing of sustainable sealing components for hydrogen mobility.
- Undoubtedly, numerous chemical compositions can be adopted and explored regarding the development of new functional elastomers.
- The virtually unlimited possibility of combining sustainable polymers that possess increased chemical resistance, with clean and circular reinforcing fillers will lead to the fabrication of functional composite seals with improved characteristics and extended service life.

BUPT

In this regard, several further research directions can be outlined:

- further optimization of the Eco-EPDM formulations by investigating different loadings of circular carbon black to maximize mechanical performance without compromising processability;
- experimental testing of these materials in an active fuel cell stack to validate the leaching impact on actual electrochemical performance (OCV decay, voltage loss);
- attempts to characterize the long-term fatigue behavior of these elastomers under combined mechanical cycling and chemical exposure;
- assessment of the influence of hydrogen gas permeation at high pressures (700 bar) on the structural integrity of the sustainable EPDM variants;
- further investigations regarding the specific identification of organic leachates using Mass Spectrometry (HPLC-MS) to pinpoint the exact additives responsible for contamination;
- further investigations on the characteristics and properties of the seals at sub-zero temperatures, specifically focusing on the influence of crystallization kinetics on cold-start sealing capability.

BUPT

REFERENCES

1. International Energy Agency World Energy Investment 2024 2024.
2. BloombergNEF Energy Transition Investment Trends 2024 2025.
3. Chart: Global Investment in the Energy Transition… | Canary Media Available online: https://www.canarymedia.com/articles/clean-energy/chart-global-investment-in-the-energy-transition-surpasses-2t?utm_source=chatgpt.com (accessed on 30 October 2025).
4. International Energy Agency Global Hydrogen Review 2024 2024.
5. Proton Exchange Membrane Fuel Cell Market Size, Trends, Share, Demand 2034 Available online: https://www.zionmarketresearch.com/report/proton-exchange-membrane-fuel-cell-market?utm_source=chatgpt.com (accessed on 30 October 2025).
6. PEM Fuel Cell Market Share, 2034 Statistics Report Available online: https://www.gminsights.com/industry-analysis/pem-fuel-cell-market?utm_source=chatgpt.com (accessed on 30 October 2025).
7. Saur, G. Wind-To-Hydrogen Project: Electrolyzer Capital Cost Study; Golden, Colorado, USA, 2008;
8. Hubert, M.; Peterson, D.; Miller, E.; Vickers, J.; Mow, R.; Howe, C.; Rustagi, N.; Gilbert, A.; Capanna, S.; Penev, M.; et al. Clean Hydrogen Production Cost Scenarios with PEM Electrolyzer Technology; Washington, D.C., 2024;
9. Badgett, A.; Brauch, J.; Thatte, A.; Rubin, R.; Skangos, C.; Wang, X.; Ahluwalia, R.; Pivovar, B.; Ruth, M. Updated Manufactured Cost Analysis for Proton Exchange Membrane Water Electrolyzers; Golden, Colorado, USA, 2024;
10. International Renewable Energy Agency Green Hydrogen Cost Reduction: Scaling up Electrolysers to Meet the 1.5C Climate Goal 2020.
11. Frieden, F.; Leker, J. Future Costs of Hydrogen: A Quantitative Review. Sustain Energy Fuels 2024, 8, 1806–1822, doi:10.1039/D4SE00137K.
12. Energy; Directory, S. Fuel Cell Degradation Mechanisms 2024.
13. Hinds, G. Performance and Durability of PEM Fuel Cells: A Review; Teddington, Middlesex, United Kingdom, 2004;
14. Luo, C.; Choo, H.L.; Ahmad, H.; Sivasankaran, P.N. Towards Enhanced Durability: A Review of Fuel Cell Electric Vehicle Development. Next Energy 2025, 9, 100399, doi:10.1016/j.nxener.2025.100399.
15. Rangel, C.M.; Silva, R.A.; Travassos, M.A.; Paiva, T.I.; Fernandes, V.R. Fuel Starvation: Irreversible Degradation Mechanisms in PEM Fuel Cells. In Proceedings of the Proceedings of the 18th World Hydrogen Energy Conference (WHEC 2010); Essen, Germany, May 2010.
16. Xie, Z.; Wang, J.; Zhao, G.; Zhang, Q.; Fan, H.; Zeng, A.; Ding, W. A Review on Durability of Key Components of PEM Fuel Cells. Catal Sci Technol 2024, 14, 4420–4431, doi:10.1039/D4CY00351A.
17. Foltuț, D.; Șerban, V.-A. Current Advancements in the Behavior Analysis of EPDM Elastomers in Peripheral Applications of the Cathodic Side of PEMFC Systems. Recent Prog Mater 2024, 06, 1–27, doi:10.21926/rpm.2404026.
18. Foltuț, D.; Vălean, E.; Șoșoi, G.-I.; Pascal, D.-T.; Pospisil, J.; Buzdugan, M. Comprehensive Study of EPDM Rubber Properties: Temperature-Dependent Stiffness, Tensile Behavior and FEA Calibration. IOP Conf Ser Mater Sci Eng 2024, 1319, 012025, doi:10.1088/1757-899X/1319/1/012025.

BUPT

19. Foltuț, D.; Șoșoi, G.-I.; Vălean, E.; Pospisil, J.; Pascal, D.-T.; Șerban, V.-A. Impact of Aging on Tensile Properties of EPDM, TPV, and Eco-TPV: A Comparative Study Across Diverse Environments. IOP Conf Ser Mater Sci Eng 2024, 1319, 012022, doi:10.1088/1757-899X/1319/1/012022.
20. Foltuț, D.; Pospisil, J.; Pascal, D.-T. Effects of Sulfuric Acid-Water Immersion on the Properties of Ethylene Propylene Diene Monomer, Thermoplastic Vulcanizates, and Eco-Friendly Thermoplastic Vulcanizates. IOP Conf Ser Mater Sci Eng 2024, 1319, 012023, doi:10.1088/1757-899X/1319/1/012023.
21. Foltuț, D.; Uțu, I.-D.; Șerban, V.-A. Tribological Performance of EPDM and TPV Elastomers Against Glass Fiber-Reinforced Polyamide 66 Composites. Materials 2025, Vol. 18, Page 2515 2025, 18, 2515, doi:10.3390/MA18112515.
22. Foltuț, D.; Șerban, V.A. Mechanical Performance Degradation of ECO EPDM Elastomers in Acidic Fuel Cell Environments. Materials 2025, 18, doi:10.3390/ma18092071.
23. Foltuț, D.; Șoșoi, G.-I.; Șerban, V.-A. Chemical Stability and Leaching Behavior of ECO EPDM in Acidic Fuel Cell-like Conditions. Materials 2025, 18, 3260, doi:10.3390/ma18143260.
24. Steele, B.C.H.; Heinzel, A. Materials for Fuel-Cell Technologies. Nature 2001 414:6861 2001, 414, 345–352, doi:10.1038/35104620.
25. Akroot, A.; Ekici, Ö.; Köksal, M. Process Modeling of an Automotive Pem Fuel Cell System. Int J Green Energy 2019, 16, 778–788, doi:10.1080/15435075.2019.1641105.
26. Daud, W.R.W.; Rosli, R.E.; Majlan, E.H.; Hamid, S.A.A.; Mohamed, R.; Husaini, T. PEM Fuel Cell System Control: A Review. Renew Energy 2017, 113, 620–638, doi:10.1016/J.RENENE.2017.06.027.
27. Dicks, A.; Rand, D. Fuel Cell Systems Explained, Third Edition; 2018;
28. Plug Power Inc. PEM Fuel Cells 101: How They Work and Why They Matter 2024.
29. Bosch Mobility Innovations GmbH Fuel Cell Stack: Key Component for Efficient Hydrogen Powertrains 2024.
30. Center for Sustainable Systems University of Michigan Hydrogen Factsheet 2024.
31. U.S. Department of Energy Hydrogen Storage 2024.
32. Council, H. Hydrogen: Scaling Up — A Sustainable Pathway for the Global Energy Transition; 2017;
33. Europe, H. CO_2 Emission Standards for Heavy-Duty Vehicles — Position Paper; 2023;
34. Analysis, I. In 2030, over 45 000 Heavy Trucks Will Run on Hydrogen in Europe 2023.
35. MobilityPortal.eu EU CO_2 Reduction Targets for Trucks and Buses 2024.
36. Commission, E. Heavy-Duty Vehicles – Transport Decarbonisation 2025.
37. Proton-Exchange Membrane Fuel Cell Market: Global Trends & Available online: https://www.openpr.com/news/4196106/proton-exchange-membrane-fuel-cell-market-global-trends (accessed on 6 November 2025).
38. Analytics, M.R. Proton Exchange Membrane Fuel Cells Vehicle — Product Insights Report; 2025;
39. Reports, W. Proton Exchange Membrane Fuel Cells Vehicle Market: Global Market Insights, Forecast, and Opportunities; 2025;
40. Group, I. Hydrogen Fuel Cell Vehicle Market: Size, Share, Trends and Forecast by Technology, Vehicle Type, and Region, 2025–2033; 2025;

BUPT

41. Insights, F.B. Proton Exchange Membrane Fuel Cell (PEMFC) Market Size, Share & COVID-19 Impact Analysis, By Type, Application, and Regional Forecast to 2032; 2025;
42. Nguyen, H.L.; Han, J.; Vu, H.N.; Yu, S. Investigation of Multiple Degradation Mechanisms of a Proton Exchange Membrane Fuel Cell under Dynamic Operation. Energies (Basel) 2022, 15, 9574, doi:10.3390/en15249574.
43. Nguyen, H.L.; Kim, Y.; Trinh, D.H.; Yu, S. Dynamic Flooding Management Strategy for Automotive Proton Exchange Membrane Fuel Cell System Using Cathode Membrane Water Content. Appl Therm Eng 2025, 273, 126485, doi:10.1016/j.applthermaleng.2025.126485.
44. Services, G. Membrane Hydration Control in Fuel Cells 2025.
45. Zhang, Z.; Mao, J.; Liu, Z. Advancements and Insights in Thermal and Water Management of Proton Exchange Membrane Fuel Cells: Challenges and Prospects. International Communications in Heat and Mass Transfer 2024, 153, 107376, doi:10.1016/j.icheatmasstransfer.2024.107376.
46. Yakubu, A.U.; Zhao, J.; Jiang, Q.; Ye, X.; Liu, J.; Yu, Q.; Xiong, S. A Comprehensive Review of Primary Cooling Techniques and Thermal Management Strategies for Polymer Electrolyte Membrane Fuel Cells PEMFC. Heliyon 2024, 10, e38556, doi:10.1016/j.heliyon.2024.e38556.
47. Nguyen, H.L.; Han, J.; Nguyen, X.L.; Yu, S.; Goo, Y.-M.; Le, D.D. Review of the Durability of Polymer Electrolyte Membrane Fuel Cell in Long-Term Operation: Main Influencing Parameters and Testing Protocols. Energies (Basel) 2021, 14, 4048, doi:10.3390/en14134048.
48. de Bruijn, F.A. PEMFC Lifetime and Durability — an Overview; 2011;
49. Commission, E. Horizon 2020 Topic # FCH-01-6-2018 "Game Changer Fuel Cell Stack for Automotive Applications" 2018.
50. Marcinkoski, J.; Vijayagopal, R.; Adams, J.; James, B.; Kopasz, J.; Ahluwalia, R. Technical Targets for Hydrogen-Fueled Long-Haul Class 8 Tractor-Trailer Trucks; 2019;
51. Turan, C.; Cora, Ö.N.; Koç, M. Contact Resistance Characteristics of Coated Metallic Bipolar Plates for PEM Fuel Cells – Investigations on the Effect of Manufacturing. Int J Hydrogen Energy 2012, 37, 18187–18204, doi:10.1016/j.ijhydene.2012.09.042.
52. Zhang, H.; Zhang, L.; Zhang, Y.; Hou, Z.; Liu, J. Effect of Gas Diffusion Layer Notch Arrangement and Gradient Depth on the Performance of Proton Exchange Membrane Fuel Cells in the Serpentine Flow Field. ACS Omega 2023, 8, 10191–10201, doi:10.1021/acsomega.2c07632.
53. Hung, C.-H.; Chiu, C.-H.; Wang, S.-P.; Chiang, I.-L.; Yang, H. Ultra Thin Gas Diffusion Layer Development for PEMFC. Int J Hydrogen Energy 2012, 37, 12805–12812, doi:10.1016/j.ijhydene.2012.05.110.
54. Pourrahmani, H.; Van Herle, J. Manufacturing Protocol and Post Processing of Ultra-Thin Gas Diffusion Layer Using Advanced Scanning Techniques. Sci Rep 2024, 14, 13078, doi:10.1038/s41598-024-63751-z.
55. Atak, N.N.; Dogan, B.; Yesilyurt, M.K. Investigation of the Performance Parameters for a PEMFC by Thermodynamic Analyses: Effects of Operating Temperature and Pressure. Energy 2023, 282, 128907, doi:10.1016/J.ENERGY.2023.128907.
56. Wang, X.Z.; Luo, H.; Luo, J.L. Effects of Hydrogen and Stress on the Electrochemical and Passivation Behaviour of 304 Stainless Steel in Simulated PEMFC Environment. Electrochim Acta 2019, 293, 60–77, doi:10.1016/J.ELECTACTA.2018.10.028.

BUPT

57. Ren, P.; Pei, P.; Chen, D.; Zhang, L.; Li, Y.; Song, X.; Wang, M.; Wang, H. Corrosion of Metallic Bipolar Plates Accelerated by Operating Conditions in a Simulated PEM Fuel Cell Cathode Environment. Renew Energy 2022, 194, 1277–1287, doi:10.1016/J.RENENE.2022.05.153.
58. Vallejo-Cervantes, C.; Espinoza-Andaluz, M.; Iranzo, A. Technical Review of Commercial LT-PEMFC Technologies: Performance, Applications and Challenges. Int J Hydrogen Energy 2025, 176, 151480, doi:10.1016/j.ijhydene.2025.151480.
59. Wu, F.; Chen, B.; Yan, Y.; Chen, Y.; Pan, M. Degradation of Silicone Rubbers as Sealing Materials for Proton Exchange Membrane Fuel Cells under Temperature Cycling. Polymers (Basel) 2018, 10, 522, doi:10.3390/polym10050522.
60. Clean Hydrogen Joint Undertaking FCH 2 JU – MAWP Key Performance Indicators (KPIs) 2024.
61. Zaghdoudi, M.; Kömmling, A.; Jaunich, M.; Wolff, D. Erroneous or Arrhenius: A Degradation Rate-Based Model for EPDM during Homogeneous Ageing. Polymers (Basel) 2020, 12, doi:10.3390/POLYM12092152.
62. Agency, I.R.E. World Energy Transitions Outlook 2023: 1.5°C Pathway; 2023;
63. Mechanical Durability of PEM Fuel Cells | Encyclopedia MDPI Available online: https://encyclopedia.pub/entry/25697 (accessed on 3 September 2025).
64. Pehlivan-Davis, S. POLYMER ELECTROLYTE MEMBRANE (PEM) FUEL CELL SEALS DURABILITY, Lounghborough University, 2016.
65. M.A., W.R.G.Esq. XXIV. On Voltaic Series and the Combination of Gases by Platinum. The London, Edinburgh, and Dublin Philosophical Magazine and Journal of Science 1839, 14, 127–130, doi:10.1080/14786443908649684.
66. Barak, M. Fuel Cells—Present Position and Outstanding Problems. Advanced Energy Conversion 1966, 6, 29–55, doi:10.1016/0365-1789(66)90011-7.
67. Niedrach, L.W.; Grubb, W.T. Ion Exchange Membrane Fuel Cells. Fuel cells. Academic, New York 1963, 253–298.
68. Peron, J.; Mani, A.; Zhao, X.; Edwards, D.; Adachi, M.; Soboleva, T.; Shi, Z.; Xie, Z.; Navessin, T.; Holdcroft, S. Properties of Nafion® NR-211 Membranes for PEMFCs. J Memb Sci 2010, 356, 44–51, doi:10.1016/j.memsci.2010.03.025.
69. Zhao, J.; Guo, H.; Xing, Y.; Ping, S.; Lin, W.; Yang, Y.; Wang, Z.; Ma, T. A Review on the Sealing Structure and Materials of Fuel-Cell Stacks. Clean Energy 2023, 7, 59–69, doi:10.1093/ce/zkac096.
70. Hong, B.K.; Kim, S.H. Recent Advances in Fuel Cell Electric Vehicle Technologies of Hyundai. ECS Trans 2018, 86, 3–11, doi:10.1149/08613.0003ecst.
71. Dolan, C.; Gangi, J.; Homann, Q.; Fink, V.; Kopasz, J. 2019 Fuel Cell Technologies Market Report; Argonne, IL (United States), 2020;
72. Barbir, F. PEM Fuel Cells: Theory and Practice; 2012;
73. Mohapatra, S.C.; Inc, D. Complex Coolant Fluid for PEM Fuel Cells, Excerpt from 2007 DOE Hydrogen Program Annual Progress Report; 2007;
74. Ramani, V.; Kunz, H.R.; Fenton, J.M. The Chalkboard: The Polymer Electrolyte Fuel Cell. Electrochem Soc Interface 2004, 13, 17.
75. Springer, T.E.; Zawodzinski, T.A.; Gottesfeld, S. Polymer Electrolyte Fuel Cell Model. J Electrochem Soc 1991, 138, 2334.
76. Fuller, T.F.; Perry, M.L. A Historical Perspective of Fuel-Cell Technology in the 20th Century. J Electrochem Soc 2002, 149, S59–S67.

BUPT

77. Kim, S.; Hong, I. Effects of Humidity and Temperature on a Proton Exchange Membrane Fuel Cell (PEMFC) Stack. Journal of Industrial and Engineering Chemistry 2008, 14, 357–364, doi:https://doi.org/10.1016/j.jiec.2008.01.007.
78. Larminie, J.; Dicks, A. Fuel Cell Systems Explained Second Edition.
79. Li, C.; Ding, Y.; Yang, Z.; Yuan, Z.; Ye, L. Compressive Stress-Thermo Oxidative Ageing Behaviour and Mechanism of EPDM Rubber Gaskets for Sealing Resilience Assessment. Polym Test 2020, 84, 106366, doi:10.1016/J.POLYMERTESTING.2020.106366.
80. Kusoglu, A.; Weber, A.Z. New Insights into Perfluorinated Sulfonic-Acid Ionomers. Chem Rev 2017, 117, 987–1104.
81. Pehlivan-Davis, S.; Clarke, J.; Armour, S. Comparison of Accelerated Aging of Silicone Rubber Gasket Material with Aging in a Fuel Cell Environment. J Appl Polym Sci 2013, 129, 1446–1454, doi:10.1002/APP.38837.
82. Gasteiger, H.A.; Kocha, S.S.; Sompalli, B.; Wagner, F.T. Activity Benchmarks and Requirements for Pt, Pt-Alloy, and Non-Pt Oxygen Reduction Catalysts for PEMFCs. Appl Catal B 2005, 56, 9–35.
83. Ono, H.; Nait-Ali, A.; Kane Diallo, O.; Benoit, G.; Castagnet, S. Influence of Pressure Cycling on Damage Evolution in an Unfilled EPDM Exposed to High-Pressure Hydrogen. Int J Fract 2018, 210, 137–152, doi:10.1007/S10704-018-0266-Y/FIGURES/14.
84. Larminie, J.; Dicks, A.; McDonald, M.S. Fuel Cell Systems Explained; J. Wiley Chichester, UK, 2003; Vol. 2;.
85. Sery, J.; Leduc, P. Fuel Cell Behavior and Energy Balance on Board a Hyundai Nexo. International Journal of Engine Research 2022, 23, 709–720, doi:10.1177/14680874211059046.
86. Yoshida, T.; Kojima, K. Toyota MIRAI Fuel Cell Vehicle and Progress Toward a Future Hydrogen Society. Interface magazine 2015, 24, 45–49, doi:10.1149/2.F03152if.
87. Hong, B.K.; Kim, S.H. Recent Advances in Fuel Cell Electric Vehicle Technologies of Hyundai. ECS Trans 2018, 86, 3–11, doi:10.1149/08613.0003ecst.
88. Zhao, Q.; Li, X.; Gao, J.; Jia, Z. Degradation Evaluation of Ethylene-Propylene-Diene Monomer (EPDM) Rubber in Artificial Weathering Environment by Principal Component Analysis. Mater Lett 2009, 63, 116–117, doi:10.1016/j.matlet.2008.09.019.
89. Mitsuo, K.; Nobuhiro, Y.; Hiroaki, T.; Takashi, I.; Ayumu, I.; Junichiro, Y. Test Method to Establish Hydrogen Compatibility of Materials in High Pressure Hydrogen Gas Environments for Fuel Cell Vehicles. ISIJ International 2021, 61, 1333–1336, doi:10.2355/ISIJINTERNATIONAL.ISIJINT-2020-358.
90. Technologies, V. Stack Control Valve (SCV) – One-Pager 1.4 (ENG); 2025;
91. Gent, A.N. A New Constitutive Relation for Rubber. Rubber Chemistry and Technology 1996, 69, 59–61, doi:10.5254/1.3538357.
92. Scherer, R.K. Seals and Sealing Handbook; 2nd ed.; Newnes-Butterworths: London, 1981; ISBN 978-0408004522.
93. Karnopp, D.; Margolis, D.; Rosenberg, R. System Dynamics: Modeling and Simulation of Mechatronic Systems; 5th ed.; Wiley: Hoboken, 2012;
94. Gent, A.N.; Lindley, P.B. The Compression of Rubber Blocks. Proceedings of the Institution of Mechanical Engineers 1959, 173, 111–122.

BUPT

95. Zhao, J.; Guo, H.; Xing, Y.; Ping, S.; Lin, W.; Yang, Y.; Wang, Z.; Ma, T. A Review on the Sealing Structure and Materials of Fuel-Cell Stacks. Clean Energy 2023, 7, 59–69, doi:10.1093/ce/zkac096.
96. Greenwood, J.A.; Williamson, J.B.P. Contact of Nominally Flat Surfaces. Proceedings of the Royal Society A 1966, 295, 300–319, doi:10.1098/rspa.1966.0242.
97. Sandler, T.; Pistor, J.; Nellesen, A. Thermo-Mechanical and Chemical Aging of EPDM Compounds. Polym Degrad Stab 2019, 168, 108941, doi:10.1016/j.polymdegradstab.2019.108941.
98. Persson, B.N.J. Rubber Friction: Role of the Flash Temperature. Journal of Physics: Condensed Matter 2006, 18, 7789, doi:10.1088/0953-8984/18/32/025.
99. Müller, H.; Kuttler, K. Contact Mechanics for Representing Surface Roughness. Tribol Int 2013, 59, 50–60, doi:10.1016/j.triboint.2012.10.017.
100. Gent, A.N.; Tobias, R.H. Threshold Stress in the Relaxation of Rubber Compression. Journal of Polymer Science: Polymer Physics Edition 1982, 20, 2051–2058, doi:10.1002/pol.1982.180201107.
101. Fukahori, Y. New Theories of Rubber Reinforcement Based on Filler–Matrix Interaction. Prog Polym Sci 2005, 30, 736–770, doi:10.1016/j.progpolymsci.2005.03.002.
102. Persson, B.N.J. Theory of Rubber Friction and Contact Mechanics. Journal of Chemical Physics 2001, 115, 3840–3861, doi:10.1063/1.1388626.
103. Myant, C.; Underwood, R.; Morales-Espejel, G.E.; Spikes, H.A. Film Thickness and Friction of Stationary Contacts in the Mixed Lubrication Regime. Tribol Int 2010, 43, 1960–1967, doi:10.1016/j.triboint.2010.05.003.
104. Comyn, J. Polymer Permeability; Springer: London, 1992; ISBN 978-94-010-5624-0.
105. Yang, D.; Ma, J.; Zhang, Q.; Li, B.; Ming, P.; Zhang, C. Accelerated Test of Silicone Rubbers Exposing to PEMFC Environment. Progress in Natural Science: Materials International 2020, 30, 882–889, doi:10.1016/J.PNSC.2020.10.008.
106. Kadri, R.; Abdelaziz, M.N.; Fayolle, B.; Hassine, M. Ben; Witz, J.F. A Unified Mechanical Based Approach to Fracture Properties Estimates of Rubbers Subjected to Aging. Int J Solids Struct 2022, 234–235, 111305, doi:10.1016/J.IJSOLSTR.2021.111305.
107. Wu, F.; Chen, B.; Yan, Y.; Chen, Y.; Pan, M. Degradation of Silicone Rubbers as Sealing Materials for Proton Exchange Membrane Fuel Cells under Temperature Cycling. Polymers (Basel) 2018, 10, 522, doi:10.3390/polym10050522.
108. Joubert, C.; Michel, A.; Choplin, L.; Cassagnau, P. Influence of the Crosslink Network Structure on Stress-relaxation Behavior: Viscoelastic Modeling of the Compression Set Experiment. J Polym Sci B Polym Phys 2003, 41, 1779–1790, doi:10.1002/polb.10530.
109. Liu, J.; Zhang, L.W.; Wang, B.; Xu, Z.Q.; Wang, W. Effect of Thermal Aging on Mechanical Properties of EPDM Rubber. Applied Mechanics and Materials 2015, 727, 318–321.
110. Bokobza, L. The Reinforcement of Elastomeric Networks by Fillers. Macromol Mater Eng 2007, 292, 607–622, doi:10.1002/mame.200700021.
111. Kraus, G. Reinforcement of Elastomers by Carbon Black. Rubber chemistry and Technology 1978, 51, 297–321.
112. Barbir, F. PEM Fuel Cells: Theory and Practice; 2nd ed.; Academic Press: Amsterdam, 2013; ISBN 978-0-12-387710-9.

BUPT

113. Van Amerongen, G.J. The Effect of Fillers on the Permeability of Rubber to Gases. Rubber Chemistry and Technology 1955, 28, 821–832, doi:10.5254/1.3542844.
114. Larminie, J.; Dicks, A. Fuel Cell Systems Explained; 2nd ed.; John Wiley & Sons: Chichester, 2003; ISBN 978-0470848579.
115. Pamela De Sousa, A.; Karla Barbosa Da Silva, A.; Ricardo, L.; Figueiredo, F.; Lates, M.T.; Gavrila, C.C. Frictional Study of the Polyamide/Rubber Contact Materials. IOP Conf Ser Mater Sci Eng 2020, 898, 012052, doi:10.1088/1757-899X/898/1/012052.
116. Zhao, J.; Guo, H.; Xing, Y.; Ping, S.; Lin, W.; Yang, Y.; Wang, Z.; Ma, T. A Review on the Sealing Structure and Materials of Fuel-Cell Stacks. Clean Energy 2023, 7, 59–69.
117. Xu, Q.; Zhao, J.; Chen, Y.; Liu, S.; Wang, Z. Effects of Gas Permeation on the Sealing Performance of PEMFC Stacks. Int J Hydrogen Energy 2021, 46, 36424–36435, doi:10.1016/J.IJHYDENE.2021.08.137.
118. Cui, T.; Chao, Y.J.; Van Zee, J.W. Sealing Force Prediction of Elastomeric Seal Material for PEM Fuel Cell under Temperature Cycling. Int J Hydrogen Energy 2014, 39, 1430–1438, doi:10.1016/j.ijhydene.2013.10.086.
119. Qiu, D.; Liang, P.; Peng, L.; Yi, P.; Lai, X.; Ni, J. Material Behavior of Rubber Sealing for Proton Exchange Membrane Fuel Cells. Int J Hydrogen Energy 2020, 45, 5465–5473, doi:10.1016/J.IJHYDENE.2019.07.232.
120. Santoprene® TPV | Thermoplastic Vulcanizates TPV | Celanese Available online: https://www.celanese.com/products/santoprene-tpv-thermoplastic-vulcanizates (accessed on 24 July 2023).
121. Drobny, J.G. Handbook of Thermoplastic Elastomers; 2nd ed.; William Andrew: Norwich, NY, 2014; ISBN 978-0-323-22136-8.
122. Schulze, M.; Knöri, T.; Gülzow, E. Interaction of Sealing Materials with the Proton Exchange Membrane Fuel Cell Environment. J Power Sources 2004, 127, 213–221, doi:10.1016/j.jpowsour.2003.09.016.
123. Chang, H.; Wan, Z.; Chen, X.; Wan, J.; Luo, L.; Zhang, H.; Shu, S.; Tu, Z. Temperature and Humidity Effect on Aging of Silicone Rubbers as Sealing Materials for Proton Exchange Membrane Fuel Cell Applications. Appl Therm Eng 2016, 104, 472–478, doi:10.1016/j.applthermaleng.2016.05.095.
124. Yang, D.; Ma, J.; Zhang, Q.; Li, B.; Ming, P.; Zhang, C. Accelerated Test of Silicone Rubbers Exposing to PEMFC Environment. Progress in Natural Science: Materials International 2020, 30, 882–889, doi:10.1016/j.pnsc.2020.10.008.
125. Sarkar, P.; Bhowmick, A.K. Sustainable Rubbers and Rubber Additives. J Appl Polym Sci 2018, 135.
126. Hern Boon, Z.; Yin Teo, Y.; Teck-Chye Ang, D. Recent Development of Biodegradable Synthetic Rubbers and Bio-Based Rubbers Using Sustainable Materials from Biological Sources. 2022, doi:10.1039/d2ra06602e.
127. Filippova, O. V.; Maksimkin, A. V.; Dayyoub, T.; Larionov, D.I.; Telyshev, D. V. Sustainable Elastomers for Actuators: "Green" Synthetic Approaches and Material Properties. Polymers (Basel) 2023, 15.
128. Meys, R.; Kätelhön, A.; Bardow, A. Towards Sustainable Elastomers from CO2: Life Cycle Assessment of Carbon Capture and Utilization for Rubbers. Green Chemistry 2019, 21, 3334–3342, doi:10.1039/c9gc00267g.
129. Costa, S.M.R.; Fowler, D.; Carreira, G.A.; Portugal, I.; Silva, C.M. Production and Upgrading of Recovered Carbon Black from the Pyrolysis of End-of-Life Tires. Materials 2022, 15.

BUPT

130. bin Samsuri, A. Evaluation of Recycled Carbon Black (r-CB) Based on Styrene Butadiene Rubber, Natural Rubber and Nitrile Rubber Compounds. In Application and Characterization of Rubber Materials; IntechOpen, 2023.
131. Bogdahn, S.; Koch, E.; Katrakova-Kr黜er, D.; Malek, C. Application of Recovered Carbon Black (RCB) by Waste Tire Pyrolysis as an Alternative Filler in Elastomer Products. Advanced Materials & Sustainable Manufacturing 2025, 2, 10008–10008, doi:10.70322/amsm.2025.10008.
132. Boonmahitthisud, A.; Boonkerd, K. Sustainable Development of Natural Rubber and Its Environmentally Friendly Composites. Curr Opin Green Sustain Chem 2021, 28.
133. Srivastava, V.K.; Maiti, M.; Basak, G.C.; Jasra, R. V Role of Catalysis in Sustainable Production of Synthetic Elastomers; 2014; Vol. 126;.
134. Surehali, S.; Singh, A.; Biligiri, K.P. A State-of-the-Art Review on Recycling Rubber in Concrete: Sustainability Aspects, Specialty Mixtures, and Treatment Methods. Developments in the Built Environment 2023, 14, doi:10.1016/j.dibe.2023.100171.
135. Tan, J.; Chao, Y.J.; Van Zee, J.W.; Li, X.; Wang, X.; Yang, M. Assessment of Mechanical Properties of Fluoroelastomer and EPDM in a Simulated PEM Fuel Cell Environment by Microindentation Test. Materials Science and Engineering: A 2008, 496, 464–470, doi:10.1016/J.MSEA.2008.05.052.
136. Tan, J.; Chao, Y.J.; Wang, H.; Gong, J.; Van Zee, J.W. Chemical and Mechanical Stability of EPDM in a PEM Fuel Cell Environment. Polym Degrad Stab 2009, 94, 2072–2078, doi:10.1016/j.polymdegradstab.2009.07.009.
137. Lin, C.W.; Chien, C.H.; Tan, J.; Chao, Y.J.; Van Zee, J.W. Dynamic Mechanical Characteristics of Five Elastomeric Gasket Materials Aged in a Simulated and an Accelerated PEM Fuel Cell Environment. Int J Hydrogen Energy 2011, 36, 6756–6767, doi:10.1016/J.IJHYDENE.2011.02.112.
138. Nah, C.; Kim, S.G.; Shibulal, G.S.; Yoo, Y.H.; Mensah, B.; Jeong, B.H.; Hong, B.K.; Ahn, J.H. Effects of Curing Systems on the Mechanical and Chemical Ageing Resistance Properties of Gasket Compounds Based on Ethylene-Propylene-Diene-Termonomer Rubber in a Simulated Fuel Cell Environment. Int J Hydrogen Energy 2015, 40, 10627–10635, doi:10.1016/J.IJHYDENE.2015.07.003.
139. Liu, Q.; Li, J.; Jiang, Y.; Cong, C.; Xu, L.; Zhang, Y.; Meng, X.; Zhou, Q. Effect of Crosslinked Structure on the Chemical Degradation of EPDM Rubber in an Acidic Environment. Polym Degrad Stab 2021, 185, 109475, doi:10.1016/J.POLYMDEGRADSTAB.2020.109475.
140. Shamsabadi, A.; Farahani, A.; Shirkavand, M.M.; Hafezi, M.J.; Tohidian, M. Carbon Black/Ethylene Propylene Diene Monomer (EPDM) Rubber as Polymer Electrolyte Membrane Fuel Cell Gaskets: Mechanical and Chemical Assessment. Iranian Polymer Journal (English Edition) 2024, 33, 169–183, doi:10.1007/S13726-023-01239-9/TABLES/4.
141. Shuang-Hong, W.; Chang-Sheng, Z.; Chao-Fan, H. The Aging Property and Storage Life Prediction of EPDM. J Phys Conf Ser 2023, 2478, 032046, doi:10.1088/1742-6596/2478/3/032046.
142. Song, J.; Wang, Z.; Ji, H.; Wang, R.; Zhou, Y.; He, Y.; Jin, H. Mechanical Behavior of Aged EPDM Insulation of High-Voltage Cable Joints in Thermal-Oxidative Environment. IOP Conf Ser Mater Sci Eng 2020, 768, 062088, doi:10.1088/1757-899X/768/6/062088.

BUPT

143. Li, X.; Qiu, Z.; Hung, W.S.T.; Olofsson, U.; Manuel, L.; Duan, C. Study on Tribological Properties of Gear Material PA66 Reinforced by Glass Fibers. Tribol Lett 2025, 73, doi:10.1007/s11249-024-01941-6.
144. Kunishima, T.; Nagai, Y.; Kurokawa, T.; Bouvard, G.; Abry, J.C.; Fridrici, V.; Kapsa, P. Tribological Behavior of Glass Fiber Reinforced-PA66 in Contact with Carbon Steel under High Contact Pressure, Sliding and Grease Lubricated Conditions. Wear 2020, 456–457, doi:10.1016/j.wear.2020.203383.
145. Kunishima, T.; Nagai, Y.; Bouvard, G.; Abry, J.C.; Fridrici, V.; Kapsa, P. Comparison of the Tribological Properties of Carbon/Glass Fiber Reinforced PA66-Based Composites in Contact with Steel, with and without Grease Lubrication. Wear 2021, 477, doi:10.1016/j.wear.2021.203899.
146. Karger-Kocsis, J.; Mousa, A.; Major, Z.; Békési, N. Dry Friction and Sliding Wear of EPDM Rubbers against Steel as a Function of Carbon Black Content. Wear 2008, 264, 359–367, doi:10.1016/J.WEAR.2007.03.021.
147. Felhös, D.; Karger-Kocsis, J. Tribological Testing of Peroxide-Cured EPDM Rubbers with Different Carbon Black Contents under Dry Sliding Conditions against Steel. Tribol Int 2008, 41, 404–415, doi:10.1016/J.TRIBOINT.2007.09.005.
148. Rikmann, E.; Mäeorg, U.; Liiv, J. Recycling of Low-Quality Carbon Black Produced by Tire Pyrolysis. Applied Sciences (Switzerland) 2024, 14, doi:10.3390/app14052192.
149. Billotte, C.; Romana, L.; Flory, A.; Kaliaguine, S.; Ruiz, E. Recycled Carbon Black/High-Density Polyethylene Composite from Waste Tires: Manufacturing, Testing, and Aging Characterization. Recycling 2024, 9, doi:10.3390/recycling9060107.
150. Ghosh, R.; Mani, C.; Krafczyk, R.; Schnell, R.; Talma, A.; Blume, A.; Dierkes, W.K. Exploring the Impact of Reinforcing Filler Systems on Devulcanizate Composites. Polymers (Basel) 2024, 16, doi:10.3390/polym16111448.
151. Brunella, V.; Aresti, V.; Romagnolli, U.; Muscato, B.; Girotto, M.; Rizzi, P.; Luda, M.P. Recycling of EPDM via Continuous Thermo-Mechanical Devulcanization with Co-Rotating Twin-Screw Extruder. Polymers (Basel) 2022, 14, doi:10.3390/polym14224853.
152. ISO 37:2024 - Rubber, Vulcanized or Thermoplastic — Determination of Tensile Stress-Strain Properties Available online: https://www.iso.org/standard/86892.html (accessed on 30 April 2025).
153. ISO 188 - Rubber, Vulcanized or Thermoplastic — Accelerated Ageing and Heat Resistance Tests; Geneva, CH, 2023; Vol. 2023;.
154. ISO 815-1-Rubber, Vulcanized or Thermoplastic — Determination of Compression Set — Part 1: At Ambient or Elevated Temperatures 2019.
155. ISO 48-4: Rubber — Determination of Hardness — Part 4: Micro-Indentation Method 2018.
156. ISO 48-2: Rubber — Determination of Hardness — Part 2: Dead-Load Hardness 2018.
157. Foltuţ, D.; Vălean, E.; Dzitac, V.; Batrîna, D.Ş.; Simoc, O.; Pascal, D.T.; Şerban, V.A. Heat Aging Effect on Tensile Behavior at Different Strain Rates of Thermoplastic Styrene Elastomer. In Proceedings of the Materials Today: Proceedings; Elsevier Ltd, January 1 2023; Vol. 78, pp. 257–262.
158. Burelo, M.; Martínez, A.; Hernández-Varela, J.D.; Stringer, T.; Ramírez-Melgarejo, M.; Yau, A.Y.; Luna-Bárcenas, G.; Treviño-Quintanilla, C.D. Recent Developments in Synthesis, Properties, Applications and Recycling of Bio-Based Elastomers. Molecules 2024, 29.

BUPT

159. Sagar, M.; Nibedita, K.; Manohar, N.; Kumar, K.R.; Suchismita, S.; Pradnyesh, A.; Reddy, A.B.; Sadiku, E.R.; Gupta, U.N.; Lachit, P.; et al. A Potential Utilization of End-of-Life Tyres as Recycled Carbon Black in EPDM Rubber. Waste Management 2018, 74, 110–122, doi:10.1016/J.WASMAN.2018.01.003.
160. Lin, C.W.; Chien, C.H.; Tan, J.; Chao, Y.J.; Van Zee, J.W. Chemical Degradation of Five Elastomeric Seal Materials in a Simulated and an Accelerated PEM Fuel Cell Environment. J Power Sources 2011, 196, 1955–1966, doi:10.1016/j.jpowsour.2010.10.012.
161. Feng, J.; Zhang, Q.; Tu, Z.; Tu, W.; Wan, Z.; Pan, M.; Zhang, H. Degradation of Silicone Rubbers with Different Hardness in Various Aqueous Solutions. Polym Degrad Stab 2014, 109, 122–128, doi:10.1016/J.POLYMDEGRADSTAB.2014.07.011.
162. Ansari, S.P.; Mohammad, F. Electrical Conductivity Studies of Conducting Polymer Nanocomposites in Ambient Conditions. https://doi.org/10.1177/096739111602400406 2016, 24, 273–280, doi:10.1177/096739111602400406.
163. Kraus, G.; Svetlik, J.F. Electrical Conductivity of Carbon Black-Reinforced Elastomers. J Electrochem Soc 1956, 103, 337, doi:10.1149/1.2430324/XML.
164. Spahr, M.E.; Rothon, R. Carbon Black as a Polymer Filler. Polymers and Polymeric Composites: A Reference Series 2016, 1–31, doi:10.1007/978-3-642-37179-0_36-2.
165. Maciejewska, M. The Effect of Zinc Oxide Nanoparticle Morphology on Activity in Crosslinking of Carboxylated Nitrile Elastomer. 2009, doi:10.3144/expresspolymlett.2009.68.

BUPT